Theory of Tunneling-Injection Quantum Dot Lasers

Dae-Seob Han

Dissertation submitted to the faculty of the
Virginia Polytechnic Institute and State University
in partial fulfillment of the requirements for the degree of

Doctor of Philosophy
In
Materials Science and Engineering

Levon V. Asryan, Chair / Advisor
Louis J. Guido
Giti Khodaparast
Guo-Quan Lu

September 2, 2009
Blacksburg, Virginia

Keywords: quantum dot lasers, semiconductor lasers

Theory of Tunneling-Injection Quantum Dot Lasers

Dae-Seob Han

Abstract

This work develops a comprehensive theoretical model for a semiconductor laser, which exploits tunneling-injection of electrons and holes into quantum dots (QDs) from two separate quantum wells (QWs). The potential of such a tunneling-injection QD laser for temperature-stable and high-power operation is studied under the realistic conditions of out-tunneling leakage of carriers from QDs (and hence parasitic recombination outside QDs) and the presence of the wetting layer (WL). The following topics are included in the dissertation:

1) Characteristic temperature of a tunneling-injection QD laser

The threshold current density j_{th} and the characteristic temperature T_0 are mainly controlled by the recombination in the QWs. Even in the presence of out-tunneling from QDs and recombination outside QDs, the tunneling-injection laser shows the potential for significant improvement of temperature stability of j_{th} — the characteristic temperature T_0 remains very high (above 300 K at room temperature) and not significantly affected by the QD size fluctuations.

2) Output power of a tunneling-injection QD laser

Closed-form expressions for the light-current characteristic (LCC) and carrier population across the layered structure are derived. Even in the presence of out-tunneling leakage from QDs, the intensity of parasitic recombination outside QDs is shown to remain restricted with increasing injection current. As a consequence, the LCC of a tunneling-injection QD laser exhibits a remarkable feature — it becomes increasingly linear, and the slope efficiency grows closer to unity at high injection currents. The linearity is due to the fact that the current paths connecting the opposite sides of the structure lie entirely within QDs — in view of the three-dimensional confinement in QDs, the out-tunneling fluxes of carriers from dots are limited.

3) Effect of the WL on the output power of a tunneling-injection QD laser

In the Stranski-Krastanow self-assembling growth mode, a two-dimensional WL is initially grown followed by the formation of QDs. Due to thermal escape of carriers from QDs, there will be bipolar population and hence electron-hole recombination in the WL, even in a tunneling-injection structure. Since the opposite sides of a tunneling-injection structure are only connected by the current paths through QDs, and the WL is located in the n-side of the structure, the only source of holes for the WL is provided by QDs. It is shown that, due to the zero-dimensional nature of QDs, the rate of the hole supply to the WL remains limited with increasing injection current. For this reason, as in the other parts of the structure outside QDs (QWs and optical confinement layer), the parasitic electron-hole recombination remains restricted in the WL. As a result, even in the presence of the WL, the LCC of a tunneling-injection QD laser becomes increasingly linear at high injection currents, which is a further demonstration of the potential of such a laser for high-power operation.

Acknowledgments

I would like to thank the following people for their encouragement, support and belief in my ability throughout my Ph.D. course:

- My advisor, Dr. Levon V. Asryan, for giving me a chance to study at Virginia Tech as well as his guidance and advice throughout my Ph.D. course. His profound knowledge and experience as a leader in our field gave me a lot of inspiration whenever I had trouble with my research. I will always remember what I have learned from him.
- Dr. Louis Guido for giving several informal lectures on laser diodes and spending his valuable time on detailed discussions and comments about my research.
- Dr. Giti Khodaparast and Guo-Quan Lu for taking the time to be on my committee and the courses taught to me. Their courses really helped me to extend my knowledge in the field of electronic materials and devices.
- Dr. Li Jiang, my former colleague, and Mr. Yuchang Wu, my current colleague, for their discussions and encouragement.

I would like to thank all the members of the MSE Department and my friends for giving me something to remember at Virginia Tech.

I would like to acknowledge the U.S. Army Research Office for funding of this work (Grant Nos. W911-NF-05-1-0308 and W911-NF-08-1-0462).

Finally, I would like to thank my loving family and girlfriend for their patient and support. Specially, I would like to thank my mother in hospital for her endless love and sacrifice.

Table of Contents

Abstract …… ii

Acknowledgements …… iv

Table of contents …… v

List of figures …… vii

List of tables …… x

Chapter 1. Introduction …… 1

1.1. Lasing in semiconductors …… 1

1.2. Homojunction lasers …… 2

1.3. Heterostructure lasers …… 2

1.3.1. Double heterostructure lasers …… 3

1.3.2. Quantum well lasers …… 3

1.3.3. Quantum wire and quantum dot lasers …… 4

1.4. Tunneling-injection heterostructure lasers …… 9

1.5. Objectives, structure, and main results of the dissertation …… 11

List of publications of the author of this dissertation …… 15

Presentations at the MSE seminar …… 15

References …… 16

Chapter 2. Characteristic temperature of a tunneling-injection quantum dot laser…… 22

Summary …… 22

2.1. Introduction …… 22

2.2. Laser structure ……. 23

2.3. Rate equations …… 26

2.4. Threshold current density …… 30

2.5. Results and discussion …… 32

2.6. Conclusion …… 42

References …… 43

Chapter 3. Output power of a tunneling-injection quantum dot laser …… 45

Summary …… 45

3.1. Introduction …… 45

3.2. Theoretical model …… 46
3.2.1. Main assumptions …… 48
3.2.2. Rate equations and main notations …… 49
3.3. Results and discussion …… 51
3.3.1. Ideal structure: no out-tunneling from QDs, no recombination outside QDs ….. 53
3.3.2. Structure with out-tunneling leakage from QDs and recombination outside QDs …… 54
3.3.2.1. Laser characteristics versus tunneling coefficients …… 63
3.4. Conclusion …… 68
Appendix I. Relationship between the carrier escape time from a QW to a bulk region and the capture velocity from a bulk region to a QW …… 69
Appendix II. Quantities n_1^{QW} and p_1^{QW} in the tunneling fluxes of electrons and holes from QDs to a QW …… 71
Appendix III. Criterion for neglecting the recombination in the OCL …… 72
Appendix IV. Closed-form solutions of the rate equations …… 74
References …… 76

Chapter 4. Effect of the wetting layer on the output power of a tunneling-injection QD laser …… 78
Summary …… 78
4.1. Introduction …… 78
4.2. Theoretical model …… 82
4.3. Results and discussion …… 86
4.3.1. Laser characteristics versus temporal cross-sections of electron and hole capture from the WL into a QD …… 95
4.4. Conclusion …… 102
Appendix I. Quantities $\widetilde{n}_1^{WL}$ and $\widetilde{p}_1^{WL}$ in the tunneling fluxes of electrons and holes from the electron-injecting QW to the WL …… 103
Appendix II. Quantities n_1^{WL} and p_1^{WL} in the thermal escape fluxes of electrons and holes from QDs to the WL…… 105
References …… 106

List of Figures

Fig. 1.1. Schematic illustration of excitation of an electron from the valence band to the conduction band and stimulated emission by an incoming photon in a semiconductor ……..……..……..…….. 2

Fig. 1.2. Energy band diagram of a double heterostructure laser ……... 5

Fig. 1.3. Evolution of the threshold current density of semiconductor lasers ……..……..... 5

Fig. 1.4. Density of states in bulk semiconductor, QW, QWR, and QD ……. 6

Fig. 1.5. Schematic diagrams of three possible modes for the heteroepitaxial growth ……. 8

Fig. 1.6. High resolution TEM image of a single self-organized QD grown by deposition of of 16 periods of 0.25 ML InAs/0.25ML GaAs separated by 5 s pauses ……..... 8

Fig. 1.7. Threshold current density (at 300 K) versus the number of layers with QDs for structures with vertically-coupled QDs ……..……..…….…..... 9

Fig. 1.8. Energy band diagram of a tunneling-injection QW laser ……..……..... 11

Fig. 1.9. Energy band diagram of a tunneling-injection QD laser and characteristic temperature against the QD fraction of threshold current density at room temperature …….....…..…….……..……..…....……12

Fig. 2.1. Threshold current density and its components, and characteristic temperature versus temperature …….……...…..…….. 24

Fig. 2.2. Energy band diagram of a tunneling-injection QD laser and the main processes ….. 25

Fig. 2.3. Temperature-dependence of the threshold current density and its components…….. 33

Fig. 2.4. Temperature-dependence of the 2-D electron and hole densities in the left-hand-side QW at the lasing threshold …….……..... 34

Fig. 2.5. Temperature-dependence of the characteristic temperature …….…….…….…… 35

Fig. 2.6. Threshold current density and characteristic temperature versus normalized surface density of QDs ……... 37

Fig. 2.7. Threshold current density and characteristic temperature versus normalized root mean square of relative QD size fluctuations ……... 38

Fig. 2.8. Threshold current density and characteristic temperature versus normalized cavity length ……... 39

Fig. 2.9. 2-D electron and hole densities in the left-hand-side QW versus normalized

surface density of QDs ……..……. 40

Fig. 2.10. Characteristic temperature versus tunneling coefficients for minority carriers $w^{L}_{\mathrm{p,tunn}}$ and $w^{R}_{\mathrm{n,tunn}}$ ……..……...……. 41

Fig. 3.1. Energy band diagram of a conventional QD laser and the main processes …….. 47

Fig. 3.2. LCC of a conventional QD laser …….……..……... 47

Fig. 3.3. Conduction band diagram in the left-hand (electron-injecting) side of the structure .. 52

Fig. 3.4. Parasitic recombination current density in the QWs and OCL (solid curve) and current density of out-tunneling from QDs to the foreign QWs (dashed line) against excess injection current density …..…… 57

Fig. 3.5. Light-current characteristic of a tunneling-injection QD laser (solid curve) at different values of the out-tunneling coefficient $w^{L}_{\mathrm{p,tunn}}$ …… 59

Fig. 3.6. Minority carrier density in the left-hand-side QW (left-axis) and OCL (right axis) against excess injection current density …….……..……... 61

Fig. 3.7. Internal quantum efficiency (dashed curve) and slope efficiency (solid curve) against excess injection current density ……. 61

Fig. 3.8. Majority carrier density in the left-hand-side QW (solid curve, left axis) and OCL (dashed curve, right axis) against excess injection current density …… 62

Fig. 3.9. 2-D density of electrons and holes and recombination current density in the left-hand-side QW against out-tunneling coefficient at an infinitely large in-tunneling coefficient ($w^{L}_{\mathrm{n,tunn}} \to \infty$) …..…… 65

Fig. 3.10. Threshold current density against out-tunneling coefficients at infinitely large in-tunneling coefficients ($w^{L}_{\mathrm{n,tunn}}$, $w^{R}_{\mathrm{p,tunn}} \to \infty$) ……..……. 66

Fig. 3.11. Optical power against out-tunneling coefficients at infinitely large in-tunneling coefficients ($w^{L}_{\mathrm{n,tunn}}$, $w^{R}_{\mathrm{p,tunn}} \to \infty$) ……. 67

Fig. 4.1. Cross-sectional bright field image of vertically aligned InAs/GaAs QD layers with the WLs ….....……....……..... 80

Fig. 4.2. Energy band diagram of a conventional QD laser with the WL and the main processes ……..……..... 80

Fig. 4.3. Energy band diagram of a tunneling-injection QD laser with the WL and the main processes ……... 81

Fig. 4.4. 2-D densities of electrons and holes and recombination current density in the WL against excess injection current density ……..…….…….……... 90

Fig. 4.5. 2-D densities of electrons and holes and recombination current density in the electron-injecting QW against injection current density for the structures with (solid curve) and without (dashed curve) the WL …….. 91

Fig. 4.6. Light-current characteristics of the tunneling-injection QD lasers with (solid curve) and without (dashed curve) the WL ……. 92

Fig. 4.7. Internal quantum efficiency and slope efficiency against injection current density for the tunneling injection QD lasers with (solid curve) and without (dashed curve) the WL ……..…….…….……...…….. 93

Fig. 4.8. Parasitic recombination current density outside QDs (solid curve) ……..... 95

Fig. 4.9. 2-D densities of electrons and holes, recombination current densities in the WL and QW, total parasitic recombination current density outside QDs and output power against temporal cross-section of majority carrier (electron) capture from the WL into a QD at a fixed temporal cross-section $w_{\mathrm{p,\,capt}} = 0.1$ cm^2/s of minority carrier (hole) capture 97

Fig. 4.10. 2-D densities of electrons and holes, recombination current densities in the WL and QW, total parasitic recombination current density outside QDs and output power against temporal cross-section $w_{\mathrm{p,\,capt}}$ of minority carrier (hole) capture from the WL into a QD at a fixed temporal cross-section $w_{\mathrm{n,\,capt}} = 0.1$ cm^2/s of majority carrier (electron) capture .....……...…….…..... 98

Fig. 4.11. 2-D densities of electrons and holes, recombination current densities in the WL and QW, total parasitic recombination outside QDs and output power against temporal cross-section of majority and minority carrier capture ……..... 99

Fig. 4.12. Optical power against the temporal cross-sections $w_{\mathrm{n,\,capt}}$ and $w_{\mathrm{p,\,capt}}$ of electron and hole capture from the WL into a QD ……...…….. 101

List of Tables

Table 2.1. Fluxes of different processes in eqs. (2.2)–(2.12) …… 28

Table 2.2. Physical quantities in eqs. (2.2)–(2.12) …….. 29

Table 3.1. Highest injection current densities (second and third columns) satisfying the criteria for neglecting recombination in, respectively, in the left- and right-hand sides of the OCL [see (A21)] for the left-hand side] at different values of the capture velocity from the O CL to the QWs …… 73

CHAPTER 1

Introduction

1.1. Lasing in semiconductors

The term laser is an acronym for “light amplification by stimulated emission of radiation”. In semiconductor lasers, the photons are emitted through the transitions of carriers in a semiconductor material. Fig. 1.1 shows schematically the stimulated emission of photons in a semiconductor. When a photon is incident on a semiconductor, it is absorbed thus creating an electron-hole pair (i.e., an electron is excited from the valence band into the conduction band) [Fig. 1.1(a)]. If such an excited electron interacts with an incident photon, an electron-hole pair recombines creating one more photon, which has the same wavelength as an incident photon [Fig. 1.1(b)]. In a system of many electrons under thermal equilibrium, the electron energy distribution follows the Fermi-Dirac statistics, and hence the population of a higher-energy state in the conduction band is smaller than that of a lower-energy state in the valence band. Hence, the incident photons are substantially absorbed and correspondingly many electrons are excited into the conduction band. If the condition of population inversion is satisfied, i.e., the population of a higher-energy state in the conduction band becomes larger than that of a lower-energy state in the valence band, the stimulated emission of photons overcomes the absorption of photons, and finally the optical amplification is achieved. In a semiconductor material, the population inversion can be realized by creating a large number of electron-hole pairs through the excitation of electrons from the valence band into the conduction band. Electrons can be excited from the valence band into the conduction band by light irradiation or electron-beam irradiation. However, the most effective way is to form a p-n junction in semiconductor materials and then inject forward currents, which provide high-energy carriers in the p-n junction. Such semiconductor lasers, wherein the population inversion is created by the current injection, are called as injection lasers or laser diodes.

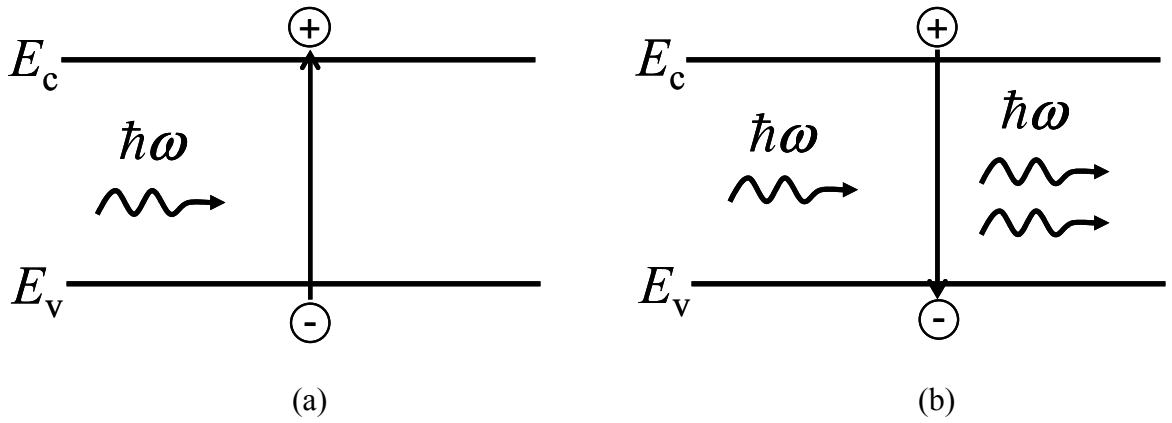

Fig. 1.1. Schematic illustration of (a) excitation of an electron from the valence band to the conduction band and (b) stimulated emission by an incoming photon in a semiconductor.

1.2. Homojunction lasers

There have been initial studies on the use of semiconductors for lasing in the late 1950s and early 1960s [1]-[3]. In 1962, narrowing of the electroluminescence spectrum has been observed in a GaAs diode at 77 K [4]. In the same year, Hall *et al.* [5] demonstrated the coherent light emission in the pulse mode using a GaAs p-n junction at 77 K; the lasing wavelength was 842 nm with a spectral width of 1.5 nm. Several other groups also observed the coherent emission in semiconductors in the infrared and visible light range [6]-[8]. At this early stage, the same semiconductor material was used to form a p-n junction, and the homojunction lasers suffered from high threshold current densities (more than 10^4 A/cm^2) at room temperature. As a result, continuous wave (CW) lasing operation was only possible at cryogenic temperature.

1.3. Heterostructure lasers

The possibility of the use of semiconductor lasers for lightwave communications motivated a further research to secure room temperature operation, low threshold current density, and reliability. After much effort, the use of heterostructures in semiconductor lasers was proposed to overcome the difficulties of lasing operation in a p-n homojunction laser, followed by the development of the crystal growth and epitaxial technologies.

1.3.1. Double heterostructure lasers

The advent of semiconductor heterostructures brought significant changes to electron devices in many areas. In 1963, the concept of double heterostructure (DHS) lasers was proposed by Alferov and Kazarinov [9] and Kroemer [10]. They proposed attaining a high density of injected carriers and population inversion in a DHS – a structure in which a layer of a narrower band gap material is sandwiched between the layers of a wider band gap material (Fig. 1.2). In a DHS, the carriers and the emitted light are efficiently confined in a middle (narrower band gap) layer. In 1970, room temperature CW operation with the threshold current density well below 10 kA/cm^2 was demonstrated in DHS lasers [11, 12]. In terms of the carrier confinement, DHS lasers have become the groundwork for a more advanced type of lasers – quantum well (QW) lasers.

1.3.2. Quantum well lasers

In 1974, Dingle *et al.* [13] observed the manifestations of quantum confinement in the optical spectra of AlGaAs-GaAs-AlGaAs semiconductor heterostructures with an ultrathin GaAs layer. In their patent [14], Dingle and Henry suggested to exploit quantum effects in semiconductor heterostructure lasers. The idea was that the use of quantum effects in semiconductor heterostructures can provide the wavelength tunability by changing the thickness of the active region and can result in a lower lasing threshold due to the change in the density of states, which came from the reduced number of the degrees of freedom for the carriers confined in the active region. In 1975, Van Der Ziel *et al.* [15] observed the lasing operation in a QW structure consisting of alternating layers of $Al_{0.2}Ga_{0.8}As$ and a very thin GaAs (50 – 500 Å), but the lasing performance fell short of that of DHS lasers.

In 1978, Dupuis *et al.* [16] reported for the first time on a $Ga_{1-x}Al_xAs$-GaAs QW laser with the performance comparable to DHS lasers. They used the term "quantum well" for the first time. Since the first observation of lasing in QW structures, the crystal growth techniques have been continuously evolving, thus allowing to grow thin films of good quality.

In 1982, through major improvements in the MBE growth technology (such as reducing the doping of the layers around the active region) and using a graded index separate confinement heterostructure, Tsang [17] achieved the threshold current density as low as 160 A/cm^2 for broad-area Fabry-Perot lasers with the cavity length of 1125 μm. By bounding the QW by a

short-period variable-step superlattice, Alferov *et al*. [18] demonstrated the GaAs-AlGaAs double-heterostructure separate-confinement QW lasers with j_{th} of about 52 A/cm^2 and, at optimized conditions, 40 A/cm^2 – the lowest value for semiconductor lasers until the late 1990s.

There have also been other approaches using the QW heterostructures. One of them was to generate the stimulated emission in semiconductor superlattices. This original concept was proposed by Kazarinov and Suris in 1971 [19]-[21] and experimentally realized by Faist and Capasso *et al.* in 1994 [22, 23]. Such a laser is called as a quantum cascade laser and is based on the electron resonant tunneling and optical transition between the quantized states in the conduction band. The quantum cascade lasers are unipolar lasers emitting in mid- to far-infrared range.

Evolution of the threshold current density, which should be as low as possible for a stable lasing action, reflects the history of semiconductor lasers (Fig. 1.3) [24]. As seen from the figure, there are four milestones in lowering the threshold current density related to the advent of a DHS laser, QW laser, short-period QW superlattices laser, and quantum dot (QD) laser.

1.3.3. Quantum wire and quantum dot lasers

The rapid development and various applications of QW lasers, in which the quantum-confinement of carriers occurs in one direction, stimulated the interest to further reducing the dimensionality of the active region. Thus, quantum wire (QWR) and QD heterostructures emerged, wherein carriers are spatially localized in two and three directions, respectively.

Fig. 1.4 shows the density of states in a bulk semiconductor, QW, QWR, and QD. The density of states in a bulk, QW, and QWR is continuous [Fig. 1.4(a)-(c)]. A true discrete energy spectrum and delta-function density of states can be realized in zero-dimensional structures, i.e., QDs only [Fig. 1.4(d)]. Due to the spatial confinement of carriers in all the three directions, QDs exhibit an electron structure similar to atoms. That is why they can be considered as ‘man-made atoms’ or ‘artificial atoms’. Structures with QDs became promising for lasing due to the expectations of low threshold current density and high temperature stability.

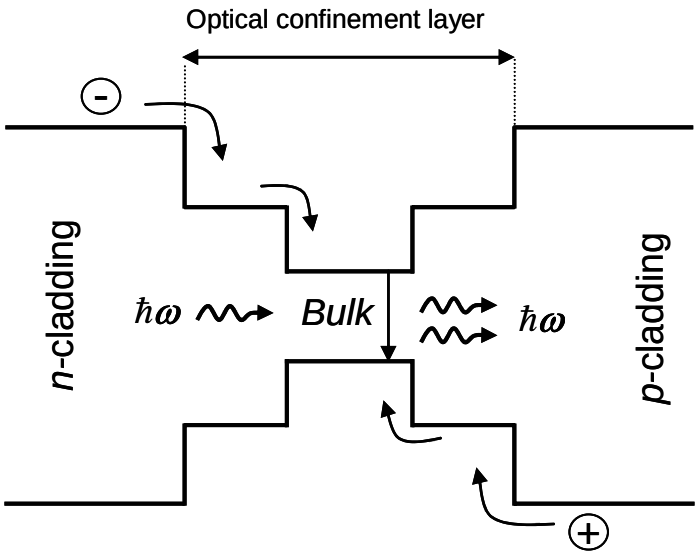

Fig. 1.2. Energy band diagram of a double heterostructure laser.

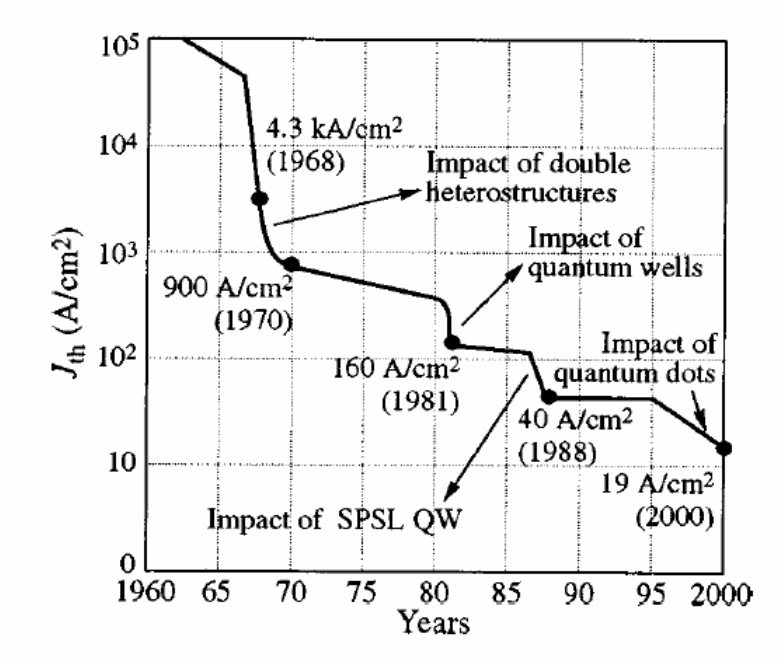

Fig. 1.3. Evolution of the threshold current density of semiconductor lasers. (Reprinted with permission from Fig. 9 of [24]. Copyright (2001) by the American Physical Society.)

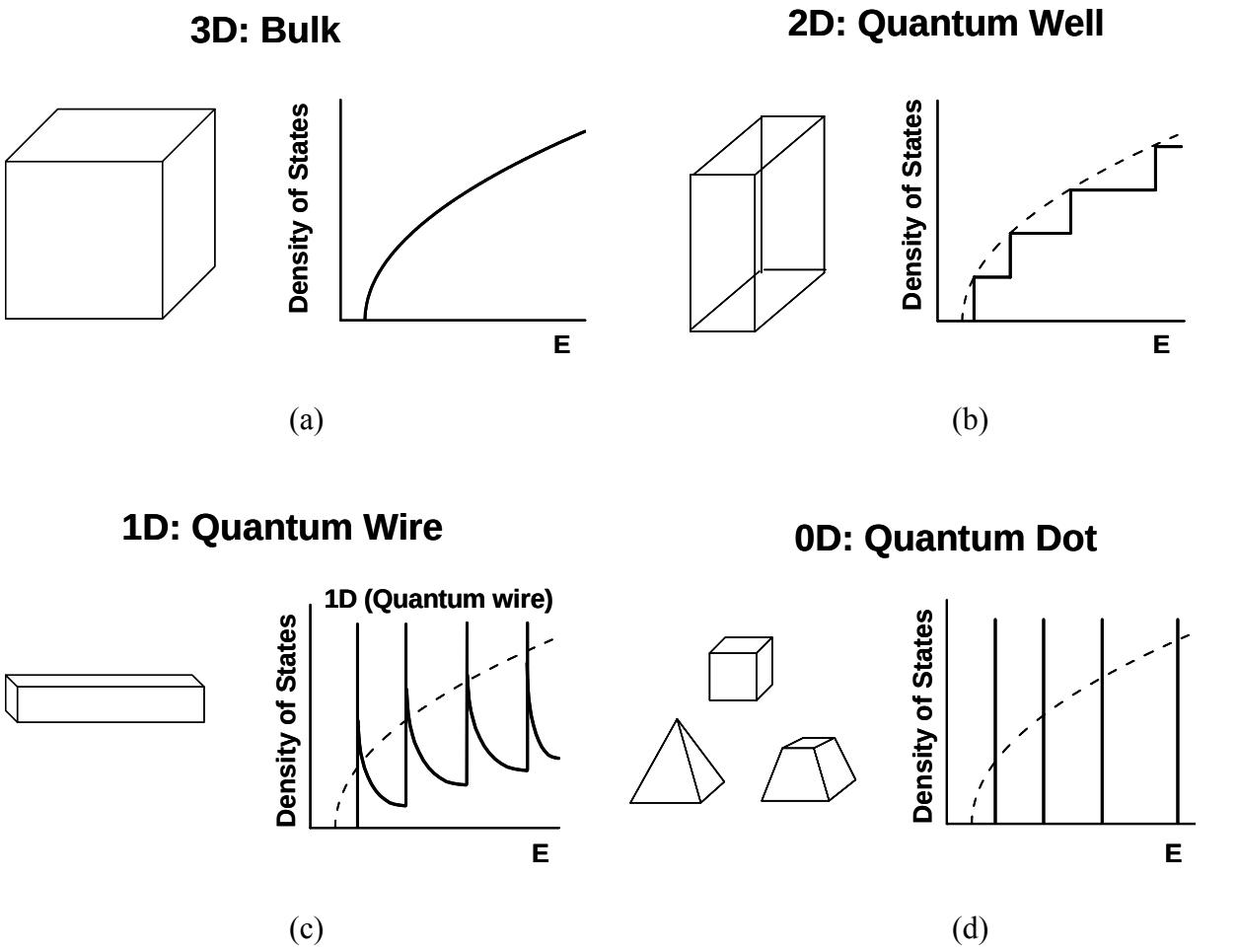

Fig. 1.4. Density of states in (a) bulk semiconductor (3D), (b) quantum well (2D), (c) quantum wire (1D), and (d) quantum dot (0D).

In 1982, Arakawa and Sakaki [25] proposed the use of QWRs and QDs for lasing. They predicted a much weaker temperature-sensitivity of the threshold current for a QWR laser compared to that of a QW laser. For an idealized QD laser, they predicted a temperature insensitive threshold current. To experimentally simulate a QWR laser, they placed a bulk (DHS) laser in a strong magnetic field and indeed observed an improvement in the temperature stability of the threshold current.

There have been much experimental efforts to realize QD lasers. Initially, the QD structures suffered from high density of defects and variance in quantum confinement energy levels due to nonuniformity in QD size and shape. The use of self-organization growth technique

for QD structures opened the door to the practical realization of QD lasers. As shown in Fig 1.5, there are three well-known growth modes for semiconductor materials – Frank van der Merwe, Volmer-Weber, and Stranski-Krastanow (SK) modes. It was the self-organized SK growth mode that allowed to grow uniform enough, dense, and defect-free QDs. In the Stranski-Krastanow growth mode, several monolayers of one material are grown first on a crystal surface of another material (substrate) having a different lattice constant. Beyond a critical thickness of the deposited layer, three-dimensional (3-D) islands (QDs) start forming from two-dimensional (2-D) monolayers thus partially relaxing the strain and reducing the elastic energy The initially grown monolayers are called as the wetting layer (WL). Hence, the 2-D WL is inherently present in self-assembled Stranski-Krastanow grown QD structures [26]-[29].

In the early stage of QD lasers, molecular beam epitaxy (MBE) was mainly used for self-organized QDs growth, which was later followed by metalorganic chemical vapor deposition (MOCVD) (Fig. 1.6) [30]. In 1994, Ledentsov *et al.* [31] demonstrated for the first time the optically-pumped lasing action in an InAs-GaAs QD structure grown by MBE. In the same year, Kirstädter *et al.* [32] reported for the first time on the QD laser diode operating at room temperature with j_{th} = 950 A/cm^2 (see also Egorov *et al.* [33]).

In 1996, Alferov *et al.* [34] used MOCVD for the fabrication of a low-threshold (j_{th} = 150 A/cm^2) QD laser. In the same year, for a QD size dispersion of 10% and other practical structure parameters, Asryan and Suris [35] predicted threshold current densities below 10 A/cm^2 at room temperature in properly optimized QD lasers.

In 1997, Ustinov *et al.* [36] demonstrated a laser based on vertically-coupled QDs with low j_{th} at the room temperature. Fig. 1.7 shows j_{th} versus the number of layers with vertically-coupled QDs [37]; with increasing number of layers, the threshold current density decreases down to 90 A/cm^2. In 1998, Zhukov *et al.* [38] reported on a QD laser with the threshold current density of 63 A/cm^2.

In 2000, the lasing with the threshold current density of 10 A/cm^2 was achieved by Park *et al.* [39] in a QD structure.

Since the beginning of the 1990s, the fabrication techniques for QD lasers have been continuously progressing. In view of the needs for telecommunication systems, many studies have been focused on QD lasers emitting at the wavelengths of 1.3 and 1.55 μm.

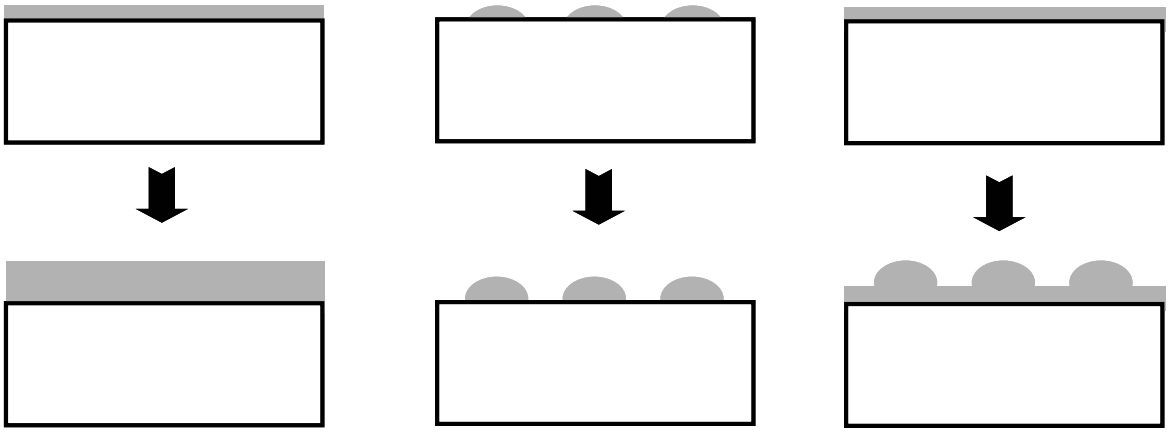

Fig. 1.5. Schematic diagrams of three possible modes for the heteroepitaxial growth: (a) Frank-van der Merwe (FM), (b) Volmer-Weber (VW), and (c) Stranski-Krastanow (SK).

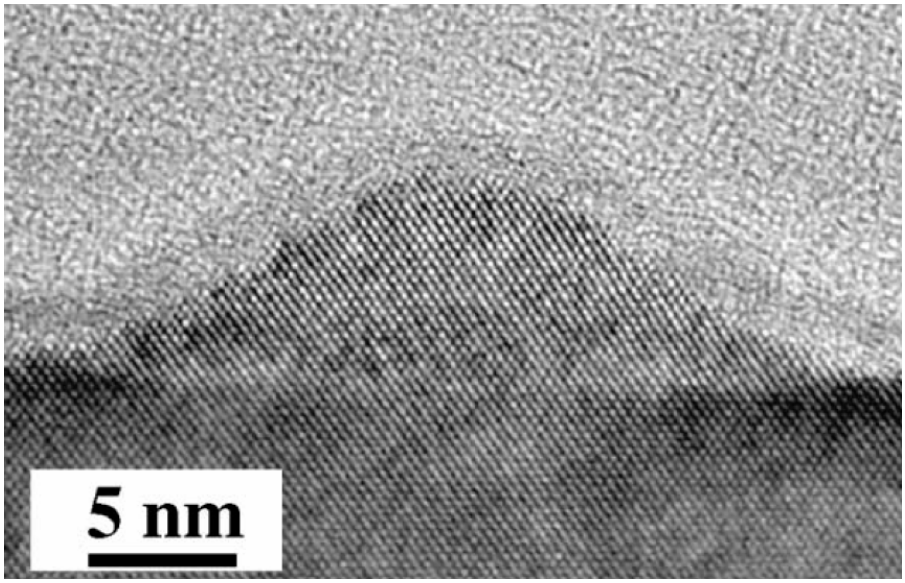

Fig. 1.6. High resolution TEM image of a single self-organized QD grown by deposition of 16 periods of 0.25 ML InAs/0.25ML GaAs separated by 5s pauses. (Reprinted from Fig. 1 of ref. [30], Copyright (2001), with permission from Elsevier.)

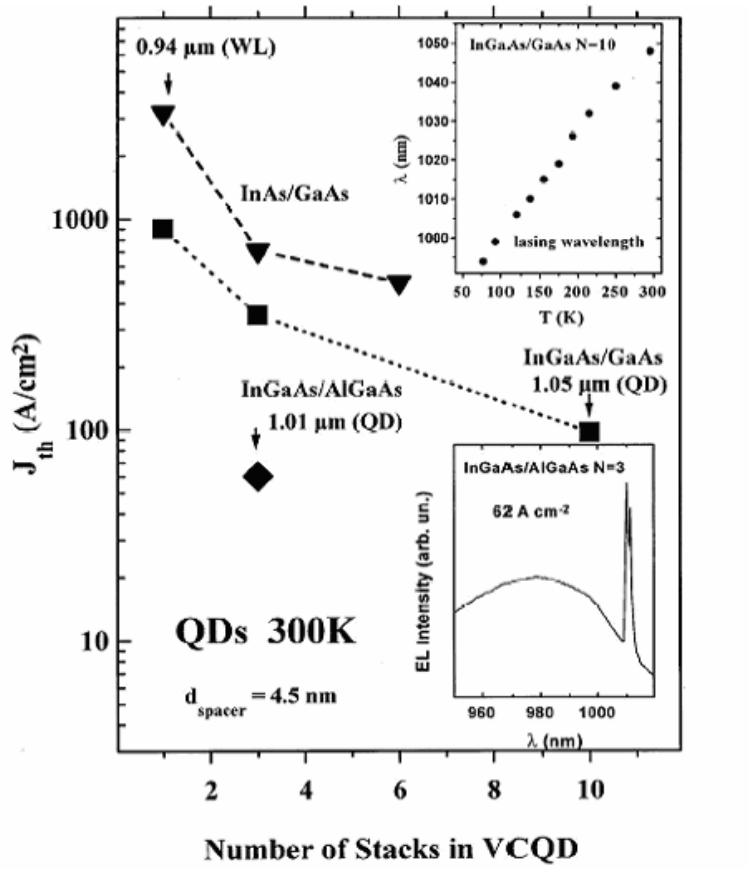

Fig. 1.7. Threshold current density (at 300 K) versus the number of layers with QDs for structures with vertically-coupled QDs. (Reprinted with permission from Fig. 6(b) of [37].)

In 2000, Lott *et al.* [40] reported on a QD vertical-cavity surface-emitting laser (VCSEL) on the GaAs substrate emitting at 1.3 μm. In [41], Homeyer *et al.* reported on an InAs/InP QD laser emitting near 1.55 μm with j_{th} = 170 A/cm^2.

1.4. Tunneling-injection heterostructure lasers

Even though the fast progress on QD lasers has been made, there are still several problems to overcome, such as temperature sensitivity of the threshold current density due to the parasitic recombination outside QDs [42] and the sublinearity of the light-current characteristic (LCC) [43]. Several approaches have been recently proposed to improve the characteristics of

QD lasers. Among them are p-type modulation doping of the active region [44, 45] and tunneling injection of carriers into QDs [46]-[48].

In 1996, tunneling-injection of electrons was proposed in single and multiple QW lasers (Fig. 1.8) [49] to alleviate hot carrier effects, which otherwise reduce the gain and increase the Auger recombination [50, 51]. Electrons injected from the cladding layer are first thermalized in a wide three dimension (bulk) region and become cold. Cold electrons then tunnel into the QW through thin barriers. Tunneling-injection QW lasers emitting at 0.98 μm showed higher modulation bandwidth, lower chirp, and weaker temperature dependence of the threshold current density.

To address the same problems in QD lasers, tunneling-injection of electrons from the QW into QDs was proposed [51]-[53]. Such a tunneling-injection QD laser did showed an enhanced small-signal modulation bandwidth and reduced temperature sensitivity of the threshold current density. However, in the structures of [51]-[53], bipolar carrier density and hence parasitic recombination still remain on the hole-injecting side.

In [54], tunneling-injection of electrons into QDs was reported for an InAs QD laser based on the InP substrate.

In [55], resonant tunneling was proposed from the bulk region into the QD excited-state separated from the QD ground-state by the energy of the longitudinal optical phonon.

In [46]-[48], to suppress the recombination outside QDs and thus to significantly improve the temperature-stability of the laser, tunneling-injection of both electrons and holes into QDs was proposed from two separate QWs [Fig. 1.9(a)]. In [46], the complete suppression of the parasitic recombination outside QDs was shown to lead to the characteristic temperature value above 1500 K [Fig. 1.9(b)].

There has been experimental work [56]-[59] related to the concept [46]-[48] of tunneling injection of both electrons and holes into QDs. Compared to a conventional QD laser, tunneling-injection can efficiently improve the uniformity of QDs by selecting the QDs of the ‘right’ size, and the carrier collection in QDs can also be improved [56]. Using tunneling-injection of both electrons and holes, the highest ground-state gain for a single-layer InAs QD laser was reported, thus allowing for ground-state lasing in short-cavity devices [57]. A more symmetrical gain shape and a smaller refractive index change at the peak gain wavelength were reported for a tunneling-injection QD laser [59].

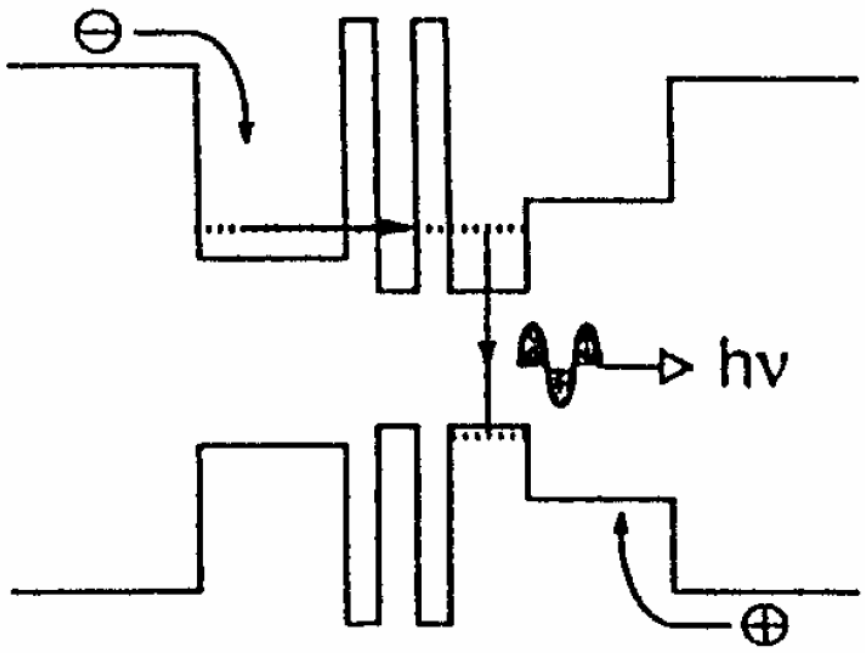

Fig. 1.8. Energy band diagram of a tunneling injection QW laser of [49]. (Fig. 1(b) of ref. [49], reprinted with kind permission of Springer Science and Business Media.)

1.5. Objectives, structure, and main results of the dissertation

In [46]-[48], tunneling-injection of both electrons and holes into QDs was proposed from two separate QWs. In the case of no out-tunneling from QDs into the foreign QWs, the characteristic temperature of the laser was shown to be above 1000 K, which means virtually temperature-insensitive threshold current density.

The main objective of this dissertation is the study of the potential of the laser, which exploits tunneling-injection of both electrons and holes into QDs, for temperature-stable and high-power operation under the realistic conditions of out-tunneling leakage of carriers from QDs into the foreign QWs and the presence of the wetting layer (WL). The structure of the dissertation, the topics of the research, and the main results are:

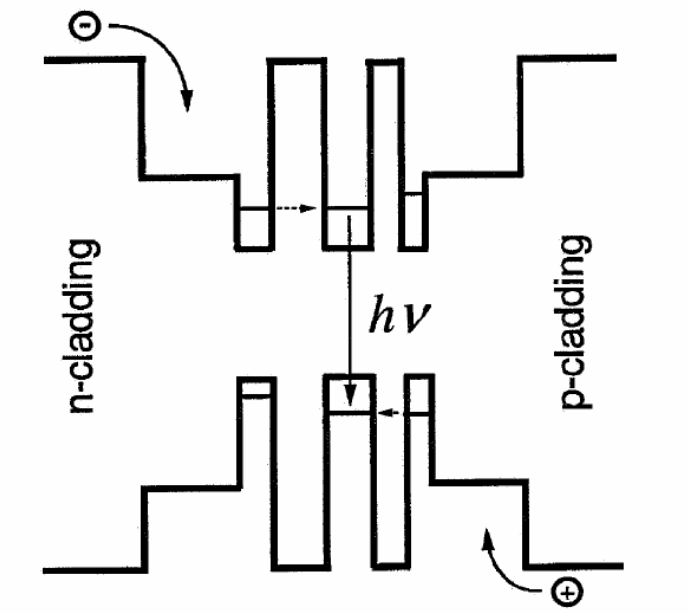

(a)

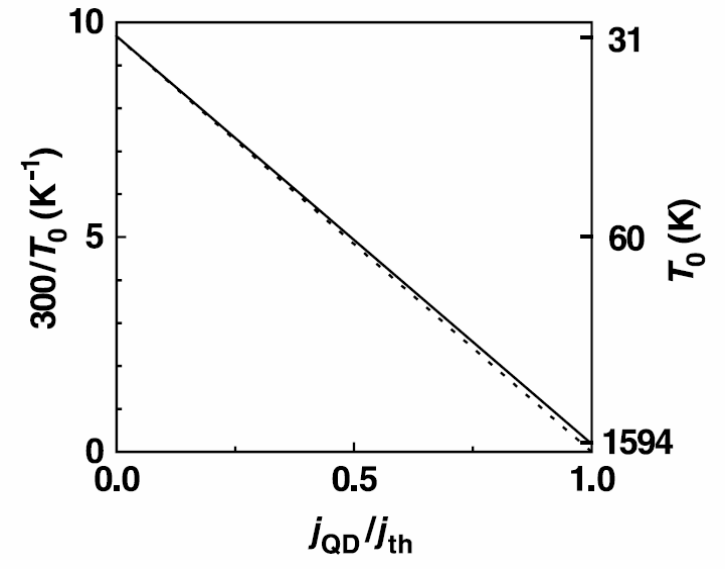

(b)

Fig. 1.9. (a) Energy band diagram of a tunneling-injection QD laser of [46]-[48] and (b) characteristic temperature against the QD fraction of threshold current density at room temperature. The dotted line depicts $1/T_0$ in the absence of inhomogeneous line broadening ($T_0^{\mathrm{QD}} = \infty$). The T_0 values are indicated on the right axis. (Reprinted from Figs. 3 and 4(b) of ref. [47], Copyright (2003), with permission from Elsevier.)

1) Characteristic temperature of a tunneling-injection QD laser (chapter 2)

A laser structure is studied, which exploits tunneling-injection of electrons and holes into QDs from two separate QWs. An extended theoretical model is developed allowing for out-tunneling leakage of carriers from QDs into the opposite-to-injection-side QWs (electrons into the p-side QW and holes into the n-side QW). Due to out-tunneling leakage, parasitic recombination of electron-hole pairs occurs outside QDs – in the QWs and optical confinement layer. The threshold current density j_{th} and the characteristic temperature T_0 are shown to be mainly controlled by the recombination in the QWs [A1, A2]. Even in the presence of out-tunneling from QDs and recombination outside QDs, a tunneling-injection laser shows potential for significant improvement of temperature stability of j_{th} — the characteristic temperature T_0 remains very high (above 300 K at room temperature) and not significantly affected by the QD size fluctuations.

2) Output power of a tunneling-injection QD laser (chapter 3)

A comprehensive theoretical model for a tunneling-injection QD laser is developed [A3]-[A5]. Both electrons and holes are injected into QDs by tunneling from two separate QWs. Ideally, out-tunneling of each type of carriers from QDs into the opposite-to-injection-side QW should be completely blocked; as a result, the parasitic electron-hole recombination outside QDs will be suppressed and the light-current characteristic (LCC) of a laser will be strictly linear. To scrutinize the potential of a tunneling-injection QD laser for high-power operation and the robustness of an actual device, the model includes out-tunneling leakage of carriers from QDs. The numerical calculations are complemented by an analytical model and closed-form expressions for the LCC and carrier population across the layered structure are derived. Even in the presence of out-tunnelling leakage, the intensity of parasitic recombination outside QDs is shown to remain restricted with increasing injection current. As a consequence, the LCC exhibits a remarkable feature distinguishing the tunneling-injection QD laser from other types of injection lasers — it becomes increasingly linear, and the slope efficiency grows closer to unity at high injection currents. The linearity is due to the fact that the current paths connecting the opposite sides of the structure lie entirely within QDs — in view of the three-dimensional confinement in QDs, the out-tunneling fluxes of carriers from dots are limited.

3) Effect of the wetting layer on the output power of a tunneling-injection QD laser (chapter 4)

To suppress bipolar population and hence electron-hole recombination outside QDs, tunneling-injection of electrons and holes into QDs from two separate QWs was proposed earlier. Close-to-ideal operating characteristics were predicted for such a tunneling-injection laser. In the Stranski-Krastanow growth mode, a two-dimensional wetting layer (WL) is initially grown followed by the formation of QDs. Due to thermal escape of carriers from QDs, there will be bipolar population and hence electron-hole recombination in the WL, even in a tunneling-injection structure. Here, the light-current characteristic (LCC) of a tunneling-injection QD laser is studied in the presence of the WL [A6, A7]. Since *(i)* the opposite sides of a tunneling-injection structure are only connected by the current paths through QDs and *(ii)* the WL is located in the n-side of the structure, the only source of holes for the WL is provided by QDs. It is shown that, due to the zero-dimensional nature of QDs, the rate of the hole supply to the WL remains limited with increasing injection current. For this reason, as in the other parts of the structure outside QDs (quantum wells and optical confinement layer), the parasitic electron-hole recombination remains restricted in the WL. As a result, even in the presence of the WL, the LCC of a tunneling-injection QD laser becomes increasingly linear at high injection currents, which is a further demonstration of the potential of such a laser for high-power operation.

List of publications of the author of this dissertation

[A1] D.-S. Han and L. V. Asryan, "Characteristic temperature of a tunneling-injection quantum dot laser," ***International Semiconductor Device Research Symposium.*** College Park, Maryland, Dec. 12–14, 2007, vols. 1 and 2, pp. 626-627.

[A2] D.-S. Han and L. V. Asryan, "Characteristic temperature of a tunneling-injection quantum dot laser: Effect of out-tunneling from quantum dots," ***Solid-State Electron.*** vol. 52, no. 10, pp. 1674-1679, Oct. 2008.

[A3] D.-S. Han and L. V. Asryan, "Light-current curve of a tunneling-injection quantum dot laser," ***Proc. SPIE,*** vol. 6902, pp. B9020-1–B9020-12, Jan. 2008.

[A4] D.-S. Han and L. V. Asryan, "Tunneling-injection of electrons and holes into quantum dots: A tool for high-power lasing," ***Appl. Phys. Lett.***, vol. 92, no. 25, pp. 251113-1–251113-3, June 2008.

[A5] D.-S. Han and L. V. Asryan, "Output power of a tunneling-injection quantum dot laser," under review.

[A6] D.-S. Han and L. V. Asryan, "Effect of the wetting layer on the output power of a tunneling-injection quantum dot laser," accepted for publication in ***IEEE/OSA J. Lightwave Technol.***

[A7] D.-S. Han and L. V. Asryan, "Tunneling-injection quantum dot laser: Effect of the wetting layer," ***Proc. SPIE,*** vol. 7610, Jan. 2010.

Presentations at the MSE seminar

1) D.-S. Han, "Output power and the light-current characteristic of a tunneling-injection quantum dot laser diode," Apr. 27, 2007.
2) D.-S. Han, "Characteristic temperature of a tunneling-injection quantum dot laser: Effect of out-tunneling from quantum dots," Jan. 25, 2008.

REFERENCES

[1] N. G. Basov, B. M. Vul, and Yu. M. Popov, "Quantum-mechanical semiconductor generators and amplifiers of electromagnetic oscillations," *Sov. Phys. JETP,* vol. 10, pp. 416, 1960 [Translated from *Zh. Eksp. Teor. Fiz.* (U.S.S.R.), vol. 37, pp. 587-588, 1959].

[2] W. S. Boyle and D. G. Tomas, "Optical maser," U. S. patent 3 059 117, Oct. 16, 1962.

[3] N. G. Basov, O. N. Krokhin, and Yu. M. Popov, "Production of negative-temperature states in P-N junctions of degenerate semiconductors," *Sov. Phys. JETP*, vol. 13, pp. 1320-1321, 1961 [Translated from *Zh. Eksp. Teor. Fiz.* (U.S.S.R.), vol. 40, pp. 1879-1880, 1961].

[4] D. N. Nasledov, A. A. Rogachev, S. M. Ryvkin, and B. V. Tsarenkov, "Recombination radiation of gallium arsenide," *Sov. Phys. Solid State*, vol. 4, pp. 782-784, 1962 [Translated from *Fiz. Tverd. Tela*, vol. 4, pp. 1062, 1962].

[5] R. N. Hall, G. E. Fenner, J. D. Kingsley, T. J. Soltys and R. O. Carlson, "Coherent light emission from GaAs Junctions," *Phys. Rev. Lett.,* vol. 9, no. 9, pp. 366, Nov. 1962.

[6] M. I. Nathan, W. P. Dumke, G. Burns, F. H. Dill, Jr., and G. Lasher, "Stimulated emission of radiation from GaAs p-n junctions," *Appl. Phys. Lett.*, vol. 1, no. 3, pp. 62-64, Nov. 1962.

[7] N. Holonyak, Jr., and S. F. Bevacqua, "Coherent (visible) light emission from $Ga(As_{1-x}P_x)$ junctions,'' *Appl. Phys. Lett.,* vol. 1, no. 4, pp. 82-83, Dec. 1962.

[8] T. M. Quist, R. H. Rediker, R. J. Keyes, W. E. Krag, B. Lax, A. L. McWhorter, and H. J. Zeilger, "Semiconductor maser of GaAs," *Appl. Phys. Lett.*, vol. 1, no. 4, pp. 91-92, Dec. 1962.

[9] Zh. I. Alferov and R. F. Kazarinov, "Semiconductor laser with electric pumping," Inventor's Certificate 181737 [in Russian], Application No. 950840, priority as of Mar. 30, 1963.

[10] H. Kroemer, "Semiconductor laser with electric pumping," U.S. Patent 3 309 553, Aug. 16, 1963.

[11] Zh. I. Alferov, V. M. Andreev, D. Z. Garbuzov, Yu. V. Zhilyaev, E. P. Morozov, E. L. Portnoi, and V. G. Trofim, "Investigation of the influence of the AlAs–GaAs heterostructure parameters on the laser threshold current and realization of continuous

emission at room temperature," *Sov. Phys. Semicond.*, vol. 4, pp. 1573–1575, 1971 [Translated from *Fiz. Tekh. Poluprovodn.*, vol. 4, pp. 1826, 1970].

[12] I. Hayashi, M. B. Panish, P. W. Foy, and S. Sumski, "Junction lasers which operate continuously at room temperature," *Appl. Phys. Lett.*, vol. 17, no. 3, pp. 109-111, Aug. 1970.

[13] R. Dingle, W. Wiegmann, and C. H. Henry, "Quantized states of confined carriers in very thin Al_xGa_{1-x} As–GaAs–Al_xGa_{1-x}As heterostructures," *Phys. Rev. Lett.*, vol. 33, no. 14, pp. 827–830, 1974.

[14] R. Dingle and C. H. Henry, "Quantum effects in heterostructure lasers," U.S. Patent 3 982 207, Sept. 21, 1976.

[15] J. P. van der Ziel, R. Dingle, R. C. Miller, W. Wiegmann, and W. A. Nordland, Jr., "Laser oscillation from quantum states in very thin GaAs–$Al_{0.2}Ga_{0.8}$As multilayer structures," *Appl. Phys. Lett.*, vol. 26, no. 8, pp. 463–465, Apr. 1975.

[16] R. D. Dupuis, P. D. Dapkus, N. Holonyak, Jr., E. A. Rezek, and R. Chin, "Room-temperature operation of quantum-well $Ga_{(1-x)}Al_xAs$–GaAs laser diodes grown by metalorganic chemical vapor deposition," *Appl. Phys. Lett.*, vol. 32, no. 5, pp. 295–297, Mar. 1978.

[17] W. T. Tsang, "Extremely low threshold (AlGa)As graded-index waveguide separate-confinement heterostructure lasers grown by molecular-beam epitaxy," *Appl. Phys. Lett.*, vol. 40, no. 3, pp. 217–219, Feb. 1982.

[18] Zh. I. Alferov, A. I. Vasil'ev, S. V. Ivanov, P. S. Kop'ev, N. N. Ledentsov, M. E. Lutsenko, B. Y. Mel'tser, and V. M. Ustinov, "Lowering the threshold current density in GaAs–AlGaAs double-heterostructure separate-confinement quantum-well lasers (J_{thr} = 52 A/cm^2 , T = 300 K) by bounding the quantum well by a short-period variable-step superlattice," *Sov. Tech. Phys. Lett.*, vol. 14, pp. 782–784, 1988.

[19] R. F. Kazarinov and R. A. Suris, "Possibility of amplification of electromagnetic waves in a semiconductor with a superlattice," *Sov. Phys. Semicond.*, vol. 5, no. 4, pp. 707–709, 1971.

[20] R. F. Kazarinov and R. A. Suris, "Electric and electromagnetic properties of semiconductors with a superlattice," *Sov. Phys. Semicond.*, vol. 6, no. 1, pp. 120–131, 1972.

[21] R. F. Kazarinov and R. A. Suris, "Theory of electrical properties of semiconductors with superlattices," *Sov. Phys. Semicond.*, vol. 7, no. 3, pp. 347–352, 1973.

[22] J. Faist, F. Capasso, D. L. Sivco, C. Sirtori, A. L. Hutchinson, and A. Y. Cho, "Quantum cascade laser," *Sci.*, vol. 264, no. 5158, pp. 553–556, Apr.1994.

[23] J. Faist, F. Capasso, D. L. Sivco, C. Sirtori, A. L. Hutchinson, and A. Y. Cho, "Quantum cascade laser: An intersub-band semiconductor laser operating above liquid nitrogen temperature," *Electron. Lett.*, vol. 30, no. 11, pp. 865–866, May 1994.

[24] Zh. I. Alferov, "Nobel lecture: The double heterostructure concept and its applications in physics, electronics, and technology," *Rev. Mod. Phys.,* vol. 73, no. 3, pp. 767–782, July 2001.

[25] Y. Arakawa and H. Sakaki, "Multidimensional quantum well laser and temperature dependence of its threshold current," *Appl. Phys. Lett.*, vol. 40, no. 11, pp. 939–941, Jun. 1982.

[26] K. Nishi, R. Mirin, D. Leonard, G. Medeiros-Ribeiro, P. M. Petroff, and A. C. Gossard, "Structural and optical characterization of InAs/InGaAs self-assembled quantum dots grown on (311)*B* GaAs," *J. Appl. Phys.,* vol. 80, no. 6, pp. 3466–3470, Sept. 1996.

[27] R. Leon, Y. Kim, C. Jagadish, M. Gal, J. Zou, and D. J. H. Cockayne, "Effects of interdiffusion on the luminescence of InGaAs/GaAs quantum dots," *Appl. Phys. Lett.*, vol. 69, no. 13, pp. 1888–1890, Sept. 1996.

[28] A. Patanè, A. Polimeni, P. C. Main, M. Henini, and L. Eaves, "High-temperature light emission from InAs quantum dots," *Appl. Phys. Lett.*, vol. 75, no. 6, pp. 814–816, Aug. 1999.

[29] J. S. Kim and I.-H. Bae, "Optical properties of wetting layer in InAs quantum dots at different growth temperatures," *J. Korean Phys. Soc.*, vol. 42, no. 92, pp. S483–S486, Feb. 2003.

[30] P. Bhattacharya, S. Krishna, J. Phillips, P. J. McCann, and K. Namjou, "Carrier dynamics in self-organized quantum dots and their application to long-wavelength sources and detectors, " *J. Cryst. Growth,* vols. 227–228, pp. 27-35, July 2001.

[31] N. N. Ledentsov, V. M. Ustinov, A. Yu. Egorov, A. E. Zhukov, M. V. Maksimov, I. G. Tabatadze, and P. S. Kop'ev, "Optical-properties of heterostructures with InGaAs-GaAs quantum clusters," *Semiconductors*, vol. 28, no. 8, pp. 832–834, Aug. 1994.

[32] N. Kirstädter, N. N. Ledentsov, M. Grundmann, D. Bimberg, V. M. Ustinov, S. S. Ruvimov, M. V. Maximov, P. S. Kop'ev, Zh. I. Alferov, U. Richter, P. Werner, U. Gösele, and J. Heydenreich, "Low threshold, large T_0 injection laser emission from (InGa)As quantum dots," *Electron. Lett.*, vol. 30, no. 17, pp. 1416–1417, Aug. 1994.

[33] A. Yu. Egorov, A. E. Zhukov, P. S. Kop'ev, N. N. Ledentsov, M. V. Maksimov, and V. M. Ustinov, "Effect of deposition conditions on the formation of (In,Ga)As quantum clusters in a GaAs matrix," *Semiconductors*, vol. 28, no. 8, pp. 809–811, Aug. 1994.

[34] Zh. I. Alferov, N. Y. Gordeev, S. V. Zaitsev, P. S. Kop'ev, I. V. Kochnev, V. V. Khomin, I. L. Krestnikov, N. N. Ledentsov, A. V. Lunev, M. V. Maksimov, S. S. Ruvimov, A. V. Sakharov, A. F. Tsatsul'nikov, Y. M. Shernyakov, and D. Bimberg, "A low-threshold injection heterojunction laser based on quantum dots, produced by gas-phase epitaxy from organometallic compounds," *Sov. Phys. Semicond.*, vol. 30, no. 2, pp. 197–200, 1996.

[35] L. V. Asryan and R. A. Suris, "Inhomogeneous line broadening and the threshold current density of a semiconductor quantum dot laser," *Semicond. Sci. Technol.*, vol. 11, no. 4, pp. 554–567, Apr. 1996.

[36] V. M. Ustinov, A. Yu. Egorov, A. R. Kovsh, A. E. Zhukov, M. V. Maksimov, A. F. Tsatsul'nikov, N. Y. Gordeev, S. V. Zaitsev, Y. M. Shernyakov, N. A. Bert, P. S. Kop'ev, Zh. I. Alferov, N. N. Ledentsov, J. Böhrer, D. Bimberg, A. O. Kosogov, P. Werner, and U. Gösele, "Low-threshold injection lasers based on vertically coupled quantum dots, " *J. Cryst. Growth,* vol. 175-176, no. 2, pp. 689-685, May. 1997.

[37] N. N. Ledentsov, V. A. Shchukin, M. Grundmann, N. Kirstaedter, J. Bo¨hrer, O. Schmidt, D. Bimberg, V. M. Ustinov, A. Yu. Egorov, A. E. Zhukov, P. S. Kop'ev, S. V. Zaitsev, N. Yu. Gordeev, Zh. I. Alferov, A. I. Borovkov, A. O. Kosogov, S. S. Ruvimov, P. Werner, U. Gosele, and J. Heydenreich, "Direct formation of vertically coupled quantum dots in Stranski-Krastanow growth," *Phys. Rev. B*, vol. 54, no. 12, pp. 8743–8750, Sept. 1996.

[38] A. E. Zhukov, V. M. Ustinov, A. Yu. Egorov, A. R. Kovsh, A. F. Tsatsul'nikov, M. V. Maximov, N. N. Ledentsov, S. V. Zaitsev, N. Y. Gordeev, V. I. Kopchatov, Y. M. Shernyakov, P. S. Kop'ev, D. Bimberg, Zh. I. Alferov, "Injection lasers based on InGaAs quantum dots in an AlGaAs matrix," *J. Electron. Mater.,* vol. 27, no. 3, pp. 106-109, Mar. 1998.

[39] G. Park, O. B. Shchekin, D. L. Huffaker, and D. G. Deppe, "Low threshold oxide-confined 1.3-μm quantum-dot laser," *IEEE Photon. Technol. Lett.*, vol. 33, no. 3, pp. 230–232, Mar. 2000.

[40] J. A. Lott, N. N. Ledentsov, V. M. Ustinov, N. A. Maleev, A. E. Zhukov, A. R. Kovsh, M. V. Maximov, B. V. Volovik, Zh. I. Alferov, and D. Bimberg, "InAs–InGaAs quantum dot VCSELs on GaAs substrates emitting at 1.3 μm," *Electron. Lett.*, vol. 36, no. 16, pp. 1384–1385, Aug. 2000.

[41] E. Homeyer, R. Piron, F. Grillot, O. Dehaese, K. Tavernier, E. Mace, J. Even, A. Le Corre, and S. Loualiche, "Demonstration of a low threshold current in 1.54 μm InAs/InP(311)B quantum dot laser with reduced quantum dot stacks," *Jpn. J. Appl. Phys.*, vol. 46, no. 10A, pp. 6903–6905, Oct. 2007.

[42] L. V. Asryan and R. A. Suris, "Temperature dependence of the threshold current density of a quantum dot laser," *IEEE. J. Quantum Electron.*, vol. 34, no. 5, pp. 841–850, May. 1998.

[43] L. V. Asryan, R. A. Suris, and S. Luryi, "Internal efficiency of semiconductor lasers with a quantum-confined active region," *IEEE. J. Quantum Electron.*, vol. 39, no. 3, pp. 404–418, Mar. 2003.

[44] O. B. Shchekin, J. Ahn, D. G. Deppe, "High temperature performance of self-organised quantum dot laser with stacked p-doped active region," *Electron. Lett.,* vol. 38, no.14, pp. 712-713, Jul. 2002.

[45] S. Fathpour, Z. Mi, P. Bhattacharya, A. R. Kovsh, S. S. Mikhrin, I. L. Krestnikov, A. V. Kozhukhov, N. N. Ledentsov, "The role of Auger recombination in the temperature-dependent output characteristics ($T_0 = \infty$) of p-doped 1.3 μm quantum dot lasers," *Appl. Phys. Lett.,* vol. 85, no. 22, pp. 5164-5166, Nov. 2004.

[46] L. V. Asryan and S. Luryi, "Tunneling-injection quantum-dot laser: Ultrahigh temperature stability," *IEEE J. Quantum Electron*., vol. 37, no. 7, pp. 905–910, Jul. 2001.

[47] L. V. Asryan and S. Luryi, "Temperature-insensitive semiconductor quantum dot laser," *Solid-State Electron*., vol. 47, no. 2, pp. 205–212, Feb. 2003.

[48] L. V. Asryan and S. Luryi, "Semiconductor laser with reduced temperature sensitivity," *U.S. Patent 6 870 178 B2*, Mar. 22, 2005.

[49] P. Bhattacharya, "Quantum well and quantum dot lasers: From strained-layer and self-organized epitaxy to high-performance devices," *Optical and Quantum Electron*., vol. 32, no. 3, pp. 211–225, Mar. 2000.

[50] X. Zhang, Y. Yuan, A. Gutierrez-Aitken, and P. Bhattacharya, "GaAs-based multiple quantum well tunneling injection lasers," *Appl*. *Phys*. *Lett*., vol. 69, no. 16, pp. 3482–3484, May 2002.

[51] K. Kamath, D. Klotzkin, and P. Bhattacharya, "Small-signal modulation characteristics of self-organized quantum dot separate confinement heterostructure and tunneling injection lasers," *Proc*. *IEEE LEOS 10th Annual Meeting*, vol. 2, pp. 498–499, Nov. 1997.

[52] P. Bhattacharya, X. K. Zhang, Y. S. Yuan, K. Kamath, D. Klotzkin, C. Caneau, R. Bhat, "High-speed tunnel injection quantum well and quantum dot lasers," *Proc. SPIE*, vol. 3283, pp. 702–709, Jan. 1998.

[53] P. Bhattacharya and S. Ghosh, "Tunnel injection $In_{0.4}Ga_{0.6}As$/GaAs quantum dot lasers with 15 GHz modulation bandwidth and at room temperature," *Appl*. *Phys*. *Lett*., vol. 80, no. 19, pp. 3482–3484, May 2002.

[54] Y. Qiu, D. Uhl, R. Chacon, and R. Q. Yang, "Lasing characteristics of InAs quantum-dot lasers on (001) InP substrate," *Appl*. *Phys*. *Lett*., vol. 83, no. 9, pp. 1704–1706, Apr. 2003.

[55] Y. Arakawa, "Fabrication of quantum wires and dots by MOCVD selective growth," *Solid-State Electron*., vol. 37, no. 4–6, pp. 523–528, Apr–Jun. 1994.

[56] T. Chung, G. Walter, and N. Holonyak, "Coupled strained-layer InGaAs quantum-well improvement of an InAs quantum dot AlGaAs-GaAs-InGaAs-InAs heterostructure laser," *Appl*. *Phys*. *Lett*., vol. 79, no. 27, pp. 4500–4502, Dec. 2001.

[57] G. Walter, T. Chung, and N. Holonyak, "High-gain coupled InGaAs quantum well InAs quantum dot AlGaAs-GaAs-InGaAs heterostructure diode laser operation," *Appl*. *Phys*. *Lett*., vol. 80, no. 7, pp. 1126–1128, Feb. 2002.

[58] G. Walter, T. Chung, and N. Holonyak, "Coupled-stripe quantum-well-assisted AlGaAs-GaAs-InGaAs-InAs quantum-dot laser," *Appl*. *Phys*. *Lett*., vol. 80, no. 17, pp. 3045–3047, Apr. 2002.

[59] P. K. Kondratko, S.-L. Chuang, G. Walter, T. Chung, and N. Holonyak, "Observations of near-zero linewidth enhancement factor in a quantum-well coupled quantum-dot laser," *Appl*. *Phys*. *Lett*., vol. 83, no. 23, pp. 4818–4820, Dec. 2003.

Chapter 2

Characteristic Temperature of a Tunneling-Injection Quantum Dot Laser

Summary

A laser structure is studied, which exploits tunneling-injection of electrons and holes into quantum dots (QDs) from two separate quantum wells (QWs). An extended theoretical model is developed allowing for out-tunneling leakage of carriers from QDs into the opposite-to-injection-side QWs (electrons into the p-side QW and holes into the n-side QW). Due to out-tunneling leakage, parasitic recombination of electron-hole pairs occurs outside QDs – in the QWs and optical confinement layer. The threshold current density j_{th} and the characteristic temperature T_0 are shown to be mainly controlled by the recombination in the QWs. Even in the presence of out-tunneling from QDs and recombination outside QDs, the tunneling-injection laser shows the potential for significant improvement of temperature stability of j_{th} — the characteristic temperature T_0 remains very high (above 300 K at room temperature) and not significantly affected by the QD size fluctuations.

2.1. Introduction

High temperature stability of threshold current has been predicted for semiconductor quantum dot (QD) lasers [1]. An ideal situation would be temperature-insensitive threshold current density j_{th}, i.e., the characteristic temperature (a widely-accepted figure of merit of any diode laser from the viewpoint of temperature-stability of j_{th} [2]) defined as

$$T_0 = \left(\frac{\partial \ln j_{th}}{\partial T} \right)^{-1} \tag{2.1}$$

would be infinitely high. In actuality, however, not all injected carriers appear in QDs — a fraction of them recombines outside QDs. The recombination current outside QDs depends strongly on T and causes such dependence of j_{th}; hence, T_0 becomes finite (Fig. 2.1) [3].

To suppress the recombination outside QDs, tunneling-injection of both electrons and holes into QDs was proposed in [4, 5]. (In [6]-[9], to minimize hot-carrier effects, tunneling-injection of only electrons into respectively the quantum well (QW) and QDs was proposed. In [10], to avoid a possible phonon bottleneck problem, resonant tunneling was proposed from the bulk optical confinement layer (OCL) into the QD-excited-state separated from the QD-ground-state by the energy of the longitudinal optical phonon.) A complete suppression of the recombination outside QDs will result in T_0 above 1000 K [4, 5], which corresponds to a virtually temperature-insensitive j_{th}.

Here we study the effect of out-tunneling leakage of carriers from QDs (shown by inclined arrows ⑤ in Fig. 2.2) and hence recombination outside QDs (vertical arrows ⑥ and ⑧ in Fig. 2.2) on the T-dependence of j_{th} [A1, A2][*)]. We show that, even in the presence of such leakage, T_0 remains very high. We analyze T_0 versus the temperature and parameters of a GaInAsP/InP heterostructure lasing near 1.55 μm.

2.2. Laser structure

The energy band diagram of the structure is shown in Fig. 2.2. The electrons (holes) are injected from the n- (p-) cladding layer into the OCL, captured in the corresponding QW, and finally tunnel into QDs (Fig. 2.2). The basic concept is that the QWs are not connected by a current path that bypasses QDs. To realize this concept, (i) the barriers separating QDs from the QWs should be high enough to suppress the thermal escape (leakage) of carriers from the QWs, and (ii) the material separating QDs from each other in the QD layer should have a wide enough bandgap to suppress all tunneling other than via the QD levels (this material may be the same as that of the barrier layers).

The probability of direct tunneling is higher than that of indirect tunneling. Hence, due to QD size fluctuations, which are always present in QD ensembles [11, 12], the tunneling will be most efficient within a certain range of QD sizes. To maximize the tunneling-injection rate and hence the number of active (pumped) QDs, the material and thickness of the injecting QW should be chosen so that the lowest subband edge in the QW matches the quantized energy level for the corresponding type of carrier in the average-sized (most represented) QD. Such an

---

[*)] "A" in the reference number indicates the publications of the author of this dissertation.

optimum situation is shown in Fig. 2.2 [the QWs may (as shown in the figure) or may not be of the same material as QDs].

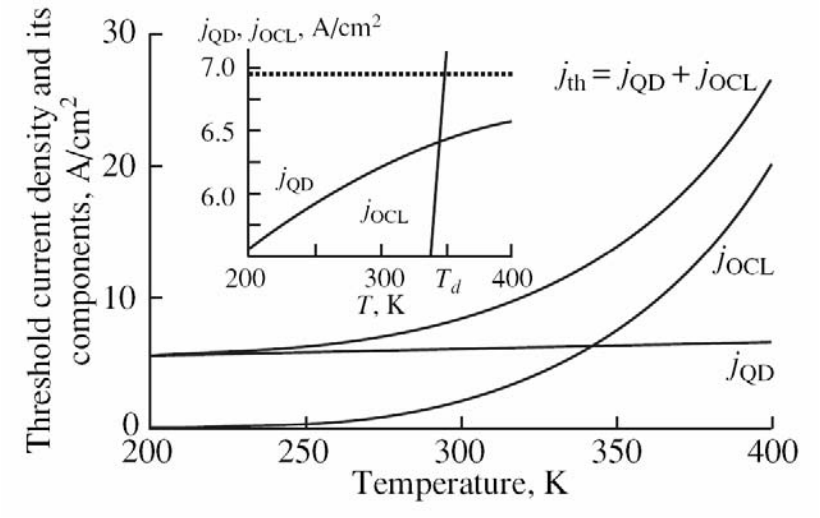

(a)

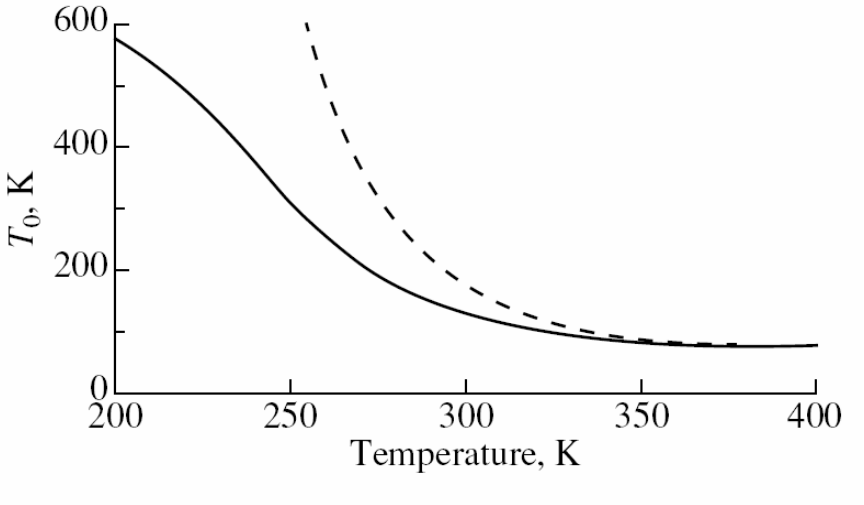

(b)

Fig. 2.1. (a) Threshold current density and its components, and (b) characteristic temperature versus temperature. Inset in (a) shows j_{QD} and j_{OCL} on enlarged (along the vertical axis) scale at $T = T_d$ = 344 K, $j_{OCL} = j_{QD}$. The dotted line of (a) and dashed line of (b) represents the current density j_{QD} and $T_{0,neutral}$ calculated on the assumption of neutrality in QDs, respectively. (Figs. 16 and 17(c) of ref. [3], reprinted with kind permission of Springer Science and Business Media.)

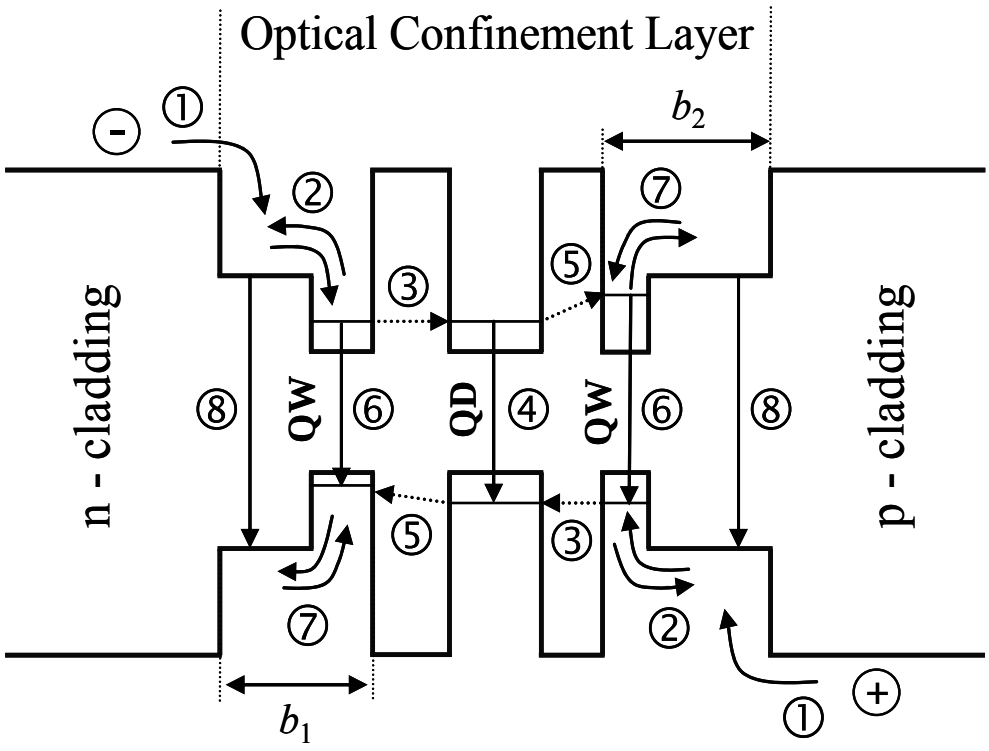

Fig. 2.2. Energy band diagram of a tunneling-injection QD laser and the main processes: ① injection from the cladding layers to the OCL, ② majority carrier capture from the OCL to the QW and thermal escape from the QW to the OCL, ③ tunneling-injection from the QW into a QD, ④ spontaneous and stimulated recombination in a QD, ⑤ out-tunneling from a QD into the "foreign" QW, ⑥ spontaneous recombination in the QWs, ⑦ minority carrier thermal escape from the QW to the OCL and capture from the OCL to the QW, and ⑧ spontaneous recombination in the OCL. (Reprinted from Fig. 1 of ref. [A1], Copyright (2008), with permission from Elsevier.)

Under certain conditions, which are described in [4, 5], there will be no second step of tunneling of electrons (holes) from QDs to the p- (n-) side QW (we refer to this second step of tunneling as out-tunneling); there will be no electrons (holes) as minority carriers in the p- (n-) side OCL and QW and hence the electron-hole recombination will be completely suppressed there.

Here, we allow for out-tunneling leakage of electrons from QDs to the right-hand-side QW and holes from QDs to the left-hand-side QW [processes ⑤ in Fig. 2.2]. Hence, electrons as minority carriers will recombine with holes as majority carriers in the right-hand-side QW and OCL [processes ⑥ and ⑧ in Fig. 2.2]. Similarly, holes as minority carriers will recombine with electrons as majority carriers in the left-hand-side QW and OCL.

2.3. Rate equations

The following set of rate equations is used:

for free electrons and holes in the left-hand side of the OCL,

$$b_1 \frac{\partial n_L}{\partial t} = \frac{j}{e} + \frac{n_{\mathrm{QW}}^L}{\tau_{\mathrm{n,esc}}^L} - v_{\mathrm{n,capt}}^L n_L - b_1 B n_L p_L , \tag{2.2}$$

$$b_1 \frac{\partial p_L}{\partial t} = \frac{p_{\mathrm{QW}}^L}{\tau_{\mathrm{p,esc}}^L} - v_{\mathrm{p,capt}}^L p_L - b_1 B n_L p_L , \tag{2.3}$$

for free holes and electrons in the right-hand side of the OCL,

$$b_2 \frac{\partial p_R}{\partial t} = \frac{j}{e} + \frac{p_{\mathrm{QW}}^R}{\tau_{\mathrm{p,esc}}^R} - v_{\mathrm{p,capt}}^R p_R - b_2 B n_R p_R , \tag{2.4}$$

$$b_2 \frac{\partial n_R}{\partial t} = \frac{n_{\mathrm{QW}}^R}{\tau_{\mathrm{n,esc}}^R} - v_{\mathrm{n,capt}}^R n_R - b_2 B n_R p_R , \tag{2.5}$$

for electrons and holes in the electron-injecting (left-hand-side) QW,

$$\frac{\partial n_{\mathrm{QW}}^L}{\partial t} = v_{\mathrm{n,capt}}^L n_L - \frac{n_{\mathrm{QW}}^L}{\tau_{\mathrm{n,esc}}^L} - w_{\mathrm{n,\,tunn}}^L N_S (1 - f_{\mathrm{n}}) n_{\mathrm{QW}}^L + w_{\mathrm{n,tunn}}^L n_1^{L,\mathrm{QW}} N_S f_{\mathrm{n}} - B_{\mathrm{2D}} n_{\mathrm{QW}}^L p_{\mathrm{QW}}^L , \tag{2.6}$$

$$\frac{\partial p_{\mathrm{QW}}^{L}}{\partial t} = v_{\mathrm{p,capt}}^{L} p_{L} - \frac{p_{\mathrm{QW}}^{L}}{\tau_{\mathrm{p,esc}}^{L}} - w_{\mathrm{p,tunn}}^{L} N_{S}(1-f_{\mathrm{p}}) p_{\mathrm{QW}}^{L} + w_{\mathrm{p,tunn}}^{L} p_{1}^{L,\mathrm{QW}} N_{S} f_{\mathrm{p}} - B_{\mathrm{2D}} n_{\mathrm{QW}}^{L} p_{\mathrm{QW}}^{L}, \tag{2.7}$$

for holes and electrons in the hole-injecting (right-hand-side) QW,

$$\frac{\partial p_{\mathrm{QW}}^{R}}{\partial t} = v_{\mathrm{p,capt}}^{R} p_{R} - \frac{p_{\mathrm{QW}}^{R}}{\tau_{\mathrm{p,esc}}^{R}} - w_{\mathrm{p,tunn}}^{R} N_{S}(1-f_{\mathrm{p}}) p_{\mathrm{QW}}^{R} + w_{\mathrm{p,tunn}}^{R} p_{1}^{R,\mathrm{QW}} N_{S} f_{\mathrm{p}} - B_{\mathrm{2D}} n_{\mathrm{QW}}^{R} p_{\mathrm{QW}}^{R}, \tag{2.8}$$

$$\frac{\partial n_{\mathrm{QW}}^{R}}{\partial t} = v_{\mathrm{n,capt}}^{R} n_{R} - \frac{n_{\mathrm{QW}}^{R}}{\tau_{\mathrm{n,esc}}^{R}} - w_{\mathrm{n,tunn}}^{R} N_{S}(1-f_{\mathrm{n}}) n_{\mathrm{QW}}^{R} + w_{\mathrm{n,tunn}}^{R} n_{1}^{R,\mathrm{QW}} N_{S} f_{\mathrm{n}} - B_{\mathrm{2D}} n_{\mathrm{QW}}^{R} p_{\mathrm{QW}}^{R}, \tag{2.9}$$

for electrons and holes confined in QDs,

$$\begin{aligned} N_{S}\frac{\partial f_{\mathrm{n}}}{\partial t} &= w_{\mathrm{n,tunn}}^{L} N_{S}(1-f_{\mathrm{n}}) n_{\mathrm{QW}}^{L} - w_{\mathrm{n,tunn}}^{L} n_{1}^{L,\mathrm{QW}} N_{S} f_{\mathrm{n}} + w_{\mathrm{n,tunn}}^{R} N_{S}(1-f_{\mathrm{n}}) n_{\mathrm{QW}}^{R} - w_{\mathrm{n,tunn}}^{R} n_{1}^{R,\mathrm{QW}} N_{S} f_{\mathrm{n}} \\ &\quad - N_{S}\frac{f_{\mathrm{n}} f_{\mathrm{p}}}{\tau_{\mathrm{QD}}} - \frac{c}{\sqrt{\in_{\mathrm{g}}}}\frac{g^{\max}}{S}(f_{\mathrm{n}} + f_{\mathrm{p}} - 1)N, \end{aligned} \tag{2.10}$$

$$\begin{aligned} N_{S}\frac{\partial f_{\mathrm{p}}}{\partial t} &= w_{\mathrm{p,tunn}}^{R} N_{S}(1-f_{\mathrm{p}}) p_{\mathrm{QW}}^{R} - w_{\mathrm{p,tunn}}^{R} p_{1}^{R,\mathrm{QW}} N_{S} f_{\mathrm{p}} + w_{\mathrm{p,tunn}}^{L} N_{S}(1-f_{\mathrm{p}}) p_{\mathrm{QW}}^{L} - w_{\mathrm{p,tunn}}^{L} p_{1}^{L,\mathrm{QW}} N_{S} f_{\mathrm{p}} \\ &\quad - N_{S}\frac{f_{\mathrm{n}} f_{\mathrm{p}}}{\tau_{\mathrm{QD}}} - \frac{c}{\sqrt{\in_{g}}}\frac{g^{\max}}{S}(f_{\mathrm{n}} + f_{\mathrm{p}} - 1)N, \end{aligned} \tag{2.11}$$

and for photons,

$$\frac{\partial N}{\partial t} = \frac{c}{\sqrt{\in_{g}}} g^{\max}(f_{\mathrm{n}} + f_{\mathrm{p}} - 1)N - \frac{c}{\sqrt{\in_{g}}}\beta N. \tag{2.12}$$

The fluxes and physical quantities entering into (2.2)–(2.12) are presented in Tables 2.1 and 2.2, respectively.

Table 2.1. Fluxes of different processes in eqs. (2.2)–(2.12)

$\frac{j}{e}$	Injection from the cladding layers to the OCL
$\frac{n_{\mathrm{QW}}^{L,R}}{\tau_{\mathrm{n,esc}}^{L,R}}$, $\frac{p_{\mathrm{QW}}^{L,R}}{\tau_{\mathrm{p,esc}}^{L,R}}$	Thermal escape of electrons and holes from the QWs to the OCL
$v_{\mathrm{n,capt}}^{L,R} n_{L,R}$, $v_{\mathrm{p,capt}}^{L,R} n_{L,R}$	Capture of electrons and holes from the OCL to the QWs
$b_1 B n_L p_L$, $b_2 B n_R p_R$	Spontaneous radiative recombination in the left- and right-hand sides of the OCL
$w_{\mathrm{n,\,tunn}}^{L} N_S (1-f_{\mathrm{n}}) n_{\mathrm{QW}}^{L}$, $w_{\mathrm{p,\,tunn}}^{R} N_S (1-f_{\mathrm{p}}) p_{\mathrm{QW}}^{R}$	Tunneling-injection of electrons and holes into the QD ensemble (processes ③ in Fig. 2.2)
$w_{\mathrm{n,tunn}}^{L} n_1^{L,\mathrm{QW}} N_S f_{\mathrm{n}}$, $w_{\mathrm{p,tunn}}^{R} p_1^{R,\mathrm{QW}} N_S f_{\mathrm{p}}$	Electron and hole backward tunneling from the QD ensemble to the injector-QWs (processes reverse to ③ in Fig. 2.2)
$w_{\mathrm{p,tunn}}^{L} p_1^{L,\mathrm{QW}} N_S f_{\mathrm{p}}$, $w_{\mathrm{n,tunn}}^{R} n_1^{R,\mathrm{QW}} N_S f_{\mathrm{n}}$	Hole and electron out-tunneling from the QD ensemble to the foreign (electron- and hole-injecting, respectively) QWs (processes ⑤ in Fig. 2.2)
$w_{\mathrm{p,tunn}}^{L} N_S (1-f_{\mathrm{p}}) p_{\mathrm{QW}}^{L}$, $w_{\mathrm{n,tunn}}^{R} N_S (1-f_{\mathrm{p}}) n_{\mathrm{QW}}^{R}$	Hole and electron backward tunneling from the foreign QWs into the QD ensemble (processes reverse to ⑤ in Fig. 2.2)
$B_{\mathrm{2D}} n_{\mathrm{QW}}^{L} p_{\mathrm{QW}}^{L}$, $B_{\mathrm{2D}} n_{\mathrm{QW}}^{R} p_{\mathrm{QW}}^{R}$	Spontaneous radiative recombination in the left- and right-hand-side QWs
$N_S \frac{f_{\mathrm{n}} f_{\mathrm{p}}}{\tau_{\mathrm{QD}}}$	Spontaneous radiative recombination in QDs
$\frac{c}{\sqrt{\epsilon_g}} \frac{g^{\max}}{S} (f_{\mathrm{n}} + f_{\mathrm{p}} - 1) N$	Stimulated radiative recombination flux

Table 2.2. Physical quantities in eqs. (2.2)–(2.12)

$f_{\mathrm{n,p}}$	Electron- and hole-level occupancies in QDs
τ_{QD}	Spontaneous radiative lifetime in a QD
$n_{\mathrm{QW}}^{L,R}$, $p_{\mathrm{QW}}^{L,R}$	2-D electron and hole densities in the QWs
$n_{L,R}$, $p_{L,R}$	Free-electron and -hole densities in the left- and right-hand side of the OCL
$n_1^{L,R,\mathrm{QW}}$, $p_1^{L,R,\mathrm{QW}}$	Quantities (measured in units of cm^{-2}) in the electron and hole tunneling fluxes from the QD ensemble to the QWs
$w_{\mathrm{n,p,\,tunn}}^{L,R}$	Tunneling coefficients (measured in units of cm^2/s) for electron and hole tunneling between the QD ensemble and the QWs
b_1 , b_2	Thicknesses of the left- and right-hand side of the OCL [separation between the *n*- (*p*-) cladding layer and the left- (right-) hand-side barrier]
N_{S}	Surface density of QDs
$S=WL$	Cross-section of the junction
W	Lateral size of the device
L	Cavity length
$g^{\max}$	Maximum value of the modal gain [12, 13]
N	Number of photons in the lasing mode
c	Light velocity in vacuum
B, $B_{2\mathrm{D}}$	Spontaneous radiative recombination constants for the bulk (OCL) and 2-D region (QWs)
$\sqrt{\epsilon_g}$	Group index of the dispersive OCL material
R	Facet reflectivity
j	Injection current density
$\beta = (1/L)\ln(1/R)$	Mirror loss coefficient
$v_{\mathrm{n,\,p,capt}}^{L,R}$	Capture velocity of electrons and holes from the OCL to the QWs
$\tau_{\mathrm{n,p,esc}}^{L,R}$	Thermal escape times of electrons and holes from the QWs to the OCL

2.4. Threshold current density

We consider a continuous-wave operation of the laser and correspondingly use the steady-state rate equations

$$\frac{\partial}{\partial t}\left(b_1 n_L,\, b_1 p_L,\, b_2 n_R,\, b_2 p_R,\, n_{\mathrm{QW}}^{L},\, p_{\mathrm{QW}}^{L},\, n_{\mathrm{QW}}^{R},\, p_{\mathrm{QW}}^{R},\, N_S f_{\mathrm{n}},\, N_S f_{\mathrm{p}},\, N\right) = 0\,. \qquad (2.13)$$

Below the lasing threshold, the stimulated recombination term vanishes in (2.10)-(2.12) (since $N = 0$).

Above the lasing threshold, the number of stimulated photons is nonvanishing ($N \neq 0$). To satisfy (2.12) at the steady-state and at nonvanishing N, the following lasing condition should hold

$$g^{\max}\left(f_n + f_p - 1\right) = \beta \qquad (2.14)$$

which is the condition of equality of the modal gain to the mirror loss at and above the lasing threshold (the internal optical loss is not considered here).

The threshold current density j_{th} is defined as the lowest injection current density at which (2.14) satisfies. At $j = j_{\mathrm{th}}$, the number of photons is still zero; for j immediately above j_{th}, N starts to build up. From the steady-state rate equations at $N = 0$, the threshold current density can be presented as the sum of the spontaneous recombination current densities in QDs, QWs, and OCL,

$$j_{\mathrm{th}} = eN_S \frac{f_{\mathrm{n}} f_{\mathrm{p}}}{\tau_{\mathrm{QD}}} + eB_{\mathrm{2D}} n_{\mathrm{QW}}^{L} p_{\mathrm{QW}}^{L} + eB_{\mathrm{2D}} n_{\mathrm{QW}}^{R} p_{\mathrm{QW}}^{R} + eb_1 B n_L p_L + eb_2 B n_R p_R \qquad (2.15)$$

where the electron and hole level occupancies in QDs, $f_{\mathrm{n,p}}$, and densities in the QWs and OCL, $n_{\mathrm{QW}}^{L,R}$, $p_{\mathrm{QW}}^{L,R}$, and $n_{L,R}$, $p_{L,R}$, should be found from the solution of the rate equations at the lasing threshold [i.e., when $N = 0$ and simultaneously eq. (2.14) satisfies].

As seen from (2.2)-(2.9), the rate equations for the carrier densities in the right-hand-side QW and OCL are similar to those in the left-hand side. For this reason, we will analyze these equations for the left-hand side only.

Using the rate equations (2.3) and (2.7) at the steady-state, the recombination flux outside QDs can be presented as follows:

$$B_{2D} n_{QW}^{L} p_{QW}^{L} + b_1 B n_L p_L = w_{p,tunn}^{L} p_1^{L,QW} N_S f_p - w_{p,tunn}^{L} N_S (1 - f_p) p_{QW}^{L} \tag{2.16}$$

and similarly for the right-hand side of the structure. In (2.16), $w_{p,tunn}^{L} p_1^{L,QW} N_S f_p$ is the hole out-tunneling flux from the QD ensemble to the left-hand-side QW, and $w_{p,tunn}^{L} N_S (1 - f_p) p_{QW}^{L}$ is the flux of backward tunneling of holes from the left-hand-side QW to the QD ensemble.

Eq. (2.16) simply states that the net out-tunneling flux of minority carriers from QDs goes into the recombination in the corresponding side of the structure. With (2.16) and a similar equation for the right-hand side of the structure, j_{th} can be written as follows:

$$\begin{aligned} j_{th} = eN_S \frac{f_n f_p}{\tau_{QD}} &+ \left[e w_{p,tunn}^{L} p_1^{L,QW} N_S f_p - e w_{p,tunn}^{L} N_S (1 - f_p) p_{QW}^{L} \right] \\ &+ \left[e w_{n,tunn}^{R} n_1^{R,QW} N_S f_n - e w_{n,tunn}^{R} N_S (1 - f_n) n_{QW}^{R} \right]. \end{aligned} \tag{2.17}$$

If the charge neutrality holds in QDs ($f_n = f_p$) [13, 14], then using (2.14) we immediately obtain that the level occupancies in QDs are temperature-insensitive at and above the lasing threshold,

$$f_n = f_p = \frac{1}{2}\left(1 + \frac{\beta}{g^{max}}\right) = \text{const}(T). \tag{2.18}$$

Consequently, the current density associated with recombination in QDs [the first term in the right-hand side of (2.15) and (2.17)] will be temperature-insensitive. If in this case out-tunneling of carriers from QDs is completely blocked, then $j_{th} = eN_S\left(f_n f_p / \tau_{QD}\right) = \text{const}(T)$ and $T_0 = \infty$.

In the presence of out-tunneling, assuming again charge neutrality in QDs, the temperature dependence of j_{th} will be due to such dependence of the recombination currents outside QDs. The characteristic temperature can be presented as

$$\frac{1}{T_0} = \frac{j_{QW}}{j_{th}} \frac{1}{T_0^{QW}} + \frac{j_{OCL}}{j_{th}} \frac{1}{T_0^{OCL}} \tag{2.19}$$

where j_{QW} is the sum of the second and third terms in the right-hand side of (2.15), j_{OCL} is the sum of the last two terms, and T_0^{QW} and T_0^{OCL} are defined similarly to T_0 but for j_{QW} and j_{OCL}.

2.5. Results and discussion

Continuous wave room-temperature operation of a GaInAsP/InP heterostructure lasing near 1.55 μm is considered here. To calculate j_{th} and T_0, we solved the steady-state rate equations for free carriers in the OCL, carriers in the QWs, and carriers confined in QDs.

Fig. 2.3 shows the temperature dependence of the threshold current density and its components. As seen from the figure, j_{th} is practically controlled by the recombination in the QWs — the contribution of the recombination in QDs and the OCL is negligible. The recombination current density j_{QW} is directly proportional to T, which stems from such dependence of both the electron and hole densities in each of the QWs — Fig. 2.4 shows the T-dependence of the 2-D electron and hole densities in the left-hand-side QW. Indeed, since the spontaneous radiative recombination constant in the 2-D region (QW) is inversely proportional to the temperature [15],

$$B_{2D} \propto \frac{1}{T} \tag{2.20}$$

then

$$B_{2D} n_{QW}^{L,R} p_{QW}^{L,R} \propto \frac{1}{T} T \cdot T = T\,. \tag{2.21}$$

The fact that $n_{QW}^{L,R}$ and $p_{QW}^{L,R}$ are proportional to T in its turn simply means that the temperature-dependences of $n_{QW}^{L,R}$ and $p_{QW}^{L,R}$ are mainly controlled by those of the 2-D effective densities of states in the conduction and valence bands in the QWs,

$$N_{c,v}^{2D} = \frac{m_{c,v}^{QW} k_B T}{\pi \hbar^2} \tag{2.22}$$

where $m_{c,v}^{QW}$ are the electron and hole effective masses in the QWs and k_B is the Boltzmann's constant.

Since $j_{QW} \propto T$, it is clear from the definition $T_0^{QW} = \left(\partial \ln j_{QW} / \partial T\right)^{-1}$ that T_0^{QW} is simply equal to the temperature (the dotted line in Fig. 2.5)

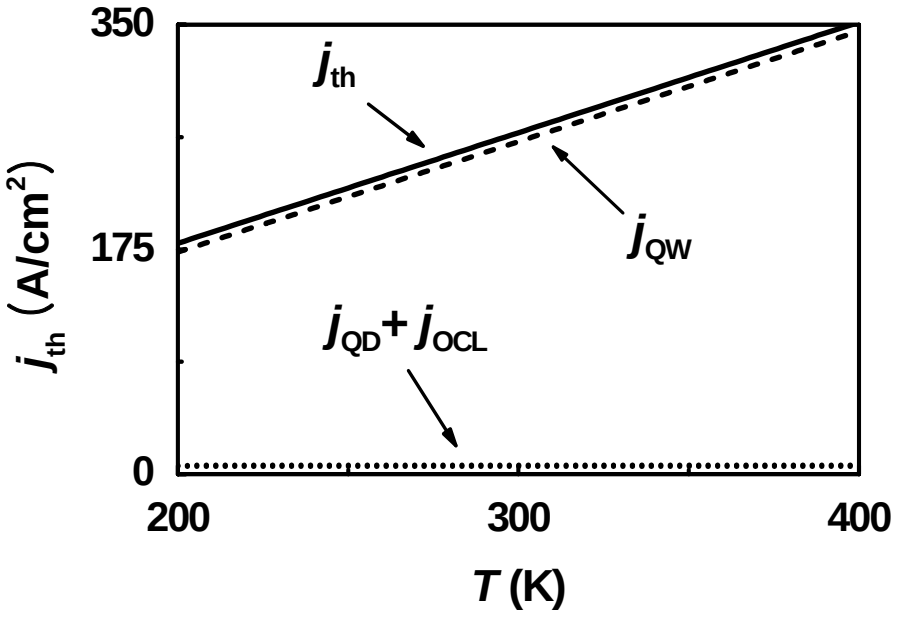

Fig. 2.3. Temperature-dependence of the threshold current density and its components. In Figs. 2.3-2.10, the structure parameters and the tunneling coefficients are as follows unless otherwise specified: $N_S = 6.1 \times 10^{10}$ cm^{-2}, $\delta = 0.05$, and $L = 1139$ μm; $w^L_{\mathrm{n,tunn}} = 16.2$ cm^2/s, $w^L_{\mathrm{p,tunn}} = 0.015$ cm^2/s, $w^R_{\mathrm{n,tunn}} = 0.016$ cm^2/s, and $w^R_{\mathrm{p,tunn}} = 1.48$ cm^2/s. (Reprinted from Fig. 2 of ref. [A1], Copyright (2008), with permission from Elsevier.)

$$T_0^{\mathrm{QW}} = T\,. \tag{2.23}$$

Not only the contribution of the recombination in the OCL to the threshold current is negligible ($j_{\mathrm{OCL}} / j_{\mathrm{th}} << 1$), but also the temperature dependence of j_{OCL} is weaker than that of j_{QW}, i.e., $T_0^{\mathrm{OCL}} > T_0^{\mathrm{QW}}$. Hence the second term in the right-hand side of (2.19) can be safely neglected to yield for the characteristic temperature (the solid line in Fig. 2.5)

$$T_0 \approx \frac{j_{\mathrm{th}}}{j_{\mathrm{QW}}} T_0^{\mathrm{QW}} = \frac{j_{\mathrm{th}}}{j_{\mathrm{QW}}} T = \left(1 + \frac{j_{\mathrm{QD}} + j_{\mathrm{OCL}}}{j_{\mathrm{QW}}}\right) T \;>\; T\,. \tag{2.24}$$

A slight excess of T_0 over T is due to the factor $j_{\mathrm{th}} / j_{\mathrm{QW}} = 1 + \left(j_{\mathrm{QD}} + j_{\mathrm{OCL}}\right) / j_{\mathrm{QW}}$, which is slightly larger than unity.

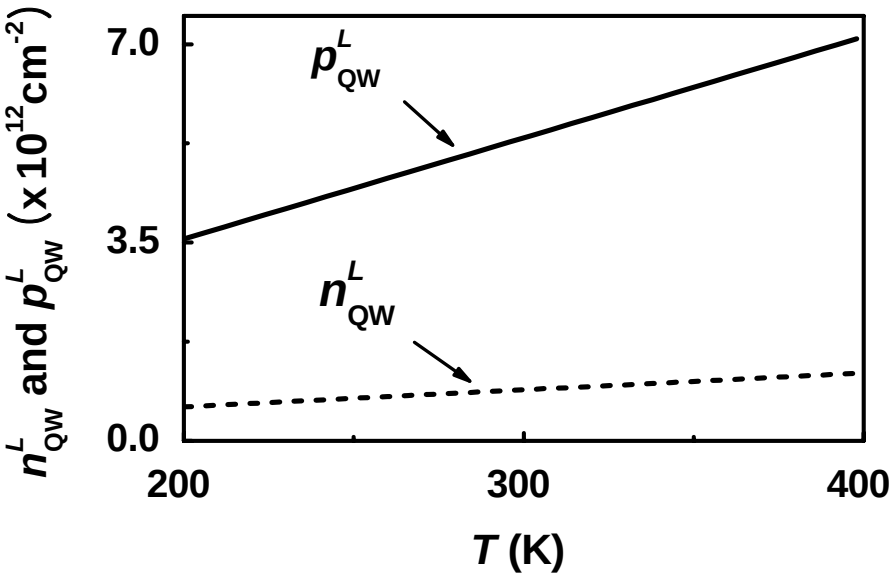

Fig. 2.4. Temperature-dependence of the 2-D electron and hole densities in the left-hand-side QW at the lasing threshold. (Reprinted from Fig. 3 of ref. [A1], Copyright (2008), with permission from Elsevier.)

Under the condition of charge neutrality in QDs [when $f_{\mathrm{n,p}}$ are given by (2.18)] and using the expression for the maximum value of the modal gain $g^{\max}$ [12, 13], the level occupancies in QDs are presented as follows in terms of the structure parameters (surface density of QDs N_S, root mean square of relative QD size fluctuations δ, and cavity length L) [12]:

$$f_{\mathrm{n,p}} = \frac{1}{2}\left(1+\frac{N_S^{\min}}{N_S}\right) = \frac{1}{2}\left(1+\frac{\delta}{\delta^{\max}}\right) = \frac{1}{2}\left(1+\frac{L^{\min}}{L}\right) \tag{2.25}$$

where $N_S^{\min}$, $\delta^{\max}$, and $L^{\min}$ are the critical tolerable values of N_S, δ, and L, respectively. When any of the structure parameters is equal to its critical value, QDs become fully occupied ($f_{\mathrm{n,p}} = 1$). For $N_S < N_S^{\min}$, or $\delta > \delta^{\max}$, or $L < L^{\min}$, the lasing condition (equality of the gain to the loss) can not be satisfied and no lasing can be attained in a QD structure [12].

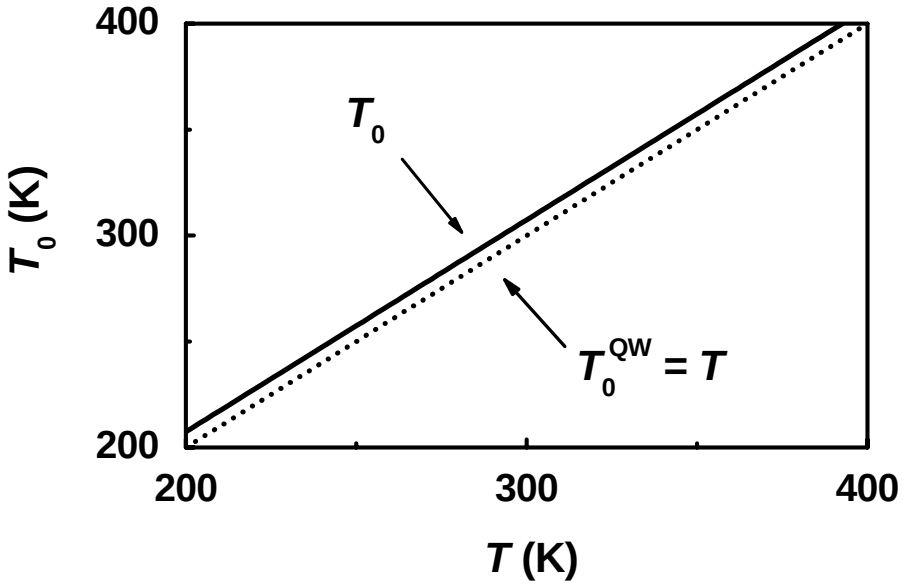

Fig. 2.5. Temperature-dependence of the characteristic temperature. The dotted line shows the characteristic temperature T_0^{QW} for the threshold current density component j_{QW} associated with the recombination in the QWs. Since $j_{\mathrm{QW}} \propto T$, $T_0^{\mathrm{QW}} = T$. (Reprinted from Fig. 4 of ref. [A1], Copyright (2008), with permission from Elsevier.)

Figs. 2.6–2.8 show j_{th} and T_0 versus the QD structure parameters normalized to their critical tolerable values. In contrast to a 'conventional' (not tunneling-injection) QD laser, in which $j_{\mathrm{th}} \to \infty$ as any of the structure parameters approaches its critical value [12], here j_{th} remains finite at $f_{\mathrm{n,p}} = 1$, i.e., when $N_S = N_S^{\min}$ [Fig. 2.6(a)], or $\delta = \delta^{\max}$ [Fig. 2.7(a)], or $L = L^{\min}$ [Fig. 2.8(a)]. As $f_{\mathrm{n,p}} \to 1$ in a conventional QD laser, both the free electron and hole densities in the OCL increase infinitely and hence so does the threshold current density component j_{OCL} associated with the recombination in the OCL. In a tunneling-injection structure with out-tunneling leakage of carriers from QDs, as already discussed above (Fig. 2.3) and also clear from Fig. 2.6(a), j_{th} is controlled by the recombination current density j_{QW} in the QWs (the dashed curve in the figure). When $f_{\mathrm{n,p}} \to 1$ (i.e., $N_S \to N_S^{\min}$, or $\delta \to \delta^{\max}$, or $L \to L^{\min}$),

j_{QW} remains finite. The point is that the 2-D majority and minority carrier densities in the QW behave oppositely when the parameter of the structure tends to its critical tolerable value. This is shown in Fig. 2.9 by the example of the dependence on N_S. While the majority carrier density (the dashed curve) increases infinitely as $N_S \to N_S^{\min}$, the minority carrier density (the solid curve) goes to zero so that their product defining j_{QW} [the dashed curve in Fig. 2.6(a)] remains finite.

Using eq. (2.17), we can easily derive the expression for the threshold current density at the critical value of the parameter. Indeed, when $f_{\mathrm{n,p}} \to 1$, not only $\left(1 - f_{\mathrm{n,p}}\right) \to 0$ but also the minority carrier densities in the left- and right-hand-side QWs, p_{QW}^{L} and n_{QW}^{R}, tend to zero. Hence the current densities of backward tunneling of minority carriers from the QWs to QDs, $ew_{\mathrm{p,tunn}}^{L} N_S (1 - f_{\mathrm{p}}) p_{\mathrm{QW}}^{L}$ and $ew_{\mathrm{n,tunn}}^{R} N_S (1 - f_{\mathrm{n}}) n_{\mathrm{QW}}^{R}$, vanish as $f_{\mathrm{n,p}} \to 1$; the maximum values (those at $f_{\mathrm{n,p}} = 1$) of the current densities of out-tunneling from QDs, $ew_{\mathrm{p,tunn}}^{L} p_1^{L,\mathrm{QW}} N_S$ and $ew_{\mathrm{n,tunn}}^{R} n_1^{R,\mathrm{QW}} N_S$, will only remain in (2.17) together with the spontaneous recombination current density in QDs. Thus we obtain

$$j_{\mathrm{th}}\Big|_{f_{\mathrm{n,p}} \to 1} = \frac{eN_S}{\tau_{QD}} + ew_{\mathrm{p,tunn}}^{L} p_1^{L,\mathrm{QW}} N_S + ew_{\mathrm{n,tunn}}^{R} n_1^{R,\mathrm{QW}} N_S \,. \tag{2.26}$$

In a particular case when $f_{\mathrm{n,p}} \to 1$ by virtue of $N_S \to N_S^{\min}$, $N_S^{\min}$ should enter into (2.26) instead of N_S.

Hence, as any of the structure parameters approaches its critical tolerable value and QDs become fully occupied, no portion of out-tunneling fluxes of minority carries returns back to QDs — these fluxes are entirely consumed via the recombination processes outside QDs (primarily in the QWs).

As a function of the QD size dispersion or the cavity length, j_{th} is at its maximum at $\delta = \delta^{\max}$ or $L = L^{\min}$ and decreases monotonically with decreasing δ or increasing L [Fig. 2.7(a) and Fig. 2.8(a), respectively].

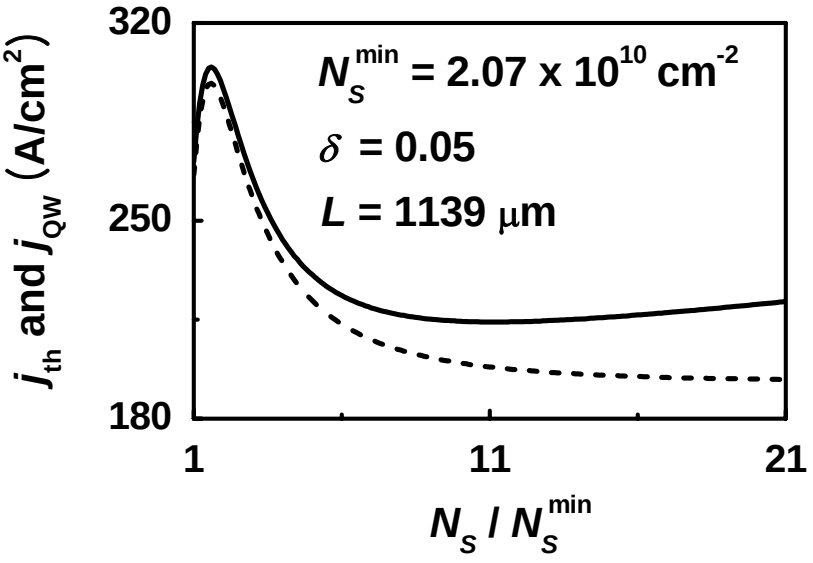

(a)

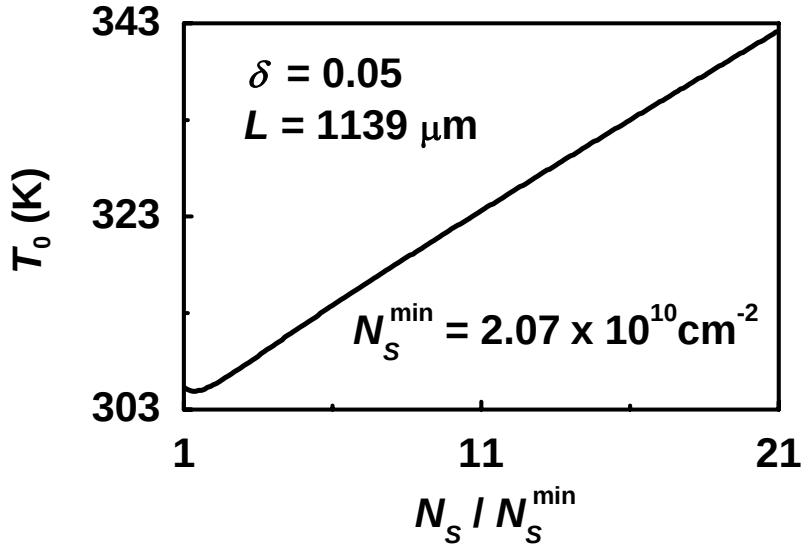

(b)

Fig. 2.6. (a) Threshold current density and (b) characteristic temperature versus normalized surface density of QDs. In Figs. 2.6-2.10, the temperature T = 300 K. The dashed curve in (a) shows the threshold current density component j_{QW} associated with the recombination in the QWs. (Reprinted from Fig. 5 of ref. [A1], Copyright (2008), with permission from Elsevier.)

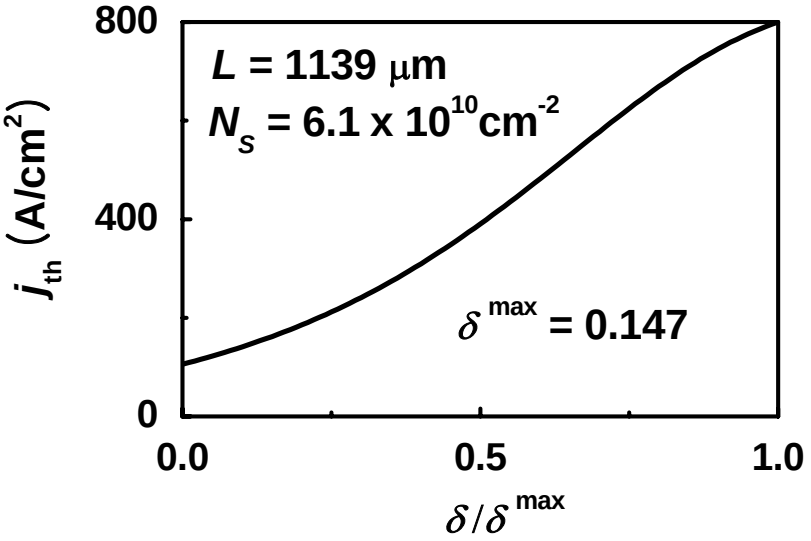

(a)

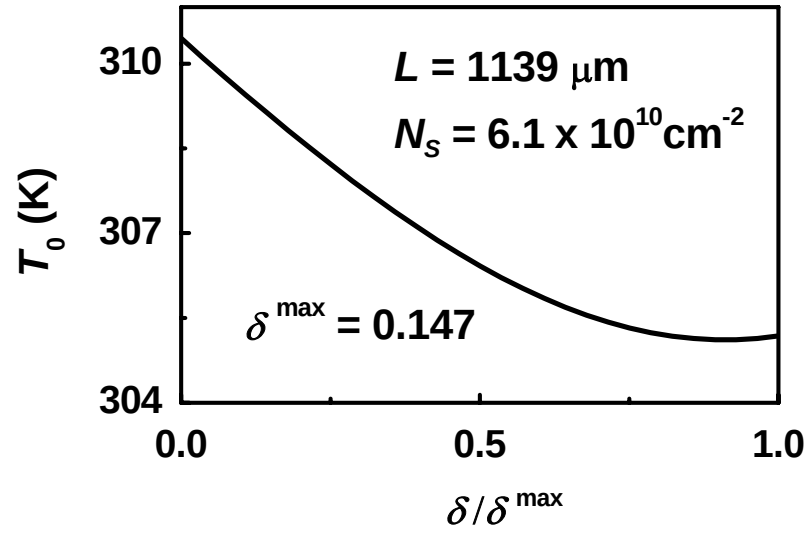

(b)

Fig. 2.7. (a) Threshold current density and (b) characteristic temperature versus normalized root mean square of relative QD size fluctuations. (Reprinted from Fig. 6 of ref. [A1], Copyright (2008), with permission from Elsevier.)

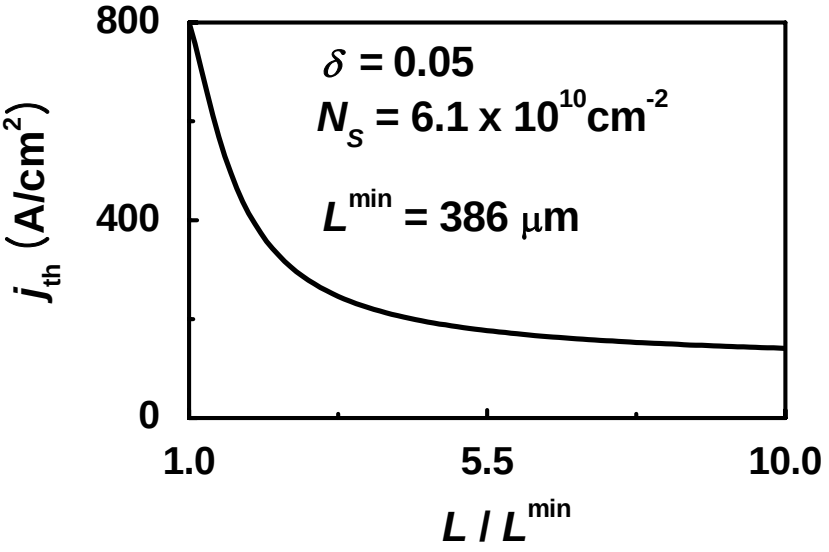

(a)

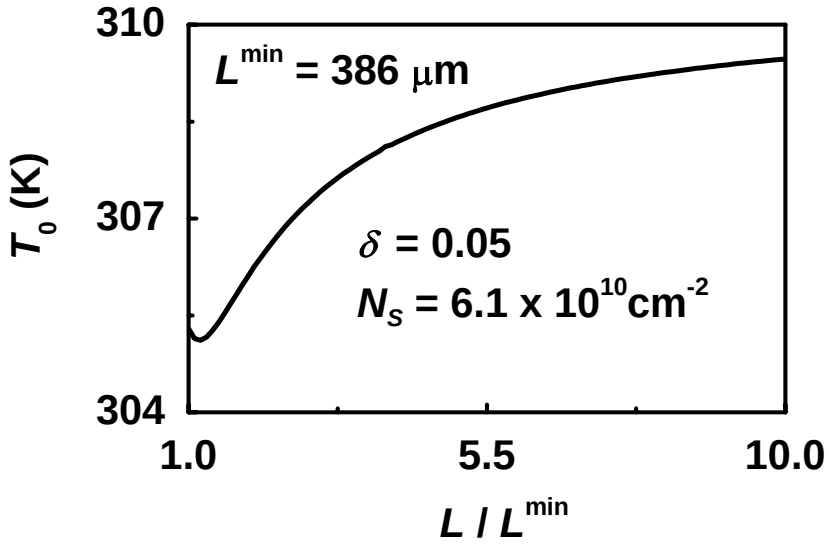

(b)

Fig. 2.8. (a) Threshold current density and (b) characteristic temperature versus normalized cavity length. (Reprinted from Fig. 7 of ref. [A1], Copyright (2008), with permission from Elsevier.)

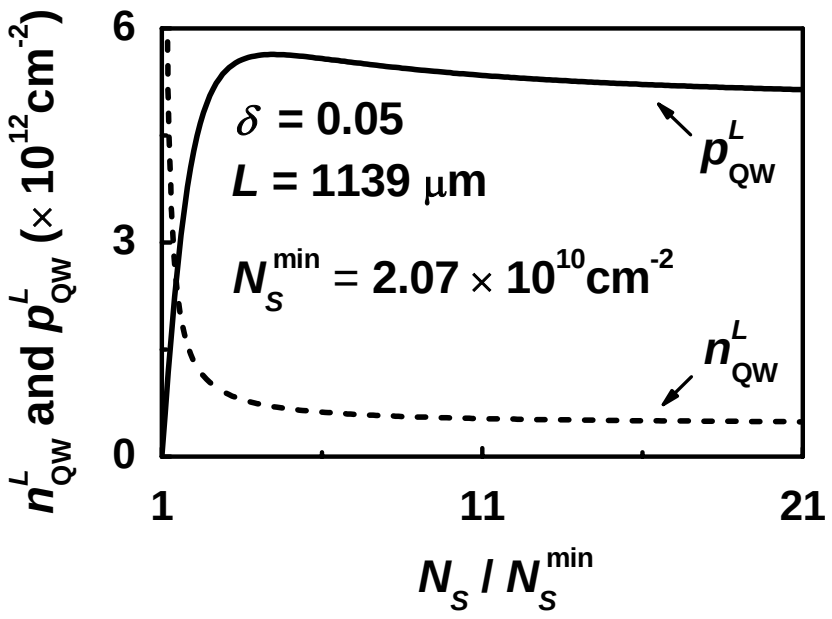

Fig. 2.9. 2-D electron and hole densities in the left-hand-side QW versus normalized surface density of QDs. (Reprinted from Fig. 8 of ref. [A1], Copyright (2008), with permission from Elsevier.)

As a function of the surface density of QDs, j_{th} is non-monotonic [Fig. 2.6(a)] — j_{th} increases rapidly with N_S and approaches its maximum at the N_S value slightly higher than N_S^{min}. On further increasing N_S, j_{th} decreases over a wide range of N_S values and then again starts to slowly increase [Fig. 2.6(a)].

As seen from Figs. 2.6-2.8, T_0 is very high throughout the entire range of the parameters shown. As each of the parameters is changed toward its critical tolerable value, T_0 decreases. This decrease is however small, particularly with changing δ and L [Fig. 2.7(b) and Fig. 2.8(b)]. There is a peculiarity in the dependence of T_0 on each of the structure parameters — the point of minimum of this dependence is slightly shifted from the critical point. Notice that even the lowest value of T_0 is above 300 K, i.e. well above (by a factor of more than three) the characteristic temperature of commercial telecommunication QW lasers [16]. At the same time, if the structure parameters are reasonably far from their critical values, the threshold current densities [Figs. 2.3, 2.6(a), 2.7(a), and 2.8(a)] are well below those of telecommunication lasers.

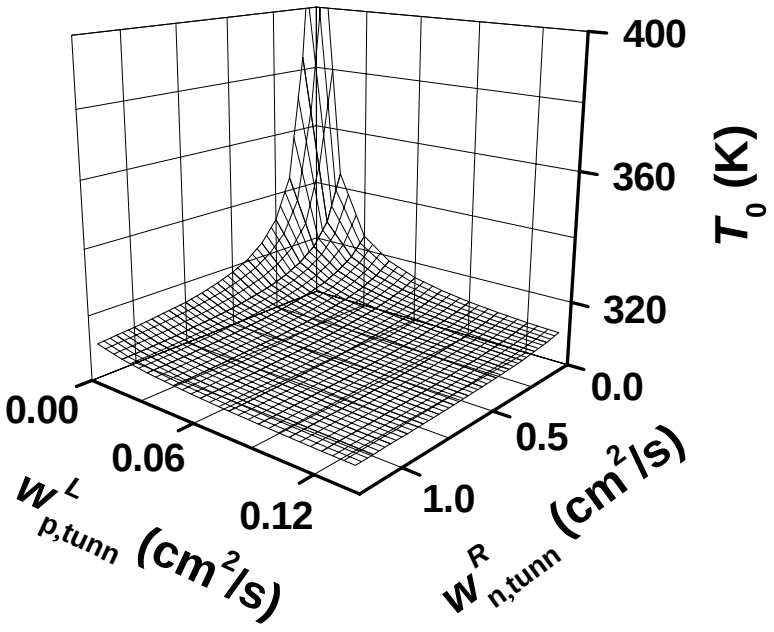

Fig. 2.10. Characteristic temperature versus tunneling coefficients for minority carriers $w^L_{\mathrm{p,tunn}}$ and $w^R_{\mathrm{n,tunn}}$. The tunneling coefficients for majority carriers are as follows: $w^L_{\mathrm{n,tunn}}$ = 16.2 cm^2/s and $w^R_{\mathrm{p,tunn}}$ = 1.48 cm^2/s. (Reprinted from Fig. 9 of ref. [A1], Copyright (2008), with permission from Elsevier.)

Shown in Fig. 2.10 is T_0 versus the tunneling coefficients $w^L_{\mathrm{p,tunn}}$ and $w^R_{\mathrm{n,tunn}}$ for minority carriers. As $w^L_{\mathrm{p,tunn}}$ and $w^R_{\mathrm{n,tunn}} \to 0$, the characteristic temperature increases infinitely, $T_0 \to \infty$. Indeed, in such situation, there is no out-tunneling of minority carriers from QDs and hence the recombination outside QDs is totally suppressed. The only remaining component of j_{th} is the recombination current density in QDs, j_{QD} [the first term in the right-hand side of (2.15) and (2.17)]. Under the condition of charge neutrality in QDs [$f_{\mathrm{n}} = f_{\mathrm{p}} = \mathrm{const}\,(T)$ – see (2.25)], this component is temperature-independent and hence so is j_{th}.

The tunneling coefficients are strongly controlled by the thicknesses of barriers separating QDs from the QWs as well as the QD and QW parameters. Using the universal

dependence of the characteristic temperature on $w^{L}_{\mathrm{p,tunn}}$ and $w^{R}_{\mathrm{n,tunn}}$ shown in Fig. 2.10, the dependences on each of the parameters controlling the tunneling coefficients can be obtained.

In commercial InP-based telecommunication lasers, the temperature-sensitivity of the threshold current can also be affected by the thermal leakage of minority carriers over the heterobarriers between the OCL and cladding layers and recombination in the latter [17]. As seen from Fig. 2.3 and discussed above, the role of recombination in the OCL is negligible compared to that in the QWs. In other words, the out-tunneling flux of minority carriers from QDs is mainly consumed by the recombination in the QWs — this flux practically does not appear in the OCL. For this reason, the recombination in the cladding layers, which could only be fed by the thermal leakage of minority carriers from the OCL, can be safely neglected in a tunneling-injection QD laser.

2.6. Conclusion

We studied the threshold characteristics of a laser, in which electrons and holes are injected into QDs by tunneling from two separate QWs. We developed an extended theoretical model allowing for out-tunneling leakage of carriers from QDs and hence recombination outside QDs. The carrier densities, threshold current density j_{th}, and characteristic temperature T_0 have been calculated as functions of temperature and structure parameters. The recombination in the QWs has been shown to control j_{th} and T_0. Even in the presence of out-tunneling from QDs and recombination outside QDs, T_0 has been shown to remain very high (above 300 K at room temperature) and not significantly affected by the QD size fluctuations, which is a clear manifestation of robustness of the tunneling-injection QD laser.

REFERENCES *)

[A1] D.-S. Han and L. V. Asryan, "Characteristic temperature of a tunneling-injection quantum dot laser: Effect of out-tunneling from quantum dots," *Solid-State Electron.* vol. 52, no. 10, pp. 1674–1679, Oct. 2008.

[A2] D.-S. Han and L. V. Asryan, "Characteristic temperature of a tunneling-injection quantum dot laser," *International Semiconductor Device Research Symposium.* College Park, Maryland, Dec. 12–14, 2007, vols. 1 and 2, pp. 626–627.

[1] Y. Arakawa and H. Sakaki, "Multidimensional quantum well laser and temperature dependence of its threshold current," *Appl. Phys. Lett.,* vol. 40, no. 11, pp. 939–941, Jun. 1982.

[2] J. I. Pankove, "Temperature dependence of emission efficiency and lasing threshold in laser diodes," *IEEE J. Quantum Electron.,* vol. 4, no. 4, pp. 119–122, Apr. 1968.

[3] L. V. Asryan and R. A. Suris, "Theory of threshold characteristics of semiconductor quantum dot lasers," *Semicond.,* vol. 38, no. 1, pp. 1–22, Jan. 2004.

[4] L. V. Asryan and S. Luryi, "Tunneling-injection quantum-dot laser: Ultrahigh temperature stability," *IEEE J. Quantum Electron.,* vol. 37, no. 7, pp. 905–910, Jul. 2001.

[5] L. V. Asryan and S. Luryi, "Temperature-insensitive semiconductor quantum dot laser," *Solid-State Electron.,* vol. 47, no. 2, pp. 205–212, 2003.

[6] H. C. Sun, L. Davis, S. Sethi, J. Singh, and P. Bhattacharya, "Properties of a tunneling injection quantum-well laser: recipe for a "cold" device with a large modulation bandwidth," *IEEE Photon. Technol. Lett.,* vol. 5, no. 8, pp. 870–872, Aug. 1993.

[7] K. Kamath, D. Klotzkin, and P. Bhattacharya, "Small-signal modulation characteristics of self-organized quantum dot separate confinement heterostructure and tunneling injection lasers," *Proc. IEEE LEOS 10th Annual Meeting*, vol. 2, pp. 498–499, Nov. 1997.

*) "A" in the reference number indicates the publications of the author of this dissertation.

[8] P. Bhattacharya, X. Zhang, Y. Yuan, K. Kamath, D. Klotzkin, C. Caneau, and R. Bhat, "High-speed tunnel-injection quantum well and quantum dot lasers," *Proc. SPIE International Symposium PHOTONICS WEST*, vol. 3283, pp. 702–709, Jan. 1998.

[9] P. Bhattacharya and S. Ghosh, "Tunnel injection $In_{0.4}Ga_{0.6}As$/GaAs quantum dot lasers with 15 GHz modulation bandwidth and $T_0 = 237$ K at room temperature," *Appl. Phys. Lett.,* vol. 80, no. 19, pp. 3482–3484, May. 2002.

[10] Y. Arakawa, "Fabrication of quantum wires and dots by MOCVD selective growth," *Solid-State Electron*., vol. 37, no. 4-6, pp. 523–528, Apr–Jun. 1994.

[11] D. Leonard, S. Fafard, K. Pond, Y. H. Zhang, J. L. Merz, and P. M. Petroff, "Structural and optical properties of self-assembled InGaAs quantum dots," *J. Vac. Sci. Technol.* B, vol. 12, no. 4, pp. 2516–2520, Jul. 1994.

[12] L. V. Asryan and R. A. Suris, "Inhomogeneous line broadening and the threshold current density of a semiconductor quantum dot laser," *Semicond. Sci. Technol.,* vol. 11, no. 4, pp. 554–567, Apr. 1996.

[13] L. V. Asryan and R. A. Suris, "Charge neutrality violation in quantum-dot lasers," *IEEE J. Select. Topics Quantum Electron.,* vol. 3, no. 2, pp. 148–157, Apr. 1997.

[14] L. V. Asryan and R. A. Suris, "Temperature dependence of the threshold current density of a quantum dot laser," *IEEE J. Quantum Electron*., vol. 34, no. 5, pp. 841–850, May 1998.

[15] L. V. Asryan, "Spontaneous radiative recombination and nonradiative Auger recombination in quantum-confined heterostructures," *Quantum Electron.,* vol. 35, no. 12, pp. 1117–1120, Dec. 2005.

[16] P. S. Zory, Jr.(Ed.), "Quantum well lasers," Boston: Academic Press; 1993.

[17] G. L. Belenky, C. L. Reynolds Jr., R. F. Kazarinov, V. Swaminathan, S. L. Luryi, and J. Lopata, "Effect of p-doping profile on performance of strained multi-quantum-well InGaAsP-InP lasers," *IEEE J. Quantum Electron.*, vol. 32, no. 8, pp. 1450–1455, Aug. 1996.

Chapter 3

Output Power of a Tunneling-Injection Quantum Dot Laser

Summary

A comprehensive theoretical model for a tunneling-injection quantum dot (QD) laser is developed. Both electrons and holes are injected into QDs by tunneling from two separate quantum wells (QWs). Ideally, out-tunneling of each type of carriers from QDs into the opposite-to-injection-side QW should be completely blocked; as a result, the parasitic electron-hole recombination outside QDs will be suppressed and the light-current characteristic (LCC) of a laser will be strictly linear. To scrutinize the potential of a tunneling-injection QD laser for high-power operation and the robustness of an actual device, our model includes out-tunneling leakage of carriers from QDs. The numerical calculations are complimented by an analytical model and closed-form expressions for the LCC and carrier population across the layered structure are derived. Even in the presence of out-tunneling leakage, the intensity of parasitic recombination outside QDs is shown to remain restricted with increasing injection current. As a consequence, the LCC of a tunneling-injection QD laser exhibits a remarkable feature — it becomes increasingly linear, and the slope efficiency grows closer to unity at high injection currents. The linearity is due to the fact that the current paths connecting the opposite sides of the structure lie entirely within QDs — in view of the three-dimensional confinement in QDs, the out-tunneling fluxes of carriers from dots are limited.

3.1. Introduction

A semiconductor quantum dot (QD) is a zero-dimensional (0-D) heterostructure formed by growth of an island of a lower band-gap material within a wider band-gap matrix. Due to quantum-confinement in all three directions, the energy spectrum of electrons and holes is discrete in a QD. There has been much effort to use QDs as an active region in diode lasers. In the ‘conventional’ design of QD lasers, the carriers are first injected from the cladding layers into

a bulk reservoir, which also serves as the optical confinement layer (OCL) and includes a two-dimensional (2-D) wetting layer, and then captured into QDs. Fig. 3.1 shows the energy band diagram of a conventional QD laser and the main processes. Due to bipolar (i.e., both electron and hole) population in the reservoir, a certain fraction of the injection current goes into the electron-hole recombination there (vertical arrows ② in Fig. 3.1). The parasitic recombination outside QDs is a major source of temperature-dependence of the threshold current. In addition, the carrier capture from the reservoir into QDs is not instantaneous. For this reason, the carrier density in the reservoir and hence the parasitic recombination rate rise, even above the lasing threshold, with injection current. This leads to sublinearity of the light-current characteristic (LCC) and limits the output power (Fig. 3.2), especially at high pump currents [1]-[3]. Hence, suppression of this parasitic recombination would be expected to significantly enhance the temperature stability and the output optical power of a laser.

In [4]–[6], to suppress the recombination outside QDs and thus to significantly improve the temperature-stability of the laser, *tunneling-injection of both electrons and holes into QDs was proposed from two separate QWs*.

In this chapter, we develop a comprehensive theoretical model for the optical power of a tunneling-injection QD laser [A1]-[A3][*)].

3.2. Theoretical model

The energy band diagram of the structure is shown in Fig. 2.2 in chapter 2. A single layer with QDs, located in the central part of the OCL, is clad on each side by a thin barrier and a QW. Electrons (holes) are injected into QDs by tunneling from the left- (right-) hand-side QW. The key idea of the device is that the QWs are not connected by a current path that bypasses QDs, which in particular assumes that (*i*) there is no thermal escape of carriers from the QWs over the barriers separating them from the QD layer, and (*ii*) there is no tunneling between the QWs through the material separating QDs in the QD layer. To realize this idea, certain conditions must be met, which were described in [4]–[6]. We discuss in this section the details of our extended model for a tunneling-injection QD laser.

[*)] "A" in the reference number indicates the publications of the author of this dissertation.

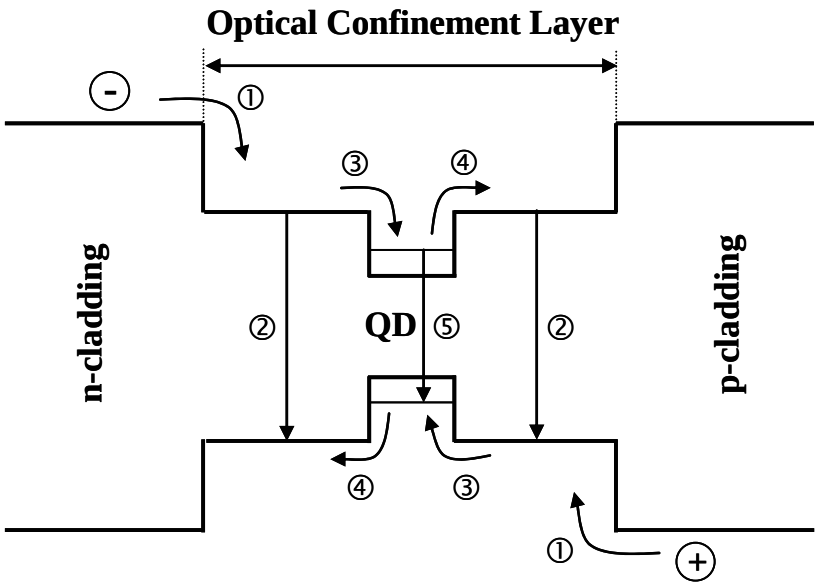

Fig. 3.1. Energy band diagram of a conventional QD laser and the main processes: ① injection from the cladding layers to the OCL, ② spontaneous recombination in the OCL, ③ carrier capture from the OCL into a QD, ④ carrier thermal escape from a QD to the OCL, and ⑤ spontaneous and stimulated recombination in a QD.

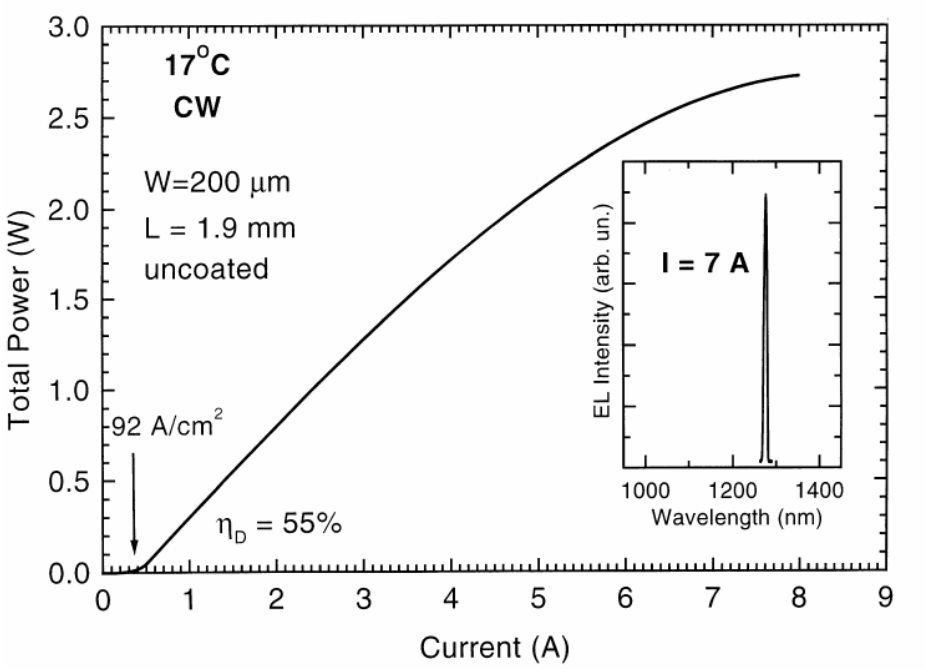

Fig. 3.2. LCC of a conventional QD laser. (Reprinted from Fig. 15 of ref. [3], Copyright (2000), with permission from Elsevier.)

3.2.1. Main assumptions

1) Fig. 2.2 shows the most optimum situation [4]–[6], when the lowest subband edge for majority carriers in the QW is in resonance with the energy level for the corresponding type of carriers in the average-sized QD, and hence the tunneling-injection rate is at its maximum. To also account for other possible situations, our model includes both direct and indirect tunneling — the effective tunneling rate from the entire QW-subband into the QD ensemble is used (see below).
2) Ideally, there should be no second tunneling step, i.e., out-tunneling from QDs into the 'foreign' QWs (electron-injecting QW for holes, and hole-injecting QW for electrons). As a result, there will be no electrons (holes) in the hole- (electron-) injecting side of the structure. As shown below, the total suppression of bipolar population and, consequently, of recombination outside QDs leads to an ideal LCC (i.e., a linear LCC with the slope efficiency equal to unity).

   Out-tunneling into the foreign QWs cannot be completely blocked in actual devices. Fig. 2.2 shows an optimized structure, in which the lowest subband edge for minority carriers in the QW is misaligned from the energy level for the corresponding type of carriers in the average-sized QD. Even in such a structure, there will be an indirect out-tunneling (shown by the inclined arrows in Fig. 2.2 in chapter 2) — electrons (holes) as minority carriers will appear in the hole- (electron-) injecting QW. Then they will thermally escape to the right- (left-) hand side of the OCL where holes (electrons) are the majority carriers. As a result, a bipolar population will establish outside QDs, and parasitic recombination will occur. Our model includes these processes and addresses their effect on the device characteristics.
3) We reasonably assume that the conduction (valence) band offset at the heteroboundary between the *p*- (*n*-) cladding and the OCL is large enough to block the further thermal escape of electrons (holes) to the *p*- (*n*-) cladding layer. In such a typical situation, the current in the *p*- (*n*-) cladding (including the boundary with the OCL) is purely hole (electron) current. Hence, the total injection current density j will enter into the rate equation for free electrons (holes) in the left- (right-) hand side of the OCL [see equations (2.2) and (2.4) in chapter 2].
4) The internal optical loss, α_{int}, is set zero here.

3.2.2. Rate equations and main notations

Our model is based on rate equations, which include the main processes in the layered structure. With the above assumptions, we have the set of equations (2.2)–(2.12) in chapter 2. The fluxes and physical quantities entering into (2.2)–(2.12) are presented in Tables 2.1 and 2.2, respectively.

We denoted the thermal escape times of electrons and holes from the QWs to the OCL by $\tau_{\mathrm{n,p,esc}}^{L,R}$ and the capture velocities from the OCL to the QWs by $v_{\mathrm{n,p,capt}}^{L,R}$. These quantities are related to each other. It is the capture velocity that describes the carrier capture to a QW [7, 8]. The general expression relating $\tau_{\mathrm{n,p,esc}}$ and $v_{\mathrm{n,p,capt}}$ is derived in Appendix I using the detailed balance condition. For undoped OCL and QW, the relation reads as follows:

$$\tau_{\mathrm{n,esc}} = \frac{1}{v_{\mathrm{n,capt}}} \frac{N_{\mathrm{c}}^{\mathrm{2D}}}{n_1}, \qquad \tau_{\mathrm{p,esc}} = \frac{1}{v_{\mathrm{p,capt}}} \frac{N_{\mathrm{v}}^{\mathrm{2D}}}{p_1}, \tag{3.1}$$

where $N_{\mathrm{c,v}}^{\mathrm{2D}} = m_{\mathrm{c,v}}^{\mathrm{QW}} T / \left(\pi \hbar^2\right)$ are the 2-D effective densities of states in the conduction and valence bands in the QWs, $m_{\mathrm{c,v}}^{\mathrm{QW}}$ are the electron and hole effective masses in the QWs, and the temperature T is measured in units of energy.

The quantities n_1 and p_1 are

$$n_1 = N_{\mathrm{c}}^{\mathrm{3D}} \exp\left(-\frac{\Delta E_{\mathrm{c}} - \varepsilon_{\mathrm{n}}^{\mathrm{QW}}}{T}\right), \qquad p_1 = N_{\mathrm{v}}^{\mathrm{3D}} \exp\left(-\frac{\Delta E_{\mathrm{v}} - \varepsilon_{\mathrm{p}}^{\mathrm{QW}}}{T}\right), \tag{3.2}$$

where $N_{\mathrm{c,v}}^{\mathrm{3D}} = 2\left[m_{\mathrm{c,v}}^{\mathrm{OCL}} T / \left(2\pi \hbar^2\right)\right]^{3/2}$ are the three-dimensional (3-D) effective densities of states in the conduction and valence bands in the OCL, $m_{\mathrm{c,v}}^{\mathrm{OCL}}$ are the electron and hole effective masses in the OCL, $\Delta E_{\mathrm{c,v}}$ are the conduction and valence band offsets between the OCL and the QW (Fig. 3.3), and $\varepsilon_{\mathrm{n,p}}^{\mathrm{QW}}$ are the energies of the lowest electron- and hole-subband edges in the QW (Fig. 3.3).

We exploit four tunneling coefficients, $w_{\mathrm{n,p,tunn}}^{L,R}$ (measured in units of cm^2/s), for electron and hole tunneling between the QD ensemble and the QWs. These tunneling coefficients are primarily controlled by the thicknesses and material parameters of the barriers, and by the QD

and QW parameters as well. In a properly designed structure, $w^{L}_{\mathrm{n,\,tunn}}$ and $w^{R}_{\mathrm{p,\,tunn}}$ should be large, and $w^{L}_{\mathrm{p,\,tunn}}$ and $w^{R}_{\mathrm{n,\,tunn}}$ small.

The quantities $n_1^{L,R,\mathrm{QW}}$ and $p_1^{L,R,\mathrm{QW}}$ entering into the electron and hole tunneling fluxes from the QD ensemble to the QWs [see (2.6)–(2.11)] are measured in units of cm^{-2}. The general expressions for n_1^{QW} and p_1^{QW} are derived in Appendix II. In the case of an undoped QW and a resonance between the energy level in a QD and the lowest subband edge in a QW,

$$n_1^{L,\mathrm{QW}} = N_{\mathrm{c}}^{2\mathrm{D}}, \qquad p_1^{R,\mathrm{QW}} = N_{\mathrm{v}}^{2\mathrm{D}}. \tag{3.3}$$

As seen from (2.2)–(2.9), the equations for the carrier densities in the right-hand-side QW and OCL are similar to those in the left-hand side. For this reason, we will analyze the rate equations and their solutions for the carrier densities in the left-hand side only. The solutions in the right-hand side are easily obtained from those in the left-hand side by an exchange between the electron and hole densities "n" and "p" and the left- and right-hand-side indices "L" and "R".

To optimize the device, it is desirable to maximize the net in-tunneling flux of electrons, $w^{L}_{\mathrm{n,tunn}} N_S (1-f_{\mathrm{n}}) n^{L}_{\mathrm{QW}} - w^{L}_{\mathrm{n,tunn}} n_1^{L,\mathrm{QW}} N_S f_{\mathrm{n}}$, from the electron-injecting QW into QDs in (2.6) and (2.10) and minimize the net out-tunneling flux of holes, $w^{L}_{\mathrm{p,tunn}} p_1^{L,\mathrm{QW}} N_S f_{\mathrm{p}} - w^{L}_{\mathrm{p,tunn}} N_S (1-f_{\mathrm{p}}) p^{L}_{\mathrm{QW}}$, from QDs to the electron-injecting QW in (2.7) and (2.11).

The flux of electron (and similarly hole) tunneling from a QD ensemble to a QW can be written as

$$w_{\mathrm{n,tunn}} n_1^{\mathrm{QW}} N_S f_{\mathrm{n}} = N_S \frac{f_{\mathrm{n}}}{\tau^{\mathrm{QD}\to\mathrm{QW}}_{\mathrm{n,tunn}}}, \tag{3.4}$$

where

$$\tau^{\mathrm{QD}\to\mathrm{QW}}_{\mathrm{n,tunn}} = \frac{1}{w_{\mathrm{n,tunn}} n_1^{\mathrm{QW}}} \tag{3.5}$$

can be viewed as the tunneling time from a QD to a QW.

The flux of electron tunneling from a QW to a QD ensemble can be written as

$$w_{\mathrm{n,tunn}} N_S (1-f_{\mathrm{n}}) n_{\mathrm{QW}} = \frac{n_{\mathrm{QW}}}{\tau^{\mathrm{QW}\to\mathrm{QDs}}_{\mathrm{n,tunn}}}, \tag{3.6}$$

where

$$\tau_{\mathrm{n,tunn}}^{\mathrm{QW}\to\mathrm{QDs}} = \frac{\tau_{\mathrm{n,tunn,0}}^{\mathrm{QW}\to\mathrm{QDs}}}{1-f_{\mathrm{n}}} \tag{3.7}$$

can be considered as the tunneling time from a QW to a QD ensemble, and

$$\tau_{\mathrm{n,tunn,0}}^{\mathrm{QW}\to\mathrm{QDs}} = \frac{1}{w_{\mathrm{n,tunn}} N_S} \tag{3.8}$$

can be correspondingly considered as the tunneling time into an unoccupied QD ensemble (when $f_{\mathrm{n}} = 0$).

As seen from (3.5) and (3.8), the tunneling times $\tau_{\mathrm{n,tunn}}^{\mathrm{QD}\to\mathrm{QW}}$ and $\tau_{\mathrm{n,tunn,0}}^{\mathrm{QW}\to\mathrm{QDs}}$ are not the same. In contrast to $\tau_{\mathrm{n,tunn}}^{\mathrm{QD}\to\mathrm{QW}}$, which describes tunneling from *an individual* QD to a QW, $\tau_{\mathrm{n,tunn,0}}^{\mathrm{QW}\to\mathrm{QDs}}$ describes tunneling from a QW to *the entire QD ensemble* — the surface density of QDs, N_S, i.e., a characteristic of the entire QD ensemble, enters into eq. (3.8) for $\tau_{\mathrm{n,tunn}}^{\mathrm{QW}\to\mathrm{QDs}}$. Both $\tau_{\mathrm{n,tunn}}^{\mathrm{QD}\to\mathrm{QW}}$ and $\tau_{\mathrm{n,tunn,0}}^{\mathrm{QW}\to\mathrm{QDs}}$ are expressed in terms of a single coefficient $w_{\mathrm{n,tunn}}$. For these reasons and to avoid possible confusion, we will not use here two separate times $\tau_{\mathrm{n,tunn}}^{\mathrm{QD}\to\mathrm{QW}}$ and $\tau_{\mathrm{n,tunn}}^{\mathrm{QW}\to\mathrm{QDs}}$ for tunneling between a QD ensemble and a QW. Instead, we use a single parameter – the tunneling coefficient $w_{\mathrm{n,tunn}}$.

3.3. Results and discussion

We consider a continuous-wave operation of the laser and correspondingly use the steady-state rate equations in chapter 2

$$\frac{\partial}{\partial t}\left(b_1 n_L,\, b_1 p_L,\, b_2 n_R,\, b_2 p_R,\, n_{\mathrm{QW}}^L,\, p_{\mathrm{QW}}^L,\, n_{\mathrm{QW}}^R,\, p_{\mathrm{QW}}^R,\, N_S f_{\mathrm{n}},\, N_S f_{\mathrm{p}},\, N\right) = 0\,, \tag{3.9}$$

which are eleven equations in total. These equations do not, however, constitute a complete set for finding eleven unknowns (n_L, p_L, n_R, p_R, n_{QW}^L, p_{QW}^L, n_{QW}^R, p_{QW}^R, f_{n}, f_{p}, and N). It is easily shown that only nine out of ten equations (2.2)–(2.11) are independent at the steady-state, which is to say that the set should be complemented by one more equation. The equation is provided by the condition of charge neutrality in QDs (see below).

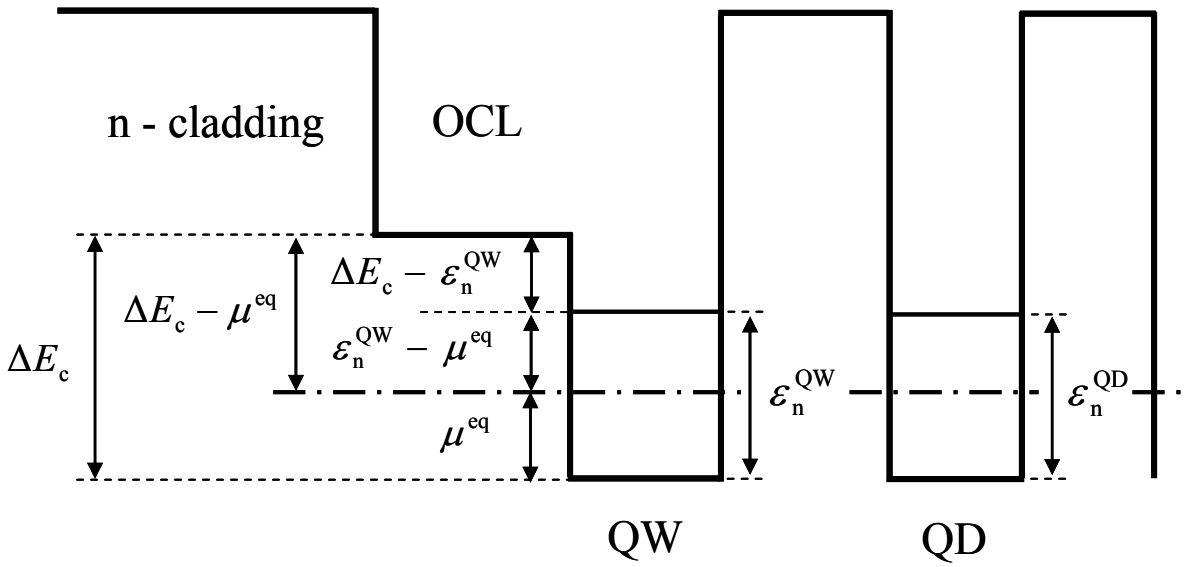

Fig. 3.3. Conduction band diagram in the left-hand (electron-injecting) side of the structure. The Fermi level μ^{eq} is shown solely as an illustration to the derivations of Appendixes I and II for the equilibrium case. No equilibrium is assumed under lasing conditions.

Above the lasing threshold, the number of stimulated photons is nonvanishing ($N \neq 0$). To satisfy eq. (2.12) at the steady-state at nonvanishing N, the following lasing condition should hold:

$$g^{\max}\left(f_n + f_p - 1\right) = \beta\,, \tag{3.10}$$

which is the condition of equality of the modal gain to the mirror loss at and above the lasing threshold (the internal optical loss is not considered here — see assumption # 4).

Using the steady-state rate equations and introducing the photon lifetime in the cavity,

$$\tau_{ph} = \frac{\sqrt{\epsilon_g}}{c}\frac{1}{\beta}, \tag{3.11}$$

the following expression is obtained for the number of photons N and output power P:

$$P = \hbar\omega\frac{N}{\tau_{ph}} = \frac{\hbar\omega}{e}S\left(j - eN_S\frac{f_n f_p}{\tau_{QD}} - eB_{2D}n_{QW}^{L}p_{QW}^{L} - eB_{2D}n_{QW}^{R}p_{QW}^{R} - eb_1Bn_Lp_L - eb_2Bn_Rp_R\right), \tag{3.12}$$

where $\hbar\omega$ is the photon energy. Expression (3.12) is general and holds no matter what a specific model is for the carrier capture from the OCL to QWs, escape from QWs to the OCL, and tunneling between QWs and QDs. What it means is that the stimulated emission is produced by an excess of the injection current density j over the current densities of spontaneous recombination in QDs (second term in the brackets), QWs (third and fourth terms), and OCL (last two terms).

The confined-carrier level occupancies in QDs, 2D-carrier densities in the QWs, and free-carrier densities in the OCL depend on the pump current density j. To calculate the LCC [i.e., P versus j given by (3.12)], these dependences should be found from the solution of the rate equations. We start with an ideal structure and next consider a structure with out-tunneling leakage from QDs.

3.3.1. Ideal structure: no out-tunneling from QDs, no recombination outside QDs

If out-tunneling from QDs into the foreign QWs is completely blocked [$w^L_{\mathrm{p,tunn}}$ and $w^R_{\mathrm{n,tunn}}$ are set zero in the rate equations (2.2)–(2.12)], there will be no minority carriers outside QDs (p_L, p^L_{QW}, n^R_{QW}, n_R = 0). The injection current will entirely go into the spontaneous and stimulated recombination in QDs. Eq. (3.12) will read as

$$P = \frac{\hbar\omega}{e} S \left(j - eN_S \frac{f_{\mathrm{n}} f_{\mathrm{p}}}{\tau_{\mathrm{QD}}} \right). \tag{3.13}$$

In general, the level occupancies $f_{\mathrm{n,p}}$, and hence the spontaneous recombination current density in QDs, $eN_S\left(f_{\mathrm{n}} f_{\mathrm{p}}/\tau_{\mathrm{QD}}\right)$, can depend on the injection current density j. Whatever the dependence is, $f_{\mathrm{n,p}}$ cannot exceed unity; consequently, $eN_S\left(f_{\mathrm{n}} f_{\mathrm{p}}/\tau_{\mathrm{QD}}\right)$ cannot exceed eN_S/τ_{QD}. For typical values of the surface density of QDs N_S (below 10^{11} cm^{-2}) and spontaneous radiative recombination time in QDs τ_{QD} (around 1 ns), eN_S/τ_{QD} is less than 20 A/cm^2. This means that for j > 100 A/cm^2, the spontaneous recombination term can be safely neglected compared to j in (3.13). Hence, the LCC of an ideal tunneling-injection QD laser, in which out-tunneling from QDs is completely blocked, is virtually linear and the slope efficiency is unity. The reason is that

the only remaining channel of nonstimulated recombination in this case is the spontaneous recombination in QDs, which is weak.

Let us show that the initial portion of the LCC [for which the term $eN_S\left(f_\mathrm{n}f_\mathrm{p}/\tau_\mathrm{QD}\right)$ cannot be neglected in (3.13)] is also linear. If charge neutrality holds in QDs ($f_\mathrm{n} = f_\mathrm{p}$), we immediately obtain from (3.10) that the level occupancies are pinned at their threshold value and do not depend on the injection current,

$$f_\mathrm{n} = f_\mathrm{p} = \frac{1}{2}\left(1 + \frac{\beta}{g^{\max}}\right) = \mathrm{const}(j)\,. \tag{3.14}$$

In this case, $eN_S\left(f_\mathrm{n}f_\mathrm{p}/\tau_\mathrm{QD}\right) = \mathrm{const}(j)$. As discussed in [2] in the context of conventional QD lasers, violation of charge neutrality ($f_\mathrm{n} \neq f_\mathrm{p}$) can disrupt pinning the level occupancies and lead to their dependence on the pump current (just as it leads to the temperature-dependence [9, 10]). Denoting $\Delta = f_\mathrm{p} - f_\mathrm{n}$, we have from (3.10)

$$f_{\mathrm{n,p}}(j) = \frac{1}{2}\left(1 + \frac{\beta}{g^{\max}}\right) \mp \frac{1}{2}\Delta(j)\,, \tag{3.15}$$

where "–" and "+" correspond to "n" and "p" subscripts, respectively. With (3.13) and (3.15), the output power can be written as

$$P(j) = \frac{\hbar\omega}{e} S\left\{ j - \frac{1}{4}\frac{eN_S}{\tau_\mathrm{QD}}\left[\left(1 + \frac{\beta}{g^{\max}}\right)^2 - \Delta^2(j)\right]\right\}. \tag{3.16}$$

Since f_p and f_n are less than unity, so is their difference Δ. As seen from (3.16), violation of charge neutrality in QDs appears as a second-order effect (Δ^2) in the expression for the LCC. Hence, in both cases of neutral and charged QDs, the LCC of an ideal tunneling-injection QD laser is also linear at low j.

3.3.2. Structure with out-tunneling leakage from QDs and recombination outside QDs

In an actual structure, there can be out-tunneling into the foreign QWs (Fig. 2.2 in chapter 2). For this reason, the electron-hole recombination outside QDs cannot be completely

suppressed. Hence, the rate equations (2.2)–(2.12) should be solved in the general case of nonvanishing tunneling coefficients $w^L_{\mathrm{p,tunn}}$ and $w^R_{\mathrm{n,tunn}}$.

We assume charge neutrality in QDs and use (3.14) for the level occupancies. The derivations lead to a quartic equation in n^L_{QW}, solution of which provides us n^L_{QW} as a function of j. The other carrier densities in the left-hand side of the structure (p^L_{QW}, n_L, and p_L) are expressed in terms of n^L_{QW}. Similarly, the carrier densities in the right-hand side are expressed in terms of p^R_{QW}. Finally, the number of photons and output power are found from (3.12) as functions of j.

Under the conditions of negligible recombination in the OCL (up to high injection current densities – see Appendix III), solving the rate equations simplifies considerably — closed-form expressions are obtained for the carrier densities and output power as functions of j (Appendix IV).

Several general conclusions can be easily made from the analysis of the rate equations.

At the steady-state, eq. (2.3) for free holes in the left-hand side of the OCL can be written as follows:

$$\frac{p^L_{\mathrm{QW}}}{\tau_{\mathrm{p,esc}}} = v^L_{\mathrm{p,capt}} p_L + b_1 B n_L p_L . \tag{3.17}$$

Substituting $p^L_{\mathrm{QW}}/\tau_{\mathrm{p,esc}} - v^L_{\mathrm{p,capt}} p_L = b_1 B n_L p_L$ in (2.7), we have

$$B_{\mathrm{2D}} n^L_{\mathrm{QW}} p^L_{\mathrm{QW}} + b_1 B n_L p_L = w^L_{\mathrm{p,tunn}} p_1^{L,\mathrm{QW}} N_S f_{\mathrm{p}} - w^L_{\mathrm{p,tunn}} N_S (1 - f_{\mathrm{p}}) p^L_{\mathrm{QW}} . \tag{3.18}$$

As seen from (3.18), bimolecular recombination in the left-hand-side QW and OCL is entirely due to the net out-tunneling of holes from QDs to the QW.

Substituting $v^L_{\mathrm{n,capt}} n_L - n^L_{\mathrm{QW}} / \tau_{\mathrm{n,esc}} = j/e - b_1 B n_L p_L$ [see (2.2)] in (2.6), we have

$$B_{\mathrm{2D}} n^L_{\mathrm{QW}} p^L_{\mathrm{QW}} + b_1 B n_L p_L = \frac{j}{e} - \left[w^L_{\mathrm{n,\,tunn}} N_S (1 - f_{\mathrm{n}}) n^L_{\mathrm{QW}} - w^L_{\mathrm{n,tunn}} n_1^{L,\mathrm{QW}} N_S f_{\mathrm{n}} \right]. \tag{3.19}$$

As seen from (3.19), the flux of bimolecular recombination in the left-hand-side QW and OCL can alternatively be presented as the difference of the electron injection flux j/e and the net in-

tunneling flux of electrons from the QW to QDs. In other words, the electron flux, which does not enter QDs, can only be consumed via recombination with holes outside QDs.

By dropping in (3.18) the flux $w^L_{\mathrm{p,tunn}} N_S (1-f_{\mathrm{p}}) p^L_{\mathrm{QW}}$ of backward tunneling of holes from the electron-injecting QW to QDs, we get the upper limit for the parasitic recombination flux in the left-hand side of the structure. Since $f_{\mathrm{n,p}} \le 1$, this limit, which presents the out-tunneling flux $w^L_{\mathrm{p,tunn}} p_1^{L,\mathrm{QW}} N_S f_{\mathrm{p}}$ of holes from QDs to the foreign (electron-injecting) QW, is itself restricted and cannot exceed $w^L_{\mathrm{p,tunn}} p_1^{L,\mathrm{QW}} N_S$ at any j (under the condition of charge neutrality [see (3.14)], $w^L_{\mathrm{p,tunn}} p_1^{L,\mathrm{QW}} N_S f_{\mathrm{p}}$ is pinned and does not change with j). Consequently, the recombination flux in the left-hand-side QW and OCL is limited by $w^L_{\mathrm{p,tunn}} p_1^{L,\mathrm{QW}} N_S$,

$$B_{2\mathrm{D}} n^L_{\mathrm{QW}} p^L_{\mathrm{QW}} + b_1 B n_L p_L \;<\; w^L_{\mathrm{p,tunn}} p_1^{L,\mathrm{QW}} N_S f_{\mathrm{p}} \;<\; w^L_{\mathrm{p,tunn}} p_1^{L,\mathrm{QW}} N_S \;=\; \mathrm{const}\,. \qquad (3.20)$$

The parasitic recombination current density [the sum of the last four terms in the brackets in (3.12)] and the out-tunneling current density,

$$j_{\mathrm{out-tunn}} = e w^L_{\mathrm{p,tunn}} p_1^{L,\mathrm{QW}} N_S f_{\mathrm{p}} + e w^R_{\mathrm{n,tunn}} n_1^{R,\mathrm{QW}} N_S f_{\mathrm{n}}\,, \qquad (3.21)$$

are shown in Fig. 3.4 versus the excess injection current density $j - j_{\mathrm{th}}$ (solid curve and horizontal dashed line, respectively).

The fact that the parasitic recombination flux outside QDs remains limited with increasing j is due to a 0-D nature of QDs — QDs constrain the carrier transfer between the opposite sides of the structure. If a QW or quantum wires would be used instead of QDs, the out-tunneling fluxes would be controlled by the 2-D or 1-D carrier densities, which, unlike $f_{\mathrm{n,p}}$, would not be limited; accordingly, the parasitic recombination flux would not be limited.

With (3.18) and a similar equation for the right-hand side of the structure, eq. (3.12) can be rewritten as follows:

$$P = \frac{\hbar\omega}{e} S \Bigg[j - e N_S \frac{f_{\mathrm{n}} f_{\mathrm{p}}}{\tau_{\mathrm{QD}}} - e w^L_{\mathrm{p,tunn}} p_1^{L,\mathrm{QW}} N_S f_{\mathrm{p}} - e w^R_{\mathrm{n,tunn}} n_1^{R,\mathrm{QW}} N_S f_{\mathrm{n}} + e w^L_{\mathrm{p,tunn}} N_S (1-f_{\mathrm{p}}) p^L_{\mathrm{QW}} + e w^R_{\mathrm{n,tunn}} N_S (1-f_{\mathrm{n}}) n^R_{\mathrm{QW}} \Bigg]. \qquad (3.22)$$

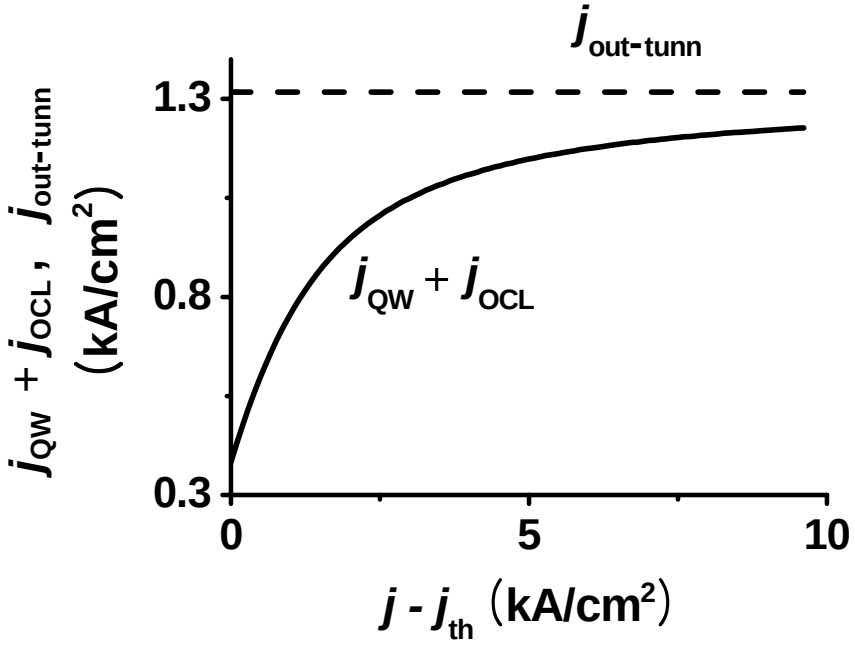

Fig. 3.4. Parasitic recombination current density in the QWs and OCL (solid curve) and current density of out-tunneling from QDs to the foreign QWs (horizontal dashed line) against excess injection current density. A GaInAsP heterostructure lasing near the telecommunication wavelength 1.55 μm is considered here. Room-temperature operation is assumed (T = 300 K). The parameters of the structure are as follows: δ = 0.05 (10% QD size fluctuations), $N_S = 6.11 \times 10^{10}$ cm^{-2}, L = 1.139 mm, R = 0.32, $\beta = 10$ cm^{-1}, W = 2 μm, $\tau_{QD} = 0.71 \times 10^{-9}$ s, $g^{max} = 29.52$ cm^{-1}, $b_1 = b_2 = 0.14$ μm, $v_{n,p,capt}^{L,R}$ = 3×10^5 cm/s, λ = 1.58 μm, $B = 1.27 \times 10^{-10}$ cm^3/s, and B_{2D} = 2.8 × 10-4 cm^2/s. In Figs. 2.3-10, the tunneling coefficients are as follows unless otherwise specified: $w_{n,tunn}^{L}$ = 0.073 cm^2/s, $w_{p,tunn}^{L}$ = 0.04 cm^2/s, $w_{n,tunn}^{R}$ = 0.013 cm^2/s, and $w_{p,tunn}^{R}$ = 0.058 cm^2/s. The threshold current density is j_{th} = 389 A/cm^2. (Reprinted with permission from Fig. 2 of ref. [A1]. Copyright [2008], American Institute of Physics.)

Whatever the dependences of p_{QW}^{L} and n_{QW}^{R} on j, it is clear from (3.22) that by dropping the last two terms in the brackets (the current densities of backward tunneling of minority carriers from the foreign QWs to QDs) we will obtain the lower limit for the output power,

$$P^{\mathrm{lowest}} = \frac{\hbar\omega}{e} S\left(j - eN_S \frac{f_{\mathrm{n}} f_{\mathrm{p}}}{\tau_{\mathrm{QD}}} - ew_{\mathrm{p,tunn}}^{L} p_1^{L,\mathrm{QW}} N_S f_{\mathrm{p}} - ew_{\mathrm{n,tunn}}^{R} n_1^{R,\mathrm{QW}} N_S f_{\mathrm{n}} \right). \tag{3.23}$$

Since $f_{\mathrm{n,p}} \le 1$, the last three terms in the brackets in (3.23) remain restricted with increasing j. Under the condition of charge neutrality in QDs, they are constant and, as clear from (3.22) and (3.23), their sum presents the upper limit for the threshold current density,

$$j_{\mathrm{th}}^{\mathrm{highest}} = eN_S \frac{f_{\mathrm{n}} f_{\mathrm{p}}}{\tau_{\mathrm{QD}}} + ew_{\mathrm{p,tunn}}^{L} p_1^{L,\mathrm{QW}} N_S f_{\mathrm{p}} + ew_{\mathrm{n,tunn}}^{R} n_1^{R,\mathrm{QW}} N_S f_{\mathrm{n}} . \tag{3.24}$$

With (3.24), eq. (3.23) reads as

$$P^{\mathrm{lowest}} = \frac{\hbar\omega}{e} S\left(j - j_{\mathrm{th}}^{\mathrm{highest}} \right). \tag{3.25}$$

The upper limit for the output power is obtained in an ideal structure discussed above and is given by (3.13), which we rewrite as follows:

$$P^{\mathrm{highest}} = \frac{\hbar\omega}{e} S\left(j - j_{\mathrm{th}}^{\mathrm{lowest}} \right), \tag{3.26}$$

where

$$j_{\mathrm{th}}^{\mathrm{lowest}} = eN_S \frac{f_{\mathrm{n}} f_{\mathrm{p}}}{\tau_{\mathrm{QD}}} \tag{3.27}$$

is the lower limit for the threshold current density.

As seen from (3.25), the lower limit for the LCC is linear (dash-dotted line in Fig. 3.5) and its slope efficiency is unity. It is parallel to the upper limit [given by (3.26) and shown by the dashed line in Fig. 3.5] and shifted from the latter by the amount of the out-tunneling current density, $j_{\mathrm{out-tunn}}$.

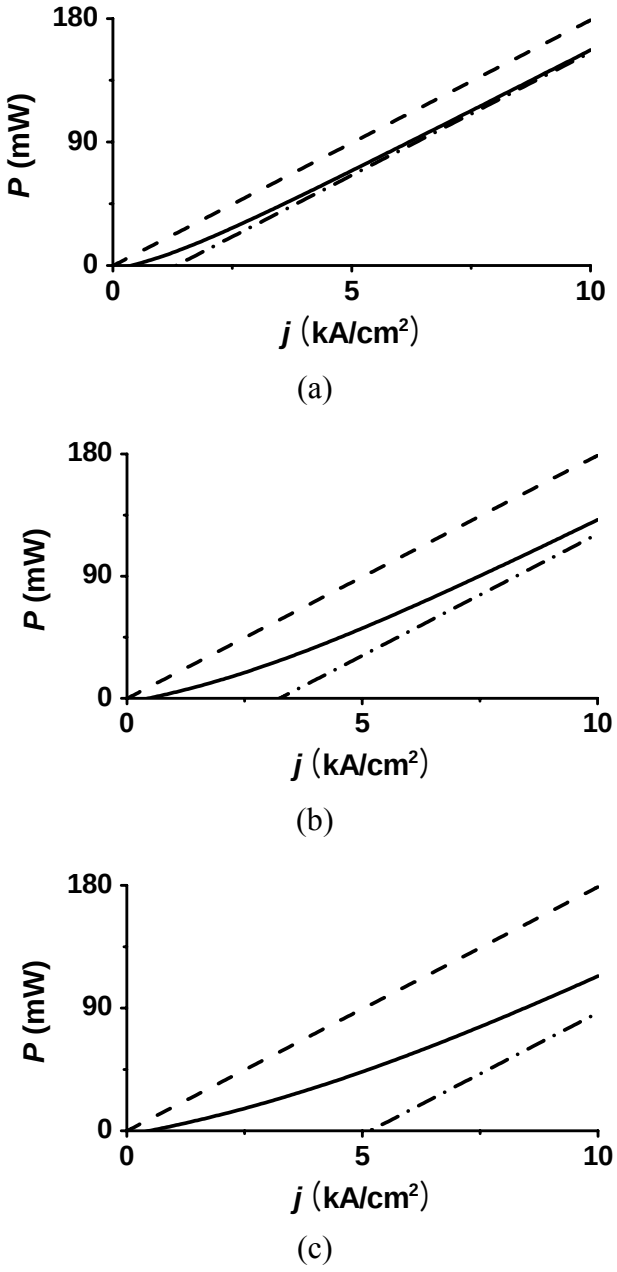

Fig. 3.5. Light-current characteristic of a tunneling-injection QD laser (solid curve) at different values of the out-tunneling coefficient $w^{L}_{\mathrm{p,tunn}}$: (a) 0.04, (b) 0.1, and (c) 0.16 cm^2/s. The threshold current density is j_{th} = 389, 457, and 479 A/cm^2 in (a), (b), and (c), respectively. The dashed line is the LCC of an ideal structure given by (3.26); $j_{\mathrm{th}}^{\mathrm{lowest}}$ = 6.21 A/cm^2 [see (3.27)]. The dash-dotted line is the asymptote given by (3.25); $j_{\mathrm{th}}^{\mathrm{highest}}$ [see (3.24)] is 1323, 3242, and 5161 A/cm^2 in (a), (b), and (c), respectively. (Reprinted with permission from Fig. 2 of ref. [A1]. Copyright [2008], American Institute of Physics.)

Hence, the actual LCC (obtained from the solution of the rate equations and shown by the solid curve in Fig. 3.5) is confined between the two parallel lines given by (3.25) and (3.26) (dash-dotted and dashed lines in Fig. 3.5). As seen from the figure and analysis below, the lower limit (3.25) presents the asymptote of the actual LCC at high injection currents.

From (3.22), we have for the slope efficiency (external differential efficiency)

$$\eta_{\text{ext}} = \frac{1}{\dfrac{\hbar\omega}{e} S} \frac{\partial P}{\partial j} = 1 + e w^{L}_{\text{p,tunn}} N_S (1 - f_{\text{p}}) \frac{\partial p^{L}_{\text{QW}}}{\partial j} + e w^{R}_{\text{n,tunn}} N_S (1 - f_{\text{n}}) \frac{\partial n^{R}_{\text{QW}}}{\partial j} . \tag{3.28}$$

Since η_{ext} should not be higher than unity, the derivatives of p^{L}_{QW} and n^{R}_{QW} with respect to j should be negative — the minority carrier density in each of the two QWs decreases with j (Fig. 3.6). Hence, the last two terms in the brackets in eq. (3.22) decrease with increasing j and the LCC asymptotically approaches the straight line given by (3.25) (Fig. 3.5).

The output power can be written as

$$P(j) = \frac{\hbar\omega}{e} S\, j_{\text{stim}}(j) = \frac{\hbar\omega}{e} S (j - j_{\text{th}}) \eta_{\text{int}}(j) , \tag{3.29}$$

where

$$j_{\text{stim}} = \frac{e}{S} \frac{N}{\tau_{\text{ph}}} \tag{3.30}$$

is the stimulated recombination current density and

$$\eta_{\text{int}} = \frac{j_{\text{stim}}}{j - j_{\text{th}}} \tag{3.31}$$

is the internal differential quantum efficiency. Since the parasitic recombination current density remains restricted [see (3.20) and Fig. 3.4], η_{int}, which presents the fraction of the excess injection current density $j - j_{\text{th}}$ that goes into the stimulated emission, should rise with j (dashed curve in Fig. 3.7). As a result, the LCC should become increasingly linear (Fig. 3.5).

With (3.29), the slope efficiency η_{ext} is expressed in terms of η_{int},

$$\eta_{\text{ext}} = \eta_{\text{int}} + (j - j_{\text{th}}) \frac{\partial \eta_{\text{int}}}{\partial j} . \tag{3.32}$$

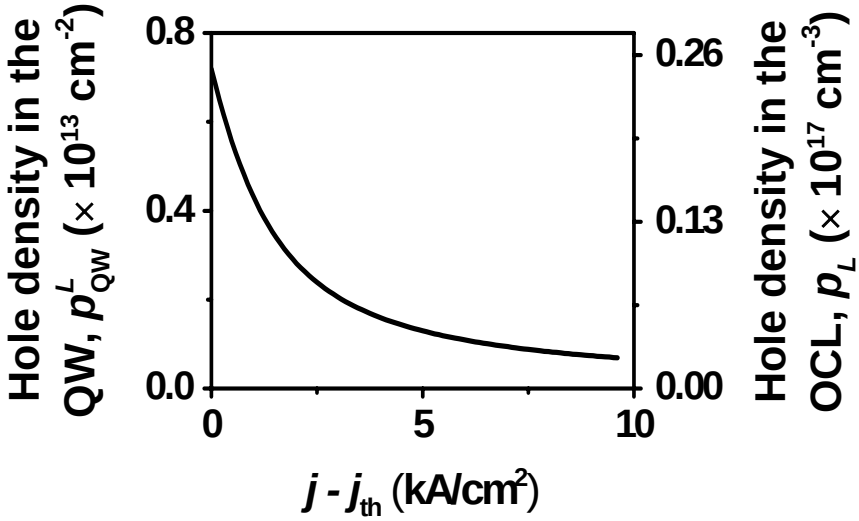

Fig. 3.6. Minority carrier density in the left-hand-side QW (left axis) and OCL (right axis) against excess injection current density. In view of a linear-proportionality relationship (A24), the same curve depicts p^L_{QW} and p_L.

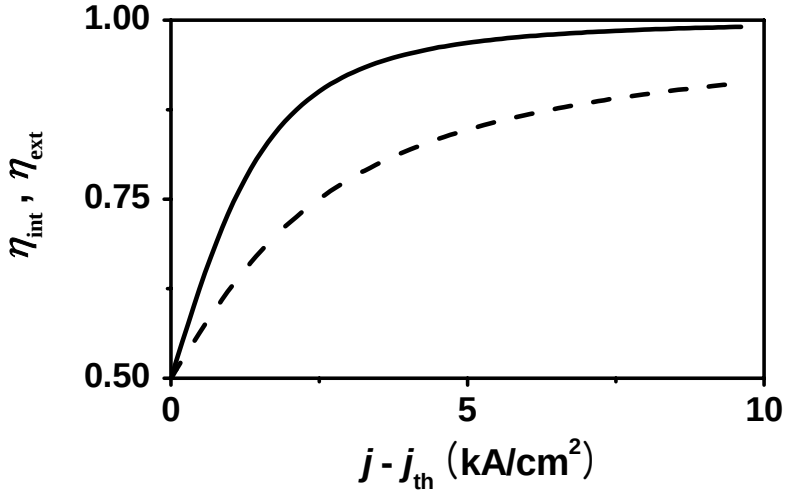

Fig. 3.7. Internal quantum efficiency (dashed curve) and slope efficiency (solid curve) against excess injection current density. (Reprinted with permission from Fig. 3 of ref. [A1]. Copyright [2008], American Institute of Physics.)

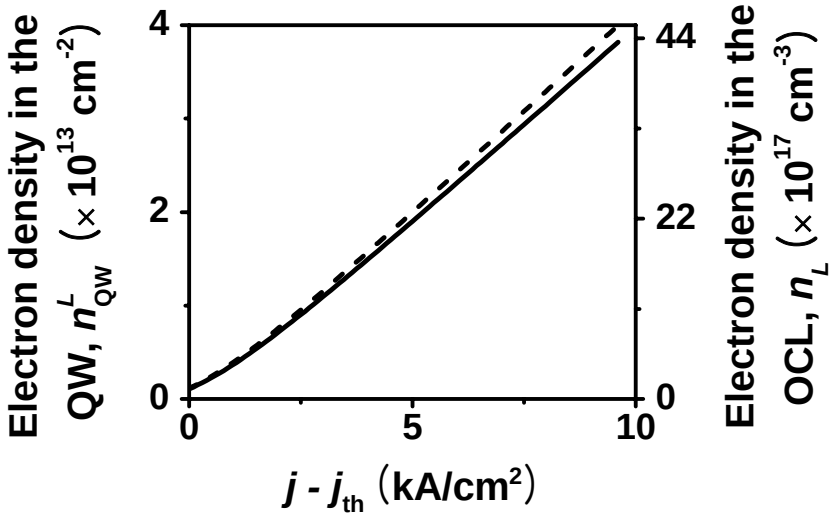

Fig. 3.8. Majority carrier density in the left-hand-side QW (solid curve, left axis) and OCL (dashed curve, right axis) against excess injection current density.

Since η_{int} increases with j, η_{ext} (solid curve in Fig. 3.7) also increases and is higher than η_{int} as is clear from (3.32). We did not consider the internal optical loss α_{int}; the inclusion of α_{int} will reduce the optical efficiency of the cavity, $\beta/(\beta + \alpha_{int})$, and hence η_{ext}.

The density of minority carriers in the left-hand-side QW and OCL is shown in Fig. 3.6. As discussed above, the minority carrier density in the QW (holes in the left-hand side) decreases with j. The minority carrier density in the OCL is directly related to that in the QW [see eq. (A24) in Appendix IV] and hence also decreases.

The density of majority carriers in the left-hand-side QW and OCL is shown in Fig. 3.8. Since majority carriers (electrons in the left-hand side) are supplied by injection, their density in the OCL and QW increases with pump current.

Auger recombination of electrons with holes in the OCL and QWs can be easily included in our model. In that case, the total parasitic recombination flux (the sum of the fluxes of bimolecular radiative recombination and trimolecular nonradiative Auger recombination) will enter into the left-hand side in (3.18) and will be equal to the net out-tunneling flux of minority carriers from QDs. Hence, the total parasitic recombination flux will remain limited with increasing j and all our conclusions about the LCC of a tunneling-injection QD laser will hold in

the presence of Auger recombination. In particular, the lower limit for the LCC and the upper limit for the threshold current density will be given by eqs. (3.23) and (3.24), respectively.

3.3.2.1. Laser characteristics versus tunneling coefficients

As discussed above, due to the fact that QDs are 0-D regions with a limited population ($f_{\mathrm{n,p}} \le 1$), the out-tunneling fluxes of minority carriers from QDs into the foreign QWs ($w^{L}_{\mathrm{p,tunn}} p_1^{L,\mathrm{QW}} N_S f_{\mathrm{p}}$ and $w^{R}_{\mathrm{n,tunn}} n_1^{R,\mathrm{QW}} N_S f_{\mathrm{n}}$) are also limited [see (3.20)]. Although the level occupancies $f_{\mathrm{n,p}}$ depend on the cavity length and other parameters of the structure, they can only change from 1/2 to 1 in the case of neutral QDs [see (3.14)]. The surface density of QDs can also be varied within a limited range (typically, from several 10^{10} to 10^{11} cm^{-2}). In contrast to $f_{\mathrm{n,p}}$ and N_S, the tunneling coefficients $w^{L}_{\mathrm{p,tunn}}$ and $w^{R}_{\mathrm{n,tunn}}$ depend strongly on the barrier thicknesses and can be easily varied within a wide range. Hence, for a given choice of materials for QDs, barriers, and QWs, the out-tunneling fluxes of minority carriers are mainly controlled by $w^{L}_{\mathrm{p,tunn}}$ and $w^{R}_{\mathrm{n,tunn}}$.

As shown in Appendix III, up to high injection current densities, the recombination in the OCL is negligible. What this means is that the out-tunneling fluxes of minority carriers from QDs are mainly consumed by the recombination in the QWs. Fig. 3.9 shows n^{L}_{QW} and p^{L}_{QW} and the recombination current density in the QW, $j^{L}_{\mathrm{QW}} = eB_{\mathrm{2D}} n^{L}_{\mathrm{QW}} p^{L}_{\mathrm{QW}}$, versus the tunneling coefficient $w^{L}_{\mathrm{p,tunn}}$. The hole density in the left-hand-side QW, which is entirely due to out-tunneling, increases considerably with $w^{L}_{\mathrm{p,tunn}}$ [Fig. 3.9(b)]. The recombination in the QW should become more intense with increasing $w^{L}_{\mathrm{p,tunn}}$. For this reason, the electron density decreases with increasing $w^{L}_{\mathrm{p,tunn}}$ [Fig. 3.9(a)]; the decrease is however negligible since electrons are majority carriers in the left-hand-side QW. Both n^{L}_{QW} and p^{L}_{QW} saturate as $w^{L}_{\mathrm{p,tunn}} \to \infty$. The barriers separating the QD layer from the QWs should block out-tunneling of minority carriers from QDs yet allowing for in-tunneling of majority carriers into QDs. It is therefore clear that, in the limiting case of infinitely large tunneling coefficients $w^{L}_{\mathrm{p,tunn}}$ and $w^{R}_{\mathrm{n,tunn}}$ for minority carriers, the tunneling coefficients $w^{L}_{\mathrm{n,tunn}}$ and $w^{R}_{\mathrm{p,tunn}}$ for majority carriers will also be infinitely large. The

expressions for the saturation values of n_{QW}^{L} and p_{QW}^{L} [obtained from (A28) and (A29)] are as follows:

$$n_{\mathrm{QW}}^{L}\Big|_{w_{\mathrm{n,p,tunn}}^{L}\to\infty} = n_{1}^{L,\mathrm{QW}}\frac{f_{\mathrm{n}}}{1-f_{\mathrm{n}}}, \tag{3.33}$$

$$p_{\mathrm{QW}}^{L}\Big|_{w_{\mathrm{n,p,tunn}}^{L}\to\infty} = p_{1}^{L,\mathrm{QW}}\frac{f_{\mathrm{p}}}{1-f_{\mathrm{p}}}. \tag{3.34}$$

The horizontal dashed lines in Fig. 3.9(a) and (b) show these saturation values.

Due to the saturation of n_{QW}^{L} and p_{QW}^{L}, the recombination current density in the QW, $j_{\mathrm{QW}}^{L} = eB_{\mathrm{2D}}n_{\mathrm{QW}}^{L}p_{\mathrm{QW}}^{L}$, also saturates with increasing $w_{\mathrm{p,tunn}}^{L}$ [Fig. 3.9(c)].

With the equilibrium level occupancies in a QD,

$$f_{\mathrm{n,p}} = \frac{1}{\exp\left(\dfrac{\varepsilon_{\mathrm{n,p}}^{\mathrm{QD}}-\mu_{\mathrm{n,p}}}{T}\right)+1}, \tag{3.35}$$

where $\varepsilon_{\mathrm{n,p}}^{\mathrm{QD}}$ are the energy levels of an electron and a hole in a QD and $\mu_{\mathrm{n,p}}$ are the quasi-Fermi levels of electrons and holes, we would obtain from (3.33) and (3.34) the equilibrium densities in the QW,

$$n_{\mathrm{QW}}^{L} = N_{\mathrm{c}}^{\mathrm{2D}}\exp\left(-\frac{\varepsilon_{\mathrm{n}}^{\mathrm{QW}}-\mu_{\mathrm{n}}}{T}\right), \qquad p_{\mathrm{QW}}^{L} = N_{\mathrm{v}}^{\mathrm{2D}}\exp\left(-\frac{\varepsilon_{\mathrm{p}}^{\mathrm{QW}}-\mu_{\mathrm{p}}}{T}\right), \tag{3.36}$$

where $\varepsilon_{\mathrm{n,p}}^{\mathrm{QW}}$ are the energies of the electron- and hole-subband edges in the QW (the quantities for electrons, $\varepsilon_{\mathrm{n}}^{\mathrm{QD}}$, $\varepsilon_{\mathrm{n}}^{\mathrm{QW}}$, and μ_{n}, are shown in Fig. 3.3). Hence, expressions (3.33) and (3.34) present the quasi-equilibrium relation between the carrier densities in the QW and level-occupancies in a QD; this is easily understood — the limiting case of $w_{\mathrm{n,p,tunn}}^{L,R}\to\infty$ describes an instant carrier exchange between the QWs and QDs.

Eq. (3.34) can also be readily obtained from (A30) by neglecting at large $w_{\mathrm{p,tunn}}^{L}$ the recombination flux in the QW, $B_{\mathrm{2D}}n_{\mathrm{QW}}^{L}p_{\mathrm{QW}}^{L}$, compared to the fluxes of out-tunneling from QDs, $w_{\mathrm{p,tunn}}^{L}p_{1}^{L,\mathrm{QW}}N_{S}f_{\mathrm{p}}$, and backward-tunneling into QDs, $w_{\mathrm{p,tunn}}^{L}N_{S}(1-f_{\mathrm{p}})p_{\mathrm{QW}}^{L}$. The balance between the two tunneling fluxes yields the quasi-equilibrium relation (3.34).

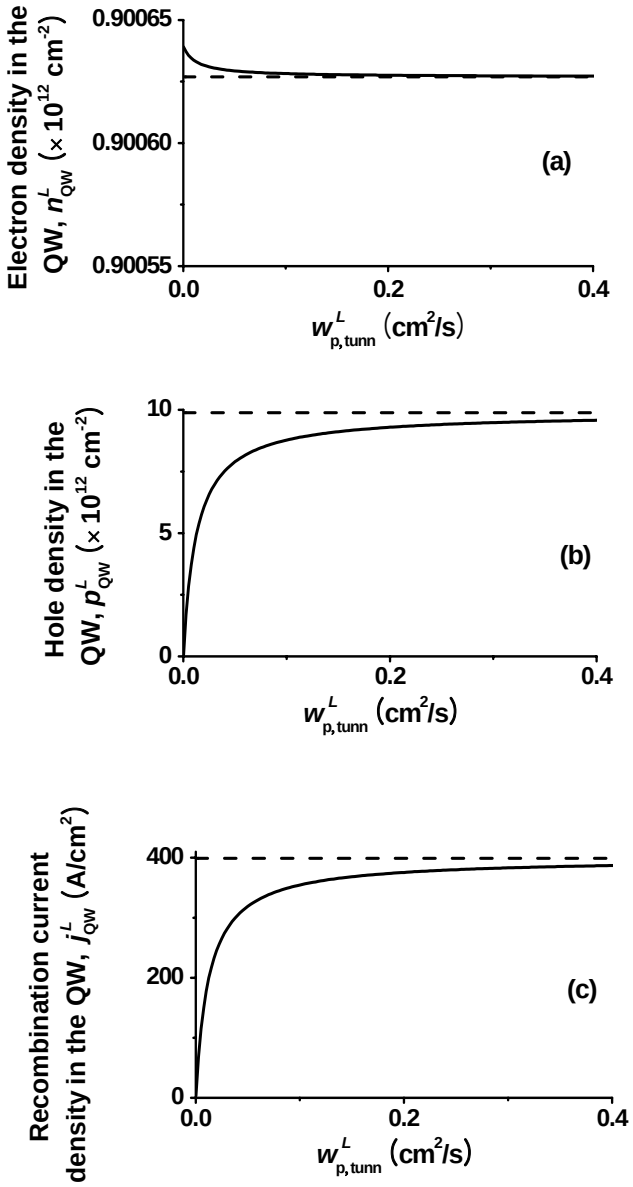

Fig. 3.9. 2-D density of electrons (a) and holes (b) and recombination current density (c) in the left-hand-side QW against out-tunneling coefficient at an infinitely large in-tunneling coefficient ($w^L_{\mathrm{n,tunn}} \to \infty$). The injection current density is j = 10 kA/cm^2. The horizontal dashed lines in (a) and (b) show the saturation values of n^L_{QW} and p^L_{QW} given by (3.33) and (3.34), respectively. The horizontal dashed line in (c) shows the saturation value of $j^L_{\mathrm{QW}} = eB_{\mathrm{2D}} n^L_{\mathrm{QW}} p^L_{\mathrm{QW}}$.

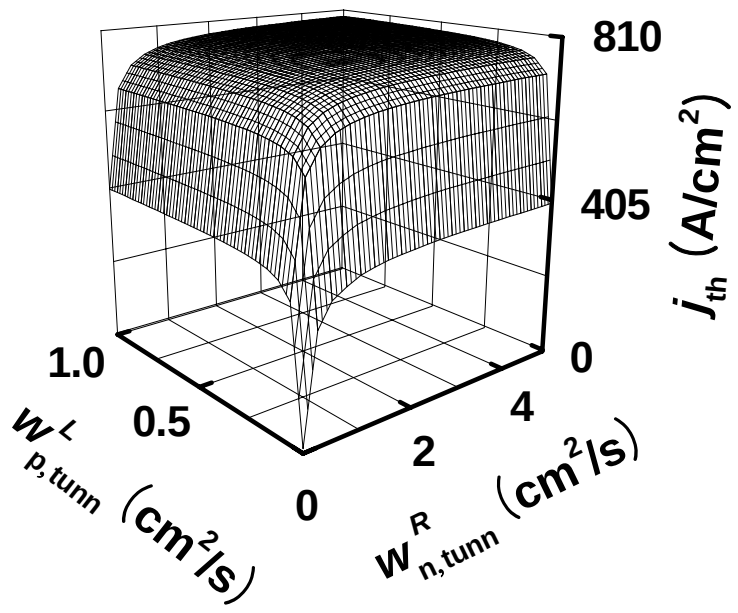

Fig. 3.10. Threshold current density against out-tunneling coefficients at infinitely large in-tunneling coefficients ($w^L_{\mathrm{n,tunn}}$, $w^R_{\mathrm{p,tunn}} \to \infty$). The j_{th} value at $w^L_{\mathrm{p,tunn}}$, $w^R_{\mathrm{n,tunn}} = 0$ (the ideal case) is given by (3.27) and is 6.21 A/cm^2. The saturation value of j_{th} is given by (3.37).

Since the recombination current density outside QDs [the sum of the last four terms in the brackets in (3.12)] increases and saturates with increasing $w^L_{\mathrm{p,tunn}}$ and $w^R_{\mathrm{n,tunn}}$, so does the threshold current density (Fig. 3.10). As a result, the output power (at a given injection current) decreases and also saturates (Fig. 3.11). The expression for the saturation value of j_{th} can be obtained by assuming that, in addition to instant exchange between the QWs and QDs, the carrier exchange between the OCL and QWs is also instantaneous ($v^{L,R}_{\mathrm{n,p,capt}} \to \infty$ or, equivalently, $\tau^{L,R}_{\mathrm{n,p,esc}} \to 0$). In such a case, quasi-equilibrium distributions will establish for electrons and holes throughout the structure and the threshold current density will be given by

$$j_{\mathrm{th}}\Big|_{w^{L,R}_{\mathrm{n,p,tunn}},\, v^{L,R}_{\mathrm{n,p,capt}} \to \infty} = eN_S \frac{f_{\mathrm{n}} f_{\mathrm{p}}}{\tau_{QD}} + eB_{2\mathrm{D}} \left(n_1^{L,\mathrm{QW}} \frac{f_{\mathrm{n}}}{1-f_{\mathrm{n}}} \right) \left(p_1^{L,\mathrm{QW}} \frac{f_{\mathrm{p}}}{1-f_{\mathrm{p}}} \right) \tag{3.37}$$

$$+ eB_{2\mathrm{D}} \left(n_1^{R,\mathrm{QW}} \frac{f_{\mathrm{n}}}{1-f_{\mathrm{n}}} \right) \left(p_1^{R,\mathrm{QW}} \frac{f_{\mathrm{p}}}{1-f_{\mathrm{p}}} \right) + eb_1 B \left(n_1^{L} \frac{f_{\mathrm{n}}}{1-f_{\mathrm{n}}} \right) \left(p_1^{L} \frac{f_{\mathrm{p}}}{1-f_{\mathrm{p}}} \right) + eb_2 B \left(n_1^{R} \frac{f_{\mathrm{n}}}{1-f_{\mathrm{n}}} \right) \left(p_1^{R} \frac{f_{\mathrm{p}}}{1-f_{\mathrm{p}}} \right),$$

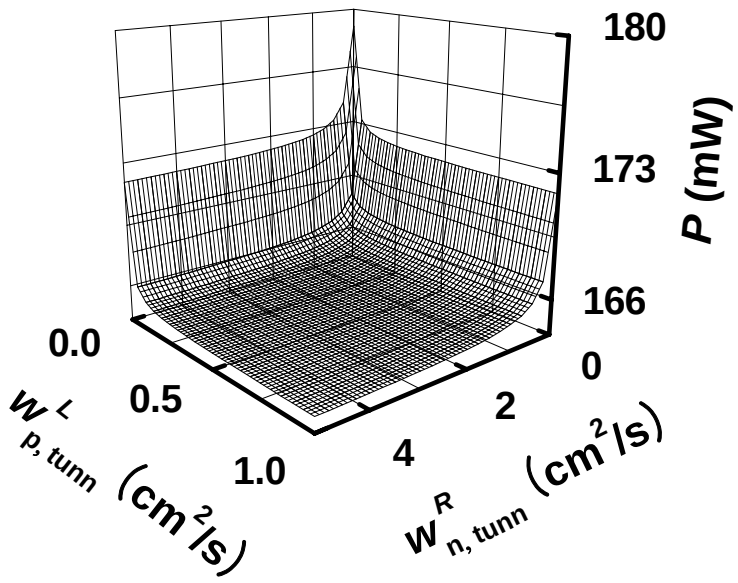

Fig. 3.11. Optical power against out-tunneling coefficients at infinitely large in-tunneling coefficients ($w^L_{n,tunn},\ w^R_{p,tunn} \to \infty$). The injection current density is j = 10 kA/cm^2. The P value at $w^L_{p,tunn},\ w^R_{n,tunn} = 0$ (the ideal case) is given by (3.26) and is 179 mW. The saturation value of P is given by (3.38).

where the terms in the brackets are the equilibrium carrier densities in the corresponding parts of the structure. In Fig. 3.10, $j_{th}\big|_{w^{L,R}_{n,p,tunn},\ \nu^{L,R}_{n,p,capt}\to\infty}$ = 806 A/cm^2.

The equilibrium carrier densities will not change with increasing injection current above the lasing threshold. Hence, the spontaneous recombination fluxes will be pinned and the excess of the injection current over the threshold current will entirely go into the stimulated recombination — the internal quantum efficiency will be unity. The output power will be given by

$$P\big|_{w^{L,R}_{n,p,tunn},\ \nu^{L,R}_{n,p,capt}\to\infty} = \frac{\hbar\omega}{e} S\left(j - j_{th}\big|_{w^{L,R}_{n,p,tunn},\ \nu^{L,R}_{n,p,capt}\to\infty} \right). \tag{3.38}$$

In Fig. 3.11, $P\big|_{w^{L,R}_{n,p,tunn},\ \nu^{L,R}_{n,p,capt}\to\infty}$ = 165 mW at j = 10 kA/cm^2.

It should be emphasized that the carrier exchange between the QWs and QDs and between the OCL and QWs cannot be instantaneous in an actual structure — the conditions

$w_{\mathrm{n,p,tunn}}^{L,R} \to \infty$ and $v_{\mathrm{n,p,capt}}^{L,R} \to \infty$ were just used to derive expressions (48) and (49) for the saturation values of j_{th} and P. For the same reason, the limiting case of $w_{\mathrm{n,p,tunn}}^{L,R} \to \infty$ does not describe a structure without the barriers — as discussed in the Introduction and in [1, 2], the carrier capture from the reservoir (be it OCL or QW) into QDs cannot be instantaneous.

3.4. Conclusion

Theory of optical power of a tunneling-injection QD laser has been developed. We have shown that tunneling-injection of electrons and holes into QDs from two separate QWs practically eliminates the adverse effect of the recombination outside QDs on the output power of such a laser. In an ideal device, out-tunneling of each type of carriers from QDs into the opposite-to-injection-side QW should be completely blocked; as a result, the parasitic recombination outside QDs will be suppressed and the LCC will be strictly linear. To scrutinize the potential of a tunneling-injection QD laser for high-power operation and the robustness of an actual device, we allowed for out-tunneling leakage of carriers from QDs. We have complemented our calculations by an analytical model and derived closed-form expressions for the LCC and carrier population in the OCL, QWs, and QDs. We have shown that, even in the presence of out-tunneling leakage in an actual device, the intensity of parasitic recombination outside QDs remains restricted with increasing injection current. Consequently, the LCC becomes increasingly linear, and the slope efficiency grows closer to unity at high injection currents. The linearity is due to the fact that the current paths connecting the opposite sides of the structure lie entirely within QDs — in view of the 3-D confinement in QDs, the out-tunneling fluxes of carriers from dots are limited.

Appendix I

Relationship between the carrier escape time from a QW to a bulk region and the capture velocity from a bulk region to a QW

For definiteness, we consider here electrons. The derivation and expressions for holes are similar. Under thermal equilibrium (no external voltage is applied to the structure and hence no current is injected), the flux $v_{\mathrm{n,capt}} n^{\mathrm{eq}}$ of electron capture from a bulk region (OCL) to a QW is equal to the flux $n_{\mathrm{QW}}^{\mathrm{eq}} / \tau_{\mathrm{n,esc}}$ of the reverse process, i.e., of thermal escape from a QW to a bulk region, to give:

$$\frac{1}{\tau_{\mathrm{n,esc}}} = \frac{n^{\mathrm{eq}}}{n_{\mathrm{QW}}^{\mathrm{eq}}} v_{\mathrm{n,capt}} . \tag{A1}$$

The equilibrium carrier density in a bulk region is

$$n^{\mathrm{eq}} = N_{\mathrm{c}}^{\mathrm{3D}} F_{1/2}\left(\frac{\mu^{\mathrm{eq}} - \Delta E_{\mathrm{c}}}{T} \right), \tag{A2}$$

where $N_{\mathrm{c}}^{\mathrm{3D}}$ is the 3-D effective density of states in the conduction band [see the expression for $N_{\mathrm{c}}^{\mathrm{3D}}$ in the text after (3.2)], $F_{1/2}$ is the Fermi-Dirac integral of order one-half, μ^{eq} is the equilibrium Fermi level (measured from the conduction band edge in a QW), and ΔE_{c} is the conduction band offset between the OCL and a QW (Fig. 3.3).

The closed-form expression for the 2-D equilibrium carrier density in a QW is (see, e.g., [11])

$$n_{\mathrm{QW}}^{\mathrm{eq}} = N_{\mathrm{c}}^{\mathrm{2D}} \ln\left[1 + \exp\left(\frac{\mu^{\mathrm{eq}} - \varepsilon_{\mathrm{n}}^{\mathrm{QW}}}{T} \right) \right], \tag{A3}$$

where $N_{\mathrm{c}}^{\mathrm{2D}}$ is the 2-D effective density of states in a QW [see the expression for $N_{\mathrm{c}}^{\mathrm{2D}}$ in the text after (3.1)] and $\varepsilon_{\mathrm{n}}^{\mathrm{QW}}$ is the energy of the lowest subband edge in a QW (Fig. 3.3).

With (A2) and (A3), (A1) becomes

$$\frac{1}{\tau_{\mathrm{n,esc}}} = \frac{N_{\mathrm{c}}^{3\mathrm{D}}}{N_{\mathrm{c}}^{2\mathrm{D}}} \frac{F_{1/2}\left(\dfrac{\mu^{\mathrm{eq}} - \Delta E_{\mathrm{c}}}{T}\right)}{\ln\left[1 + \exp\left(\dfrac{\mu^{\mathrm{eq}} - \varepsilon_{\mathrm{n}}^{\mathrm{QW}}}{T}\right)\right]} v_{\mathrm{n,capt}} . \tag{A4}$$

Neglecting the difference between the effective masses in a bulk region and a QW, the ratio of the 3-D to 2-D effective density of states can be written as

$$\frac{N_{\mathrm{c}}^{3\mathrm{D}}}{N_{\mathrm{c}}^{2\mathrm{D}}} = \frac{\sqrt{\pi}}{\lambda_{\mathrm{dB,T}}}, \tag{A5}$$

where

$$\lambda_{\mathrm{dB,T}} = \frac{2\pi\hbar}{\sqrt{2m_{\mathrm{c}}T}} \tag{A6}$$

is the thermal de Broglie wavelength, i.e., the de Broglie wavelength of an electron having energy equal to the thermal energy T (alternatively, in an infinitely deep square QW of thickness $\lambda_{\mathrm{dB,T}}/2$, the energy of the lowest quantized level is T).

We can now write (A4) as

$$\frac{1}{\tau_{\mathrm{n,esc}}} = \frac{F_{1/2}\left(\dfrac{\mu^{\mathrm{eq}} - \Delta E_{\mathrm{c}}}{T}\right)}{\ln\left[1 + \exp\left(\dfrac{\mu^{\mathrm{eq}} - \varepsilon_{\mathrm{n}}^{\mathrm{QW}}}{T}\right)\right]} \sqrt{\pi}\, \frac{v_{\mathrm{n,capt}}}{\lambda_{\mathrm{dB,T}}} . \tag{A7}$$

Eq. (A4) [or (A7)] presents the general relationship between the escape time and capture velocity. If both bulk and QW materials are nondegenerate (the Fermi level μ^{eq} is below $\varepsilon_{\mathrm{n}}^{\mathrm{QW}}$ by several T), which is the case of undoped OCL and QW considered here, then

$$F_{1/2}\left(\frac{\mu^{\mathrm{eq}} - \Delta E_{\mathrm{c}}}{T}\right) \approx \exp\left(-\frac{\Delta E_{\mathrm{c}} - \mu^{\mathrm{eq}}}{T}\right), \tag{A8}$$

$$\ln\left[1 + \exp\left(\frac{\mu^{\mathrm{eq}} - \varepsilon_{\mathrm{n}}^{\mathrm{QW}}}{T}\right)\right] \approx \exp\left(-\frac{\varepsilon_{\mathrm{n}}^{\mathrm{QW}} - \mu^{\mathrm{eq}}}{T}\right). \tag{A9}$$

With (A8) and (A9), eq. (3.1) is obtained from (A4), which can also be written in the form of eq. (1.3) of [7].

Appendix II

Quantities n_1^{QW} and p_1^{QW} in the tunneling fluxes of electrons and holes from QDs to a QW

As in Appendix I, we use the detailed balance condition under thermal equilibrium – here, for the fluxes of carrier tunneling from a QW to QDs, $w_{n,tunn} N_S (1 - f_n^{eq}) n_{QW}^{eq}$, and from QDs to a QW, $w_{n,tunn} n_1^{QW} N_S f_n^{eq}$. Thus we obtain

$$n_{QW}^{eq} = n_1^{QW} \frac{f_n^{eq}}{1 - f_n^{eq}}, \tag{A10}$$

where n_{QW}^{eq} is given by (A3) and

$$f_n^{eq} = \frac{1}{\exp\left(\dfrac{\varepsilon_n^{QD} - \mu^{eq}}{T} \right) + 1}, \tag{A11}$$

is the equilibrium occupancy of the energy level ε_n^{QD} in a QD (Fig. 3.3).

With (A3), (A10), and (A11), we have for n_1^{QW}

$$n_1^{QW} = N_c^{2D} \exp\left(\frac{\varepsilon_n^{QD} - \mu^{eq}}{T} \right) \ln\left[1 + \exp\left(\frac{\mu^{eq} - \varepsilon_n^{QW}}{T} \right) \right]. \tag{A12}$$

If a QW material is nondegenerate (which is the case of an undoped QW considered here), we have from (A9) and (A12)

$$n_1^{QW} = N_c^{2D} \exp\left(- \frac{\varepsilon_n^{QW} - \varepsilon_n^{QD}}{T} \right). \tag{A13}$$

The quantity n_1^{QW} (measured in units of cm^{-2}) is a 2-D analog of n_1 (measured in units of cm^{-3}) — while n_1 characterizes the electron excitation from a QW to a bulk region [and thus $\Delta E_c - \varepsilon_n^{QW}$ and N_c^{3D} enter into (3.2)], n_1^{QW} characterizes excitation from a QD to a QW [which is why $\varepsilon_n^{QW} - \varepsilon_n^{QD}$ and N_c^{2D} enter into (A13)].

If the energy level in a QD is in resonance with the subband edge in a QW ($\varepsilon_n^{QD} = \varepsilon_n^{QW}$), eq. (3.3) is obtained from (A13).

Appendix III

Criterion for neglecting the recombination in the OCL

We derive here the criterion for neglecting the recombination flux in the left-hand side of the OCL compared to the hole capture flux from the OCL to the QW [in view of (3.17), also compared to the hole escape flux from the QW to the OCL, $p^L_{\rm QW}/\tau^L_{\rm p,esc}$], i.e., the criterion for holding the inequality

$$b_1 B n_L p_L << v^L_{\rm p,capt} p_L \,, \tag{A14}$$

or, equivalently,

$$b_1 B n_L << v^L_{\rm p,capt} \,. \tag{A15}$$

From (2.6) at the steady-state, we have

$$n_L = \frac{1}{v^L_{\rm n,capt}} \left[\frac{n^L_{\rm QW}}{\tau^L_{\rm n,esc}} + w^L_{\rm n,tunn} N_s (1-f_{\rm n}) n^L_{\rm QW} - w^L_{\rm n,tunn} n_1^{L,{\rm QW}} N_s f_{\rm n} + B_{\rm 2D} n^L_{\rm QW} p^L_{\rm QW} \right]. \tag{A16}$$

Since the left-hand side in (3.19) is positive, the right-hand side should also be positive to give:

$$n^L_{\rm QW} \le \frac{1}{w^L_{\rm n,tunn} N_S (1-f_{\rm n})} \left(\frac{j}{e} + w^L_{\rm n,tunn} n_1^{L,{\rm QW}} N_S f_{\rm n} \right). \tag{A17}$$

Substituting the expression in the right-hand side of (A17) for $n^L_{\rm QW}$ in the first two terms in the right-hand side in (A16), we obtain the following inequality:

$$n_L < \frac{1}{v^L_{\rm n,capt}} \left\{ \left[1 + \frac{1}{\tau^L_{\rm n,esc}} \frac{1}{w^L_{\rm n,tunn} N_S (1-f_{\rm n})} \right] \frac{j}{e} + \frac{1}{\tau^L_{\rm n,esc}} n_1^{L,{\rm QW}} \frac{f_{\rm n}}{1-f_{\rm n}} + B_{\rm 2D} n^L_{\rm QW} p^L_{\rm QW} \right\}. \tag{A18}$$

Substituting $w^L_{\rm p,tunn} p_1^{L,{\rm QW}} N_S f_{\rm p}$ for $B_{\rm 2D} n^L_{\rm QW} p^L_{\rm QW}$ [see (3.20)] in (A18), a stronger inequality is obtained,

$$n_L < \frac{1}{v^L_{\rm n,capt}} \left\{ \left[1 + \frac{1}{\tau^L_{\rm n,esc}} \frac{1}{w^L_{\rm n,tunn} N_S (1-f_{\rm n})} \right] \frac{j}{e} + \frac{1}{\tau^L_{\rm n,esc}} n_1^{L,{\rm QW}} \frac{f_{\rm n}}{1-f_{\rm n}} + w^L_{\rm p,tunn} p_1^{L,{\rm QW}} N_S f_{\rm p} \right\}, \tag{A19}$$

or, by multiplying both sides of (A19) by $b_1 B$,

Table 3.1. Highest injection current densities (second and third columns) satisfying the criteria for neglecting recombination in, respectively, the left- and right-hand sides of the OCL [see (A21) for the left-hand side] at different values of the capture velocity from the OCL to the QWs.

$v^{L,R}_{\mathrm{n,p,capt}}$ (cm/s)	j (A/cm^2)	j (A/cm^2)
3×10^5	7.3×10^6	7.8×10^6
3×10^4	7.9×10^4	8.0×10^4
1×10^4	8.3×10^3	8.9×10^3

$$b_1 B n_L < \frac{b_1 B}{v^L_{\mathrm{n,capt}}} \left\{ \left[1 + \frac{1}{\tau^L_{\mathrm{n,esc}}} \frac{1}{w^L_{\mathrm{n,tunn}} N_S (1 - f_{\mathrm{n}})} \right] \frac{j}{e} + \frac{1}{\tau^L_{\mathrm{n,esc}}} n_1^{L,\mathrm{QW}} \frac{f_{\mathrm{n}}}{1 - f_{\mathrm{n}}} + w^L_{\mathrm{p,tunn}} p_1^{L,\mathrm{QW}} N_S f_{\mathrm{p}} \right\}. \quad \text{(A20)}$$

As seen from (A20), a sufficient condition for holding (A15) is the condition that the right-hand side of (A20) is less than $v^L_{\mathrm{p,capt}}$. Thus we arrive at the following criterion:

$$j << e \frac{\dfrac{v^L_{\mathrm{p,capt}} v^L_{\mathrm{n,capt}}}{b_1 B} - \dfrac{1}{\tau^L_{\mathrm{n,esc}}} n_1^{L,\mathrm{QW}} \dfrac{f_{\mathrm{n}}}{1 - f_{\mathrm{n}}} - w^L_{\mathrm{p,tunn}} p_1^{L,\mathrm{QW}} N_S f_{\mathrm{p}}}{1 + \dfrac{1}{\tau^L_{\mathrm{n,esc}}} \dfrac{1}{w^L_{\mathrm{n,tunn}} N_S (1 - f_{\mathrm{n}})}}. \quad \text{(A21)}$$

The capture velocities to QWs are typically on the order of 10^5 cm/s [7, 12, 13]. The second column in Table I shows the highest injection current density j satisfying (A21) at different values of $v^L_{\mathrm{n,p,\,capt}}$. Even for a low capture velocity of 10^4 cm/s, (A21) satisfies up to j = 8.3 kA/cm2. Hence, criterion (A21) for neglecting the parasitic recombination in the left-hand side of the OCL holds up to very high j; that is to say that the out-tunneling flux of minority carriers from QDs is mainly consumed by the recombination in the QW — this flux practically does not reach the OCL.

The criterion for neglecting the recombination throughout the OCL is given by the strongest of inequality (A21) and a similar inequality for the right-hand side of the structure (the highest j satisfying the inequality for the right-hand side is shown in the third column in Table 3.1).

Appendix IV

Closed-form solutions of the rate equations

As shown in Appendix III, the recombination in the OCL can be neglected up to very high j. Thus eqs. (2.2) and (2.3) are simplified as follows at the steady-state:

$$0 = \frac{j}{e} + \frac{n_{\mathrm{QW}}^{L}}{\tau_{\mathrm{n,esc}}^{L}} - v_{\mathrm{n,capt}}^{L} n_{L}\,, \tag{A22}$$

$$0 = \frac{p_{\mathrm{QW}}^{L}}{\tau_{\mathrm{p,esc}}^{L}} - v_{\mathrm{p,capt}}^{L} p_{L}\,. \tag{A23}$$

From (A23), the minority carrier density in the OCL is expressed in terms of the minority carrier density in the QW,

$$p_{L} = \frac{1}{v_{\mathrm{p,capt}}^{L}\tau_{\mathrm{p,esc}}^{L}}\, p_{\mathrm{QW}}^{L}\,. \tag{A24}$$

From (A22), the majority carrier density in the OCL is expressed in terms of the majority carrier density in the QW,

$$n_{L} = \frac{1}{v_{\mathrm{n,capt}}^{L}\tau_{\mathrm{n,esc}}^{L}}\, n_{\mathrm{QW}}^{L} + \frac{j}{e v_{\mathrm{n,capt}}^{L}}\,. \tag{A25}$$

Substituting $v_{\mathrm{n,capt}}^{L} n_{L} - n_{\mathrm{QW}}^{L} / \tau_{\mathrm{n,esc}}^{L} = j/e$ [see (A22)] in eq. (2.6) at the steady-state, we obtain the following equation relating the 2-D electron and hole densities in the QW:

$$n_{\mathrm{QW}}^{L} = \frac{1}{1 + \dfrac{B_{\mathrm{2D}} p_{\mathrm{QW}}^{L}}{w_{\mathrm{n,\,tunn}}^{L} N_{S} (1 - f_{\mathrm{n}})}} \left[n_{1}^{L,\mathrm{QW}} \frac{f_{\mathrm{n}}}{1 - f_{\mathrm{n}}} + \frac{j}{e w_{\mathrm{n,\,tunn}}^{L} N_{S} (1 - f_{\mathrm{n}})} \right]. \tag{A26}$$

By using (A23) in eq. (2.7) at the steady-state, we obtain the second [in addition to (A26)] equation relating n_{QW}^{L} and p_{QW}^{L},

$$p_{\mathrm{QW}}^{L} = \frac{1}{1 + \dfrac{B_{\mathrm{2D}} n_{\mathrm{QW}}^{L}}{w_{\mathrm{p,tunn}}^{L} N_{S} (1 - f_{\mathrm{p}})}}\, p_{1}^{L,\mathrm{QW}} \frac{f_{\mathrm{p}}}{1 - f_{\mathrm{p}}}\,. \tag{A27}$$

From (A26) and (A27), a quadratic equation in n_{QW}^{L} (or p_{QW}^{L}) is obtained, solution of which gives n_{QW}^{L} and then p_{QW}^{L} as functions of the injection current density j,

$$n_{\mathrm{QW}}^{L}(j)=\frac{1}{2}\Bigg[\Bigg\{\Bigg[n_{1}^{L,\mathrm{QW}}\frac{f_{\mathrm{n}}}{1-f_{\mathrm{n}}}+\frac{j}{ew_{\mathrm{n,tunn}}^{L}N_{S}(1-f_{n})}-\frac{w_{\mathrm{p,tunn}}^{L}}{w_{\mathrm{n,tunn}}^{L}}p_{1}^{L,\mathrm{QW}}\frac{f_{\mathrm{p}}}{1-f_{\mathrm{n}}}-\frac{1}{B_{\mathrm{2D}}}w_{\mathrm{p,tunn}}^{L}N_{S}(1-f_{\mathrm{p}})\Bigg]^{2}$$
$$+4\frac{1}{B_{\mathrm{2D}}}w_{\mathrm{p,tunn}}^{L}N_{S}(1-f_{\mathrm{p}})\Bigg[n_{1}^{L,\mathrm{QW}}\frac{f_{\mathrm{n}}}{1-f_{\mathrm{n}}}+\frac{j}{ew_{\mathrm{n,tunn}}^{L}N_{S}(1-f_{\mathrm{n}})}\Bigg]\Bigg\}^{\frac{1}{2}} \tag{A28}$$
$$+n_{1}^{L,\mathrm{QW}}\frac{f_{\mathrm{n}}}{1-f_{\mathrm{n}}}+\frac{j}{ew_{\mathrm{n,tunn}}^{L}N_{S}(1-f_{\mathrm{n}})}-\frac{w_{\mathrm{p,tunn}}^{L}}{w_{\mathrm{n,tunn}}^{L}}p_{1}^{L,\mathrm{QW}}\frac{f_{\mathrm{p}}}{1-f_{\mathrm{n}}}-\frac{1}{B_{\mathrm{2D}}}w_{\mathrm{p,\,tunn}}^{L}N_{S}(1-f_{\mathrm{p}})\Bigg],$$

$$p_{\mathrm{QW}}^{L}(j)=\frac{1}{2}\Bigg[\Bigg\{\Bigg[p_{1}^{L,\mathrm{QW}}\frac{f_{\mathrm{p}}}{1-f_{\mathrm{p}}}-\frac{j}{ew_{\mathrm{p,tunn}}^{L}N_{S}(1-f_{\mathrm{p}})}-\frac{w_{\mathrm{n,tunn}}^{L}}{w_{\mathrm{p,tunn}}^{L}}n_{1}^{L,\mathrm{QW}}\frac{f_{\mathrm{n}}}{1-f_{\mathrm{p}}}-\frac{1}{B_{\mathrm{2D}}}w_{\mathrm{n,tunn}}^{L}N_{S}(1-f_{\mathrm{n}})\Bigg]^{2}$$
$$+4\frac{1}{B_{\mathrm{2D}}}w_{\mathrm{n,tunn}}^{L}N_{S}(1-f_{\mathrm{n}})p_{1}^{L,\mathrm{QW}}\frac{f_{\mathrm{p}}}{1-f_{\mathrm{p}}}\Bigg\}^{\frac{1}{2}} \tag{A29}$$
$$+p_{1}^{L,\mathrm{QW}}\frac{f_{\mathrm{p}}}{1-f_{\mathrm{p}}}-\frac{j}{ew_{\mathrm{p,tunn}}^{L}N_{S}(1-f_{\mathrm{p}})}-\frac{w_{\mathrm{n,tunn}}^{L}}{w_{\mathrm{p,tunn}}^{L}}n_{1}^{L,\mathrm{QW}}\frac{f_{\mathrm{n}}}{1-f_{\mathrm{p}}}-\frac{1}{B_{\mathrm{2D}}}w_{\mathrm{n,tunn}}^{L}N_{S}(1-f_{\mathrm{n}})\Bigg].$$

By using (A24), (A25), (A28), (A29), and similar expressions for the carrier densities in the right-hand side of the structure, a closed-form expression for the LCC is obtained from (3.12).

By analyzing eq. (3.28) in the general case, we already showed that the minority carrier density in the QW decreases with increasing j (Fig. 3.6). This result can also be easily obtained from (3.18). Neglecting the recombination flux in the OCL in (3.18), we get

$$w_{\mathrm{p,tunn}}^{L}N_{S}(1-f_{\mathrm{p}})p_{\mathrm{QW}}^{L}+B_{\mathrm{2D}}n_{\mathrm{QW}}^{L}p_{\mathrm{QW}}^{L}=w_{\mathrm{p,tunn}}^{L}p_{1}^{L,\mathrm{QW}}N_{S}f_{\mathrm{p}}\,. \tag{A30}$$

The right-hand side of (A30) remains limited (constant if charge neutrality holds in QDs) with j. Since the majority carrier density (n_{QW}^{L}) should increase with j (Fig. 3.8), keeping limited the left-hand side of (A30) requires decreasing p_{QW}^{L}. The decrease of p_{QW}^{L} with j can also be seen from the analytical expression (A29).

REFERENCES[*)]

[A1] D.-S. Han and L. V. Asryan, "Tunneling-injection of electrons and holes into quantum dots: A tool for high-power lasing," *Appl. Phys. Lett.*, vol. 92, no. 25, pp. 251113-1–251113-3, June 2008.

[A2] D.-S. Han and L. V. Asryan, "Light-current curve of a tunneling-injection quantum dot laser," *Proc. SPIE*, vol. 6902, pp. B9020-1–B9020-12, Jan. 2008.

[A3] D.-S. Han and L. V. Asryan, "Output power of a tunneling-injection quantum dot laser," under review.

[1] L. V. Asryan, S. Luryi, and R. A. Suris, "Intrinsic nonlinearity of light-current characteristic of semiconductor lasers with a quantum-confined active region," *Appl. Phys. Lett.*, vol. 81, no. 12, pp. 2154–2156, Sept. 2002.

[2] L. V. Asryan, S. Luryi, and R. A. Suris, "Internal efficiency of semiconductor lasers with a quantum-confined active region," *IEEE J. Quantum Electron.*, vol. 39, no. 3, pp. 404–418, Mar. 2003.

[3] D. Bimberg, M. Grundmann, F. Heinrichsdorff, N. N. Ledentsov, V. M. Ustinov, A. E. Zhukov, A. R. Kovsh, M. V. Maximov, Y. M. Shernyakov, B. V. Volovik, A. F. Tsatsul'nikov, P. S. Kop'ev, and Zh. I. Alferov, "Quantum dot lasers: breakthrough in optoelectronics," *Thin Solid Films,* vol. 367, no. 1, pp. 235-249, May 2000.

[4] L. V. Asryan and S. Luryi, "Tunneling-injection quantum-dot laser: ultrahigh temperature stability," *IEEE J. Quantum Electron.*, vol. 37, no. 7, pp. 905–910, Jul. 2001.

[5] L. V. Asryan and S. Luryi, "Temperature-insensitive semiconductor quantum dot laser," *Solid-State Electron.*, vol. 47, no. 2, pp. 205–212, Feb. 2003.

[6] L. V. Asryan and S. Luryi, "Semiconductor laser with reduced temperature sensitivity," U.S. Patent 6 870 178 B2, Mar. 22, 2005.

[*)] "A" in the reference number indicates the publications of the author of this dissertation.

[7] I. N. Yassievich, K. Schmalz, and M. Beer, “Capture and emission of carriers in semiconductor quantum wells,’ *Semicond. Sci. Technol.*, vol. 9, no. 10, pp. 1763–1774, Oct. 1994.

[8] C.-Y. Tsai, Y. H. Lo, R. M. Spencer, and L. F. Eastman, “Nonlinear gain coefficients in semiconductor quantum-well lasers: Effects of carrier diffusion, capture, and escape,” *IEEE J. Select. Topics Quantum Electron.*, vol. 1, no. 2, pp. 316-330, June 1995.

[9] L. V. Asryan and R. A. Suris, “Charge neutrality violation in quantum-dot lasers,” *IEEE J. Select. Topics Quantum Electron.*, vol. 3, no. 2, pp. 148–157, Apr. 1997.

[10] L. V. Asryan and R. A. Suris, “Temperature dependence of the threshold current density of a quantum dot laser,” *IEEE J. Quantum Electron.*, vol. 34, no. 5, pp. 841–850, May 1998.

[11] K. J. Vahala and C. E. Zah, “Effect of doping on the optical gain and the spontaneous noise enhancement factor in quantum well amplifiers and lasers studied by simple analytical expressions,” *Appl*. *Phys*. *Lett*., vol. 52, no. 23, pp. 1945–1947, Jun. 1988.

[12] S. A. Solov'ev, I. N. Yassievich, and V. M. Chistyakov, “Capture of carriers in quantum-wells and thermal emission of carriers in III-V semiconductors,” *Semiconductors*, vol. 29, no. 7, pp. 654–660, Jul. 1995.

[13] A. Dargys and J. Kundrotas, “Impact ionization of excitons by hot carriers in quantum wells,” *Semicond*. *Sci*. *Technol*., vol. 13, no. 11, pp. 1258–1261, Nov. 1998.

Chapter 4

Effect of the Wetting Layer on the Output Power of a Tunneling-Injection Quantum Dot Laser

Summary

To suppress bipolar population and hence electron-hole recombination outside quantum dots (QDs), tunneling-injection of electrons and holes into QDs from two separate quantum wells was proposed earlier. Close-to-ideal operating characteristics were predicted for such a tunneling-injection laser. In the Stranski-Krastanow growth mode, a two-dimensional wetting layer (WL) is initially grown followed by the formation of QDs. Due to thermal escape of carriers from QDs, there will be bipolar population and hence electron-hole recombination in the WL, even in a tunneling-injection structure. In this chapter, the light-current characteristic (LCC) of a tunneling-injection QD laser is studied in the presence of the WL. Since *(i)* the opposite sides of a tunneling-injection structure are only connected by the current paths through QDs and *(ii)* the WL is located in the n-side of the structure, the only source of holes for the WL is provided by QDs. It is shown that, due to the zero-dimensional nature of QDs, the rate of the hole supply to the WL remains limited with increasing injection current. For this reason, as in the other parts of the structure outside QDs (quantum wells and optical confinement layer), the parasitic electron-hole recombination remains restricted in the WL. As a result, even in the presence of the WL, the LCC of a tunneling-injection QD laser becomes increasingly linear at high injection currents, which is a further demonstration of the potential of such a laser for high-power operation.

4.1. Introduction

Semiconductor quantum dots (QDs) can be conveniently used as an active medium for stimulated emission in injection lasers [1]-[7]. Conventionally, QDs are grown by a strain-induced island formation method, which is called as the Stranski-Krastanow growth mode [8]. In the Stranski-Krastanow growth mode, several monolayers of one material are grown first on a

crystal surface of another material (substrate) having a different lattice constant. Beyond a critical thickness of the deposited layer, three-dimensional (3-D) islands (QDs) start forming from two-dimensional (2-D) monolayers thus partially relaxing the strain and reducing the elastic energy. The initially grown monolayers are called as the wetting layer (WL). Hence, the 2-D WL is inherently present in self-assembled Stranski-Krastanow grown QD structures [9]-[13]. Fig. 4.1 shows the TEM image of self-assembled Stranski-Krastanow grown QDs and the WL.

In the conventional design of QD lasers, the carriers are first injected from the cladding layers into the optical confinement layer (OCL), and then captured into the WL and QDs (Fig. 4.2). A certain fraction of carriers thermally escapes back from QDs to the WL and OCL. Due to bipolar (both electron and hole) population in the OCL and WL, parasitic electron-hole recombination occurs there [14]–[16] in addition to recombination in QDs.

To suppress the parasitic recombination outside QDs, tunneling-injection of both electrons and holes into QDs was proposed [17]-[19]. As shown in chapter 3, in such a tunneling injection QD laser, the parasitic recombination rate remains restricted even if there is out-tunneling leakage of carriers from QDs [A1]-[A3][*)]. As a result, the light-current characteristic (LCC) of a tunneling-injection QD laser is essentially linear. No WL was assumed in the structures of [17]-[19], [A1]-[A3]. If the Stranski-Krastanow mode is used for the growth of QDs, the WL should be properly taken into account. As seen from Fig. 4.3, even if there is no tunneling between the electron-injecting quantum well (QW) and the WL, there will be bipolar population in the WL. This is because (*i*) there is such population in QDs (which is maintained to have stimulated emission) and (*ii*) the WL is coupled to QDs by the processes of thermal escape and capture. Besides, while QDs present the sole source for the hole supply to the WL, electrons can directly tunnel to the WL from the electron-injecting QW (Fig. 4.3). Hence, even in an ideal case of total suppression of parasitic recombination in the QWs and OCL, such recombination will occur in the WL [A4, A5].

In this chapter, we develop a theoretical model for the optical power of a tunneling-injection QD laser, which includes the WL and processes therein.

[*)] "A" in the reference number indicates the publications of the author of this dissertation.

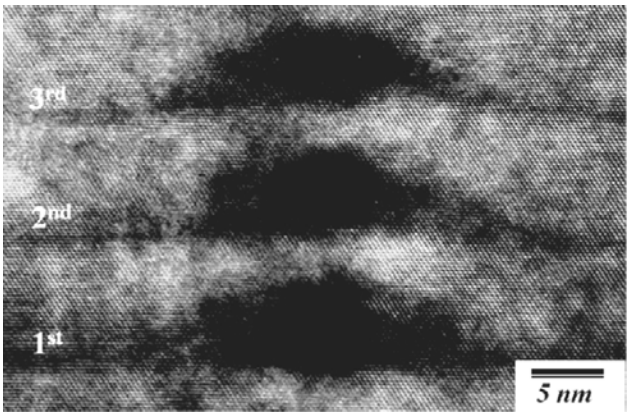

Fig. 4.1. Cross-sectional bright field image of vertically aligned InAs/GaAs QD layers with the WLs. (Reprinted from Fig. 5 of ref. [13], Copyright (2009), with permission from Elsevier.)

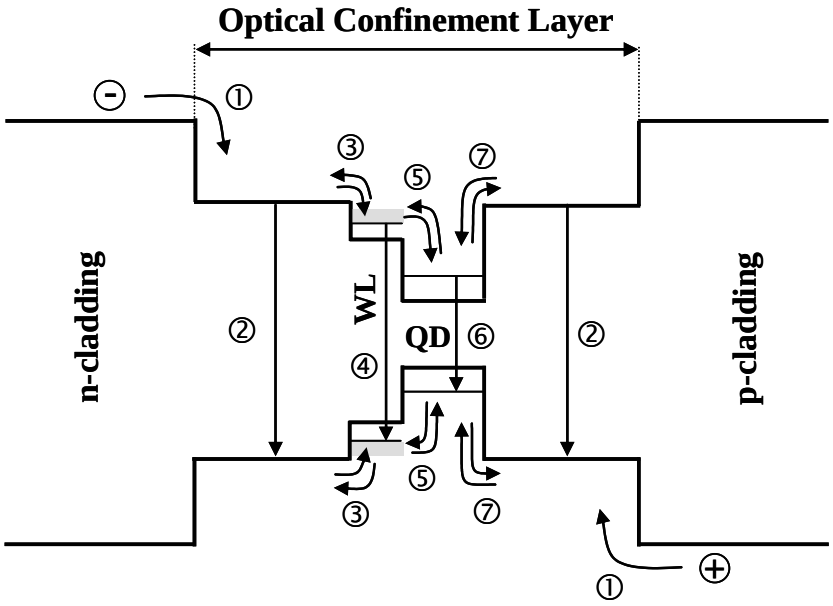

Fig. 4.2. Energy band diagram of a conventional QD laser with the WL and the main processes: ① carrier injection from the cladding layers to the OCL, ② spontaneous recombination in the OCL, ③ carrier capture from the OCL to the WL and thermal escape from the WL to the OCL, ④ spontaneous recombination in the WL, ⑤ carrier capture from the WL into a QD and thermal escape from a QD to the WL, ⑥ spontaneous and stimulated recombination in a QD, ⑦ carrier capture from the OCL into a QD and thermal escape from a QD to the OCL.

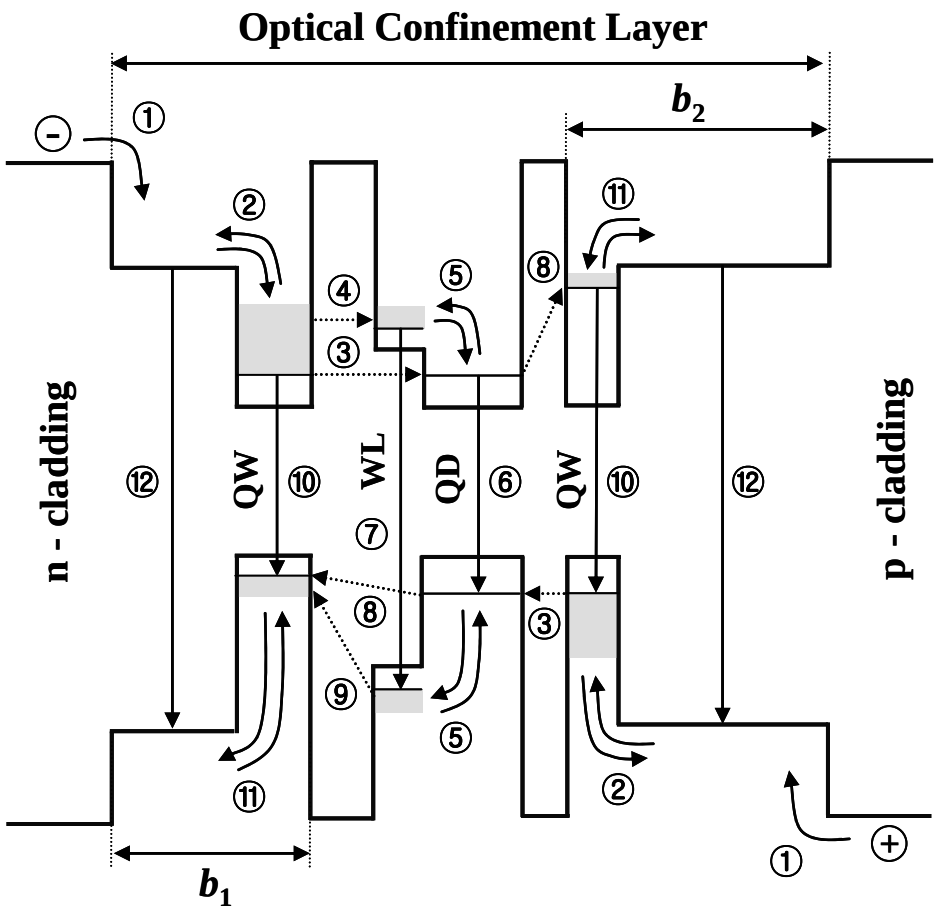

Fig. 4.3. Energy band diagram of a tunneling-injection QD laser with the WL and the main processes: ① carrier injection from the cladding layers to the OCL, ② majority carrier capture from the OCL to the QW and thermal escape from the QW to the OCL, ③ majority carrier tunneling-injection from the QW into a QD, ④ electron tunneling from the QW to the WL, ⑤ thermal escape from a QD to the WL and capture from the WL into a QD, ⑥ spontaneous and stimulated recombination in a QD, ⑦ spontaneous recombination in the WL, ⑧ out-tunneling from a QD into the "foreign" QW, ⑨ hole tunneling from the WL into the electron-injecting QW, ⑩ spontaneous recombination in the QWs, ⑪ minority carrier thermal escape from the QW to the OCL and capture from the OCL to the QW, and ⑫ spontaneous recombination in the OCL.

4.2. Theoretical model

Fig. 4.3 shows the energy band diagram of a tunneling-injection QD laser with the WL, which follows the barrier separating the electron-injecting QW from QDs. As seen from the figure, the holes can only be supplied to the WL by thermal escapes from QDs. In contrast, in addition to thermal escapes from QDs, electrons can directly tunnel to the WL from the left-hand-side (electron-injecting) QW.

We assume that the material separating QDs in the QD layer (it may be the same as the material of barriers) has high enough bandgap to suppress all tunneling other than via QDs, in particular, tunneling between the QWs, and between the hole-injecting (right-hand side) QW and the WL. Hence, the opposite sides of the structure are only connected to each other by the current paths through QDs.

We use the following set of rate equations:

for free electrons and holes in the left-hand side of the OCL,

$$b_1 \frac{\partial n_L}{\partial t} = \frac{j}{e} + \frac{n_{\mathrm{QW}}^L}{\tau_{\mathrm{n,esc}}^L} - v_{\mathrm{n,capt}}^L n_L - b_1 B n_L p_L , \tag{4.1}$$

$$b_1 \frac{\partial p_L}{\partial t} = \frac{p_{\mathrm{QW}}^L}{\tau_{\mathrm{p,esc}}^L} - v_{\mathrm{p,capt}}^L p_L - b_1 B n_L p_L , \tag{4.2}$$

for free holes and electrons in the right-hand side of the OCL,

$$b_2 \frac{\partial p_R}{\partial t} = \frac{j}{e} + \frac{p_{\mathrm{QW}}^R}{\tau_{\mathrm{p,esc}}^R} - v_{\mathrm{p,capt}}^R p_R - b_2 B n_R p_R , \tag{4.3}$$

$$b_2 \frac{\partial n_R}{\partial t} = \frac{n_{\mathrm{QW}}^R}{\tau_{\mathrm{n,esc}}^R} - v_{\mathrm{n,capt}}^R n_R - b_2 B n_R p_R , \tag{4.4}$$

for electrons and holes in the electron-injecting (left-hand-side) QW,

$$\begin{aligned} \frac{\partial n_{\mathrm{QW}}^L}{\partial t} = {} & v_{\mathrm{n,capt}}^L n_L - \frac{n_{\mathrm{QW}}^L}{\tau_{\mathrm{n,esc}}^L} - w_{\mathrm{n,\,tunn}}^L N_S (1 - f_{\mathrm{n}}) n_{\mathrm{QW}}^L + w_{\mathrm{n,tunn}}^L n_1^{L,\mathrm{QW}} N_S f_{\mathrm{n}} \\ & - w_{\mathrm{n,\,tunn}}^{\mathrm{QW}\leftrightarrow\mathrm{WL}} \tilde{n}_1^{\mathrm{WL}} n_{\mathrm{QW}}^L + w_{\mathrm{n,\,tunn}}^{\mathrm{QW}\leftrightarrow\mathrm{WL}} N_{\mathrm{c,2D}}^{\mathrm{QW}} n_{\mathrm{WL}} - B_{\mathrm{2D}} n_{\mathrm{QW}}^L p_{\mathrm{QW}}^L , \end{aligned} \tag{4.5}$$

$$\frac{\partial p_{\mathrm{QW}}^{L}}{\partial t} = v_{\mathrm{p,capt}}^{L} p_{L} - \frac{p_{\mathrm{QW}}^{L}}{\tau_{\mathrm{p,esc}}^{L}} - w_{\mathrm{p,tunn}}^{L} N_{S}(1-f_{\mathrm{p}}) p_{\mathrm{QW}}^{L} + w_{\mathrm{p,tunn}}^{L} p_{1}^{L,\mathrm{QW}} N_{S} f_{\mathrm{p}} - w_{\mathrm{p,\,tunn}}^{\mathrm{QW}\leftrightarrow\mathrm{WL}} \widetilde{p}_{1}^{\mathrm{WL}} p_{\mathrm{QW}}^{L} + w_{\mathrm{p,\,tunn}}^{\mathrm{QW}\leftrightarrow\mathrm{WL}} N_{\mathrm{v,2D}}^{\mathrm{QW}} p_{\mathrm{WL}} - B_{\mathrm{2D}} n_{\mathrm{QW}}^{L} p_{\mathrm{QW}}^{L}, \tag{4.6}$$

for holes and electrons in the hole-injecting (right-hand-side) QW,

$$\frac{\partial p_{\mathrm{QW}}^{R}}{\partial t} = v_{\mathrm{p,capt}}^{R} p_{R} - \frac{p_{\mathrm{QW}}^{R}}{\tau_{\mathrm{p,esc}}^{R}} - w_{\mathrm{p,tunn}}^{R} N_{S}(1-f_{\mathrm{p}}) p_{\mathrm{QW}}^{R} + w_{\mathrm{p,tunn}}^{R} p_{1}^{R,\mathrm{QW}} N_{S} f_{\mathrm{p}} - B_{\mathrm{2D}} n_{\mathrm{QW}}^{R} p_{\mathrm{QW}}^{R}, \tag{4.7}$$

$$\frac{\partial n_{\mathrm{QW}}^{R}}{\partial t} = v_{\mathrm{n,capt}}^{R} n_{R} - \frac{n_{\mathrm{QW}}^{R}}{\tau_{\mathrm{n,esc}}^{R}} - w_{\mathrm{n,tunn}}^{R} N_{S}(1-f_{\mathrm{n}}) n_{\mathrm{QW}}^{R} + w_{\mathrm{n,tunn}}^{R} n_{1}^{R,\mathrm{QW}} N_{S} f_{\mathrm{n}} - B_{\mathrm{2D}} n_{\mathrm{QW}}^{R} p_{\mathrm{QW}}^{R}, \tag{4.8}$$

for electrons and holes confined in QDs,

$$\begin{aligned} N_{S}\frac{\partial f_{\mathrm{n}}}{\partial t} &= w_{\mathrm{n,tunn}}^{L} N_{S}(1-f_{\mathrm{n}}) n_{\mathrm{QW}}^{L} - w_{\mathrm{n,tunn}}^{L} n_{1}^{L,\mathrm{QW}} N_{S} f_{\mathrm{n}} + w_{\mathrm{n,tunn}}^{R} N_{S}(1-f_{\mathrm{n}}) n_{\mathrm{QW}}^{R} - w_{\mathrm{n,tunn}}^{R} n_{1}^{R,\mathrm{QW}} N_{S} f_{\mathrm{n}} \\ &+ w_{\mathrm{n,capt}} N_{S}(1-f_{\mathrm{n}}) n_{\mathrm{WL}} - w_{\mathrm{n,capt}} n_{1}^{\mathrm{WL}} N_{S} f_{\mathrm{n}} - N_{S}\frac{f_{\mathrm{n}} f_{\mathrm{p}}}{\tau_{\mathrm{QD}}} - \frac{c}{\sqrt{\epsilon_{\mathrm{g}}}}\frac{g^{\max}}{S}(f_{\mathrm{n}}+f_{\mathrm{p}}-1)N, \end{aligned} \tag{4.9}$$

$$\begin{aligned} N_{S}\frac{\partial f_{\mathrm{p}}}{\partial t} &= w_{\mathrm{p,tunn}}^{R} N_{S}(1-f_{\mathrm{p}}) p_{\mathrm{QW}}^{R} - w_{\mathrm{p,tunn}}^{R} p_{1}^{R,\mathrm{QW}} N_{S} f_{\mathrm{p}} + w_{\mathrm{p,tunn}}^{L} N_{S}(1-f_{\mathrm{p}}) p_{\mathrm{QW}}^{L} - w_{\mathrm{p,tunn}}^{L} p_{1}^{L,\mathrm{QW}} N_{S} f_{\mathrm{p}} \\ &+ w_{\mathrm{p,capt}} N_{S}(1-f_{\mathrm{p}}) p_{\mathrm{WL}} - w_{\mathrm{p,capt}} p_{1}^{\mathrm{WL}} N_{S} f_{\mathrm{p}} - N_{S}\frac{f_{\mathrm{n}} f_{\mathrm{p}}}{\tau_{\mathrm{QD}}} - \frac{c}{\sqrt{\epsilon_{g}}}\frac{g^{\max}}{S}(f_{\mathrm{n}}+f_{\mathrm{p}}-1)N, \end{aligned} \tag{4.10}$$

for electrons and holes in the WL,

$$\begin{aligned} \frac{\partial n_{\mathrm{WL}}}{\partial t} &= w_{\mathrm{n,capt}} n_{1}^{\mathrm{WL}} N_{S} f_{\mathrm{n}} - w_{\mathrm{n,capt}} N_{S}(1-f_{\mathrm{n}}) n_{\mathrm{WL}} \\ &+ w_{\mathrm{n,\,tunn}}^{\mathrm{QW}\leftrightarrow\mathrm{WL}} \widetilde{n}_{1}^{\mathrm{WL}} n_{\mathrm{QW}}^{L} - w_{\mathrm{n,\,tunn}}^{\mathrm{QW}\leftrightarrow\mathrm{WL}} N_{\mathrm{c,2D}}^{\mathrm{QW}} n_{\mathrm{WL}} - B_{\mathrm{2D}} n_{\mathrm{WL}} p_{\mathrm{WL}}, \end{aligned} \tag{4.11}$$

$$\begin{aligned} \frac{\partial p_{\mathrm{WL}}}{\partial t} &= w_{\mathrm{p,capt}} p_{1}^{\mathrm{WL}} N_{S} f_{\mathrm{p}} - w_{\mathrm{p,capt}} N_{S}\left(1-f_{\mathrm{p}}\right) p_{\mathrm{WL}} \\ &+ w_{\mathrm{p,\,tunn}}^{\mathrm{QW}\leftrightarrow\mathrm{WL}} \widetilde{p}_{1}^{\mathrm{WL}} p_{\mathrm{QW}}^{L} - w_{\mathrm{p,\,tunn}}^{\mathrm{QW}\leftrightarrow\mathrm{WL}} N_{\mathrm{v,2D}}^{\mathrm{QW}} p_{\mathrm{WL}} - B_{\mathrm{2D}} n_{\mathrm{WL}} p_{\mathrm{WL}}, \end{aligned} \tag{4.12}$$

and for photons,

$$\frac{\partial N}{\partial t} = \frac{c}{\sqrt{\epsilon_{g}}} g^{\max}(f_{\mathrm{n}}+f_{\mathrm{p}}-1)N - \frac{c}{\sqrt{\epsilon_{g}}}\beta N. \tag{4.13}$$

In eqs. (4.1)-(4.13), b_1 (b_2) is the thickness of the left- (right-) hand side of the OCL [the separation between the n- (p-) cladding layer and the left- (right-) hand-side barrier – Fig. 4.3] and n_L (n_R) and p_L (p_R) are the free-electron and -hole densities there, j is the injection current density, e is the electron charge, $n_{\rm QW}^{L}$ ($n_{\rm QW}^{R}$) and $p_{\rm QW}^{L}$ ($p_{\rm QW}^{R}$) are the 2-D electron and hole densities in the left- (right-) hand-side QW (Fig. 4.3), $n_{\rm WL}$ and $p_{\rm WL}$ are the 2-D electron and hole densities in the WL, B and $B_{\rm 2D}$ are the spontaneous radiative recombination constants for the bulk (OCL) and 2-D regions (QWs and WL) measured in units of cm^3/s and cm^2/s, respectively, N_S is the surface density of QDs, $f_{\rm n,p}$ are the electron- and hole-level occupancies in QDs, $\tau_{\rm QD}$ is the spontaneous radiative lifetime in QDs, c is the velocity of light in vacuum, $\sqrt{\epsilon_g}$ is the group index of the dispersive OCL material, $g^{\rm max}$ is the maximum value of the modal gain [14], $S = WL$ is the cross-section of the junction, W is the lateral size of the device, L is the cavity length, $\beta = (1/L)\ln(1/R)$ is the mirror loss, R is the facet reflectivity, and N is the number of photons in the lasing mode; $\tau_{\rm n,p,esc}^{L,R}$ are the thermal escape times of electrons and holes from the QWs to the OCL and $v_{\rm n,p,capt}^{L,R}$ are the capture velocities from the OCL to the QWs.

We exploit six tunneling coefficients (measured in units of cm^2/s) – these are four coefficients $w_{\rm n,p,tunn}^{L,R}$ for electron and hole tunneling between the QD ensemble and the QWs, and two coefficients $w_{\rm n,p\,tunn}^{\rm QW\leftrightarrow WL}$ for electron and hole tunneling between the WL and the electron-injecting QW. These tunneling coefficients are primarily controlled by the thicknesses and material parameters of the barriers, and by the QD, QW, and WL parameters as well.

The quantities $n_1^{L,R,\rm QW}$ and $p_1^{L,R,\rm QW}$ entering into the electron and hole tunneling fluxes from the QD ensemble to the QWs [see (4.5)-(4.10)] are measured in units of cm^{-2}. In the case of an undoped QW and a resonance between the energy level in a QD and the lowest subband edge in a QW,

$$n_1^{L,\rm QW} = N_{\rm c,2D}^{\rm QW}, \qquad p_1^{R,\rm QW} = N_{\rm v,2D}^{\rm QW}, \tag{4.14}$$

where $N_{\rm c,v,2D}^{\rm QW} = m_{\rm c,v}^{\rm QW} T/\left(\pi\hbar^2\right)$ are the 2-D effective densities of states in the conduction and valence bands in the QWs, $m_{\rm c,v}^{\rm QW}$ are the electron and hole effective masses in the QWs, and the temperature T is measured in units of energy.

The terms $w_{\mathrm{n,\,tunn}}^{\mathrm{QW}\leftrightarrow\mathrm{WL}}\widetilde{n}_1^{\mathrm{WL}}n_{\mathrm{QW}}^{L}$ and $w_{\mathrm{n,\,tunn}}^{\mathrm{QW}\leftrightarrow\mathrm{WL}}N_{\mathrm{c,2D}}^{\mathrm{QW}}n_{\mathrm{WL}}$ in the right-hand side in (4.5) and (4.11) are the fluxes of electron tunneling from the electron-injecting QW to the WL and backward tunneling from the WL to the electron-injecting QW, respectively. The difference $w_{\mathrm{n,\,tunn}}^{\mathrm{QW}\leftrightarrow\mathrm{WL}}\widetilde{n}_1^{\mathrm{WL}}n_{\mathrm{QW}}^{L}-w_{\mathrm{n,\,tunn}}^{\mathrm{QW}\leftrightarrow\mathrm{WL}}N_{\mathrm{c,2D}}^{\mathrm{QW}}n_{\mathrm{WL}}$ is the net in-tunneling flux of electrons from the electron-injecting QW to the WL.

The quantities $\widetilde{n}_1^{\mathrm{WL}}$ and $\widetilde{p}_1^{\mathrm{WL}}$ entering into the electron and hole tunneling fluxes from the electron-injecting QW to the WL [see (4.5), (4.6), (4.11), and (4.12)] are measured in units of cm^{-2}. The general expressions for $\widetilde{n}_1^{\mathrm{WL}}$ and $\widetilde{p}_1^{\mathrm{WL}}$ are derived in Appendix I [see eq. (A3)]. In the case of undoped QW and WL considered here,

$$\widetilde{n}_1^{\mathrm{WL}}=N_{\mathrm{c,2D}}^{\mathrm{WL}}\exp\left(-\frac{\varepsilon_{\mathrm{n}}^{\mathrm{WL}}-\varepsilon_{\mathrm{n}}^{\mathrm{QW}}}{T}\right),\qquad \widetilde{p}_1^{\mathrm{WL}}=N_{\mathrm{v,2D}}^{\mathrm{WL}}\exp\left(-\frac{\varepsilon_{\mathrm{p}}^{\mathrm{WL}}-\varepsilon_{\mathrm{p}}^{\mathrm{QW}}}{T}\right), \tag{4.15}$$

where $\varepsilon_{\mathrm{n,p}}^{\mathrm{WL}}$ and $\varepsilon_{\mathrm{n,p}}^{\mathrm{QW}}$ are the energies of the lowest electron- and hole-subband edges in the WL and QW, respectively, $N_{\mathrm{c,v,2D}}^{\mathrm{WL}}=m_{\mathrm{c,v}}^{\mathrm{WL}}T/\left(\pi\hbar^2\right)$ are the 2-D effective densities of states in the conduction and valence bands in the WL, and $m_{\mathrm{c,v}}^{\mathrm{WL}}$ are the electron and hole effective masses in the WL.

The terms $w_{\mathrm{n,capt}}n_1^{\mathrm{WL}}N_S f_{\mathrm{n}}$ and $w_{\mathrm{n,capt}}N_S(1-f_{\mathrm{n}})n_{\mathrm{WL}}$ in the right-hand side in (4.9) and (4.11) are the fluxes of thermal escape of electrons from QDs to the WL and capture from the WL into QDs, respectively. The difference $w_{\mathrm{n,capt}}n_1^{\mathrm{WL}}N_S f_{\mathrm{n}}-w_{\mathrm{n,capt}}N_S(1-f_{\mathrm{n}})n_{\mathrm{WL}}$ is the net electron escape flux from QDs to the WL. The coefficients $w_{\mathrm{n,p,\,capt}}$ in (4.9)-(4.12) describe the electron and hole capture from the WL into a QD and escape from a QD to the WL. They are measured in units of cm^2/s and were referred to as the temporal cross-sections in [20, 21].

The quantities n_1^{WL} and p_1^{WL} entering into the electron and hole thermal escape fluxes from QDs to the WL [see (4.9)-(4.12)] are measured in units of cm^{-2}. The general expressions for n_1^{WL} and p_1^{WL} are derived in Appendix II [see eq. (A7)]. In the case of an undoped WL,

$$n_1^{\mathrm{WL}}=N_{\mathrm{c,2D}}^{\mathrm{WL}}\exp\left(-\frac{\varepsilon_{\mathrm{n}}^{\mathrm{WL}}-\varepsilon_{\mathrm{n}}^{\mathrm{QD}}}{T}\right),\qquad p_1^{\mathrm{WL}}=N_{\mathrm{v,2D}}^{\mathrm{WL}}\exp\left(-\frac{\varepsilon_{\mathrm{p}}^{\mathrm{WL}}-\varepsilon_{\mathrm{p}}^{\mathrm{QD}}}{T}\right), \tag{4.16}$$

where $\varepsilon_{\mathrm{n,p}}^{\mathrm{QD}}$ are the energies of the electron and hole levels in a QD.

The last term in the right-hand side in (4.11) is the spontaneous radiative recombination flux in the WL.

The terms describing the processes related to the WL for holes in (4.6), (4.10), and (4.12) are similar to those for electrons in (4.5), (4.9), and (4.11).

4.3. Results and discussion

We consider a continuous-wave operation of the laser and correspondingly use the set of rate equations (4.1)-(4.13) at the steady-state,

$$\frac{\partial}{\partial t}\left(b_1 n_L, b_1 p_L, b_2 n_R, b_2 p_R, n_{\mathrm{QW}}^L, p_{\mathrm{QW}}^L, n_{\mathrm{QW}}^R, p_{\mathrm{QW}}^R, n_{\mathrm{WL}}, p_{\mathrm{WL}}, N_S f_{\mathrm{n}}, N_S f_{\mathrm{p}}, N\right) = 0 . \tag{4.17}$$

It can be shown that only eleven out of twelve equations (4.1)–(4.12) are independent at the steady-state. Hence, to solve the set, we should complement it by one more equation. The equation is provided by the charge neutrality condition in QDs.

Above the lasing threshold, the number of stimulated photons is nonvanishing ($N \neq 0$). To satisfy eq. (4.13) at the steady-state at nonvanishing *N*, the following lasing condition should hold:

$$g^{\max}\left(f_{\mathrm{n}} + f_{\mathrm{p}} - 1\right) = \beta , \tag{4.18}$$

which is the condition of equality of the modal gain to the mirror loss at and above the lasing threshold (the internal optical loss is not considered here).

If charge neutrality holds in QDs ($f_{\mathrm{n}} = f_{\mathrm{p}}$), we immediately obtain from (4.18) that the level occupancies in QDs are pinned at their threshold value and do not depend on the injection current density *j*,

$$f_{\mathrm{n}} = f_{\mathrm{p}} = \frac{1}{2}\left(1 + \frac{\beta}{g^{\max}}\right) = \mathrm{const}(j) . \tag{4.19}$$

Since the opposite sides of the structure are only connected to each other by the current paths through QDs, the fact, that $f_{\mathrm{n,p}}$ do not change with *j*, means that the steady-state rate equations for the left- and right-hand sides of the structure present two independent sets. Hence, the solutions of the rate equations (4.3), (4.4), (4.7) and (4.8) for the right-hand side of the structure are unaffected by the presence of the WL.

Using the steady-state rate equations, the following expression is obtained for the number of photons N and output power P from the rate equations:

$$P = \hbar\omega \frac{c}{\sqrt{\in_{\mathrm{g}}}} \beta N$$
$$= \frac{\hbar\omega}{e} S \left(j - eN_S \frac{f_{\mathrm{n}} f_{\mathrm{p}}}{\tau_{\mathrm{QD}}} - eB_{\mathrm{2D}} n_{\mathrm{WL}} p_{\mathrm{WL}} - eB_{\mathrm{2D}} n_{\mathrm{QW}}^{L} p_{\mathrm{QW}}^{L} - eB_{\mathrm{2D}} n_{\mathrm{QW}}^{R} p_{\mathrm{QW}}^{R} - eb_1 B n_L p_L - eb_2 B n_R p_R \right) \quad (4.20)$$

where $\hbar\omega$ is the photon energy. Eq. (4.20) states that the stimulated emission is produced by an excess of the injection current density j over the current densities of spontaneous recombination in QDs (second term in the brackets), WL (third term), QWs (fourth and fifth terms), and OCL (last two terms).

To calculate the LCC [i.e., P versus j given by (4.20)], the dependences of the carrier densities on the injection current density j are found from the solution of the rate equations.

As seen from Fig. 4.4(a), the electron density n_{WL} in the WL increases with j, which is due to the increase of the electron density n_{QW}^{L} in the electron-injecting QW [Fig. 4.5(a)]. At the same time, the hole densities p_{WL} and p_{QW}^{L} decrease [Figs. 4.4(a) and 4.5(b)] [see also the text after eq. (4.34)]. The electron densities increase faster than the hole densities decrease. For this reason, the recombination current densities increase with j [Figs. 4.4(b) and 4.5(c)].

Since the WL consumes a certain fraction of electrons from the electron-injecting QW, the electron density in the latter is reduced compared to the case of no WL [Fig. 4.5(a)]. At the same time, the hole density in the electron-injecting QW is increased [Fig. 4.5(b)]. This is because the holes from the WL tunnel to the electron-injecting QW in addition to the holes from QDs. At high injection currents, the increase of p_{QW}^{L} due to the presence of the WL outweighs the decrease of n_{QW}^{L}. As a result, the recombination current density j_{QW}^{L} in the electron-injecting QW is increased [Fig. 4.5(c)].

Hence, not only an additional electron-hole recombination channel appears [Fig. 4.4(b)], but the recombination in the electron-injecting QW becomes stronger as well in the presence of the WL [Fig. 4.5(c)]. Since the recombination in the right-hand side of the structure is unaffected, the total parasitic recombination current density outside QDs is increased. For this reason, the output power is reduced in a structure with the WL (solid curve in Fig. 4.6). The output power

depends strongly on the temporal cross-section $w_{\mathrm{p,capt}}$ of hole capture from the WL into a QD [see (4.29)–(4.33)]. The larger $w_{\mathrm{p,capt}}$, the lower is the power and the stronger is the deviation of the LCC from that for a structure without the WL (dashed curve in Fig. 4.6). Clearly the internal quantum efficiency [Fig. 4.7(a)] and the slope efficiency [Fig. 4.7(b)] are reduced in the presence of the WL.

Despite the fact that the output power is reduced in the presence of the WL, it is clear from Fig. 4.6 that the LCC becomes increasingly linear with j. This remarkable feature can be understood and several general conclusions can be made from the analysis of the rate equations.

At the steady-state, eqs. (4.2) and (4.12) for holes in the left-hand side of the OCL and in the WL can be written as follows:

$$\frac{p_{\mathrm{QW}}^{L}}{\tau_{\mathrm{p,esc}}^{L}} - v_{\mathrm{p,capt}}^{L} p_{L} = b_{1} B n_{L} p_{L}\,, \tag{4.21}$$

$$w_{\mathrm{p,\,tunn}}^{\mathrm{QW}\leftrightarrow\mathrm{WL}} N_{\mathrm{v,2D}}^{\mathrm{QW}} p_{\mathrm{WL}} - w_{\mathrm{p,\,tunn}}^{\mathrm{QW}\leftrightarrow\mathrm{WL}} \widetilde{p}_{1}^{\mathrm{WL}} p_{\mathrm{QW}}^{L} = w_{\mathrm{p,capt}} p_{1}^{\mathrm{WL}} N_{S} f_{\mathrm{p}} - w_{\mathrm{p,capt}} N_{S} (1 - f_{\mathrm{p}}) p_{\mathrm{WL}} - B_{\mathrm{2D}} n_{\mathrm{WL}} p_{\mathrm{WL}}. \tag{4.22}$$

Using (4.21) and (4.22) in (4.6), we have

$$\begin{aligned} B_{\mathrm{2D}} n_{\mathrm{WL}} p_{\mathrm{WL}} + B_{\mathrm{2D}} n_{\mathrm{QW}}^{L} p_{\mathrm{QW}}^{L} + b_{1} B n_{L} p_{L} = {} & \left[w_{\mathrm{p,\,tunn}}^{L} p_{1}^{L,\mathrm{QW}} N_{S} f_{\mathrm{p}} - w_{\mathrm{p,\,tunn}}^{L} N_{S} (1 - f_{\mathrm{p}}) p_{\mathrm{QW}}^{L} \right] \\ & + \left[w_{\mathrm{p,capt}} p_{1}^{\mathrm{WL}} N_{S} f_{\mathrm{p}} - w_{\mathrm{p,capt}} N_{S} (1 - f_{\mathrm{p}}) p_{\mathrm{WL}} \right]. \end{aligned} \tag{4.23}$$

As seen from (4.23), bimolecular recombination in the WL and in the left-hand-side QW and OCL is entirely due to the net out-tunneling of holes from QDs to the electron-injecting QW [first brackets in (4.23)] and the net escape of holes from QDs to the WL (second brackets).

Bimolecular recombination in the right-hand-side QW and OCL is entirely due to the net out-tunneling of electrons from QDs to the hole-injecting QW and is not affected by the presence of the WL,

$$B_{\mathrm{2D}} n_{\mathrm{QW}}^{R} p_{\mathrm{QW}}^{R} + b_{1} B n_{R} p_{R} = w_{\mathrm{n,\,tunn}}^{R} n_{1}^{R,\mathrm{QW}} N_{S} f_{\mathrm{n}} - w_{\mathrm{n,\,tunn}}^{R} N_{S} (1 - f_{\mathrm{n}}) n_{\mathrm{QW}}^{R}\,. \tag{4.24}$$

By dropping in (4.23) the flux $w_{\mathrm{p,\,tunn}}^{L} N_{S} (1 - f_{\mathrm{p}}) p_{\mathrm{QW}}^{L}$ of backward tunneling of holes from the electron-injecting QW to QDs and the flux $w_{\mathrm{p,capt}} N_{S} (1 - f_{\mathrm{p}}) p_{\mathrm{WL}}$ of hole capture from the WL into QDs, we obtain the upper limit for the parasitic recombination flux in the left-hand side of the structure. Since $f_{\mathrm{n,p}} \le 1$, this limit, which presents the sum of the out-tunneling flux

$w^{L}_{\mathrm{p,tunn}} p_1^{L,\mathrm{QW}} N_S f_\mathrm{p}$ of holes from QDs to the electron-injecting QW and the thermal escape flux $w_{\mathrm{p,capt}} p_1^{\mathrm{WL}} N_S f_\mathrm{p}$ of holes from QDs to the WL, is itself restricted and cannot exceed $w^{L}_{\mathrm{p,tunn}} p_1^{L,\mathrm{QW}} N_S + w_{\mathrm{p,capt}} p_1^{\mathrm{WL}} N_S$ at any j [under the condition of charge neutrality (4.19), $w^{L}_{\mathrm{p,tunn}} p_1^{L,\mathrm{QW}} N_S f_\mathrm{p}$ and $w_{\mathrm{p,capt}} p_1^{\mathrm{WL}} N_S f_\mathrm{p}$ are pinned and do not change with j]. Consequently, we have for the recombination flux in the left-hand side of the structure

$$\begin{aligned} & b_1 B n_L p_L + B_{2\mathrm{D}} n^{L}_{\mathrm{QW}} p^{L}_{\mathrm{QW}} + B_{2\mathrm{D}} n_{\mathrm{WL}} p_{\mathrm{WL}} \\ < \; & w^{L}_{\mathrm{p,tunn}} p_1^{L,\mathrm{QW}} N_S f_\mathrm{p} + w_{\mathrm{p,capt}} p_1^{\mathrm{WL}} N_S f_\mathrm{p} \; < \; w^{L}_{\mathrm{p,tunn}} p_1^{L,\mathrm{QW}} N_S + w_{\mathrm{p,capt}} p_1^{\mathrm{WL}} N_S \; = \; \text{const.} \end{aligned} \tag{4.25}$$

From (4.24), we have for the recombination flux in the right-hand side of the structure

$$b_2 B n_R p_R + B_{2\mathrm{D}} n^{R}_{\mathrm{QW}} p^{R}_{\mathrm{QW}} \; < \; w^{R}_{\mathrm{n,tunn}} n_1^{R,\mathrm{QW}} N_S f_\mathrm{n} \; < \; w^{R}_{\mathrm{n,tunn}} n_1^{R,\mathrm{QW}} N_S \; = \; \text{const} \, . \tag{4.26}$$

Fig. 4.8 (solid curve) shows the recombination current density outside QDs [the sum of the last five terms in the brackets in (4.20)]. The horizontal dashed line is the sum of the current densities of electron and hole out-tunneling from QDs to the foreign QWs

$$j_{\mathrm{out-tunn}} = e w^{L}_{\mathrm{p,tunn}} p_1^{L,\mathrm{QW}} N_S f_\mathrm{p} + e w^{R}_{\mathrm{n,tunn}} n_1^{R,\mathrm{QW}} N_S f_\mathrm{n} \tag{4.27}$$

and hole thermal escape from QDs to the WL

$$j^{\mathrm{QDs}\to\mathrm{WL}}_{\mathrm{p,esc}} = e w_{\mathrm{p,capt}} p_1^{\mathrm{WL}} N_S f_\mathrm{p} \, . \tag{4.28}$$

As in a structure without the WL [A1], in the presence of the WL too, the fact that the parasitic recombination flux outside QDs remains limited with increasing j is due to the zero-dimensional nature of QDs — the flux of escape from QDs (be it out-tunneling escape to the foreign QW or thermal escape to the WL) is controlled by the level occupancy in a QD $f_{\mathrm{n,p}}$ [see (4.27) and (4.28)], which cannot exceed unity with increasing j [$f_\mathrm{n} = f_\mathrm{p}$ = const in the case of charge neutrality – see (4.19)].

With (4.23) and (4.24), eq. (4.20) can be rewritten as follows:

$$\begin{aligned} P = \frac{\hbar\omega}{e} S \Bigg[& j - e N_S \frac{f_\mathrm{n} f_\mathrm{p}}{\tau_{\mathrm{QD}}} - e w^{L}_{\mathrm{p,tunn}} p_1^{L,\mathrm{QW}} N_S f_\mathrm{p} - e w^{R}_{\mathrm{n,tunn}} n_1^{R,\mathrm{QW}} N_S f_\mathrm{n} - e w_{\mathrm{p,capt}} p_1^{\mathrm{WL}} N_S f_\mathrm{p} \\ & + e w^{L}_{\mathrm{p,tunn}} N_S (1 - f_\mathrm{p}) p^{L}_{\mathrm{QW}} + e w^{R}_{\mathrm{n,tunn}} N_S (1 - f_\mathrm{n}) n^{R}_{\mathrm{QW}} + e w_{\mathrm{p,capt}} N_S (1 - f_\mathrm{p}) p_{\mathrm{WL}} \Bigg] . \end{aligned} \tag{4.29}$$

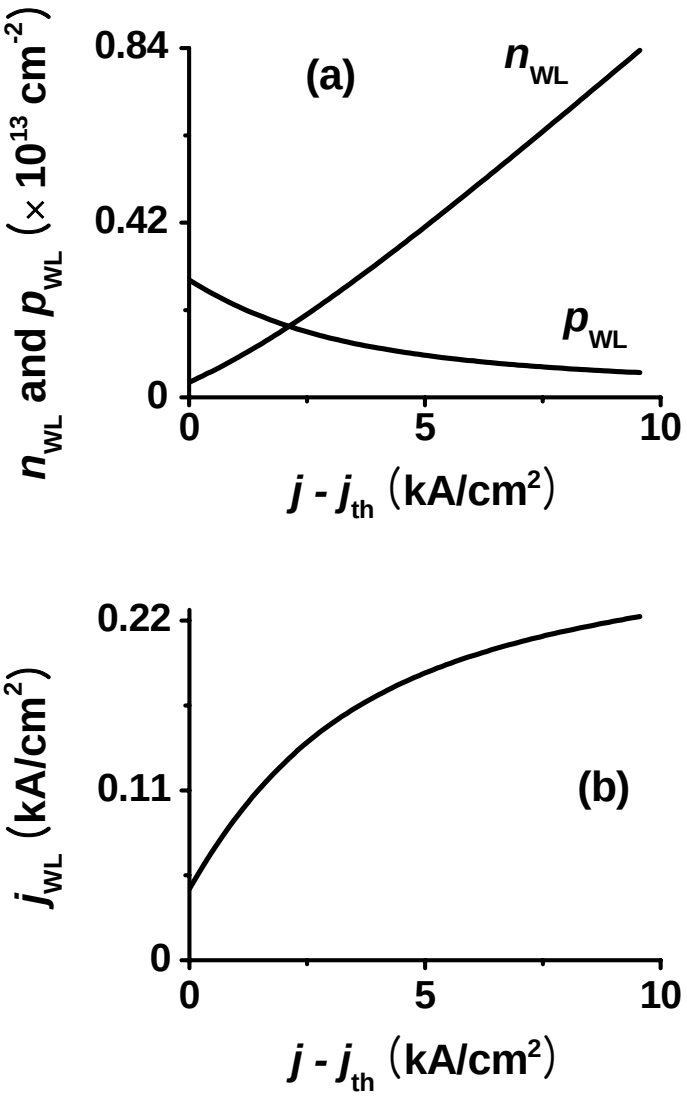

Fig. 4.4. 2-D densities of electrons and holes (a) and recombination current density (b) in the WL against excess injection current density. A GaInAsP heterostructure lasing at room-temperature (T = 300 K) near the telecommunication wavelength 1.55 μm is considered here. 10% QD size fluctuations are assumed. In Figs. 4.4 – 4.8 the parameters of the structure are as follows: $N_S = 6.11 \times 10^{10}$ cm^{-2}, L = 1.139 mm, R = 0.32, α = 10 cm^{-1}, W = 2 μm, $\tau_{QD} = 0.71 \times 10^{-9}$ s, g^{max} = 29.52 cm^{-1}, $b_1 = b_2$ = 0.14 μm, $v^{L,R}_{n,p,capt} = 3 \times 10^5$ cm/s, λ= 1.58 μm, B = 1.27×10^{-10} cm^3/s, and $B_{2D} = 2.8 \times 10^{-4}$ cm^2/s. The tunneling coefficients and temporal cross-sections are as follows unless otherwise specified: $w^L_{n,tunn} = w^{QW \leftrightarrow WL}_{n,tunn} = 0.073$ cm^2/s, $w^L_{p,tunn} = w^{QW \leftrightarrow WL}_{p,tunn} = 0.04$ cm^2/s, $w^R_{n,tunn} = 0.013$ cm^2/s, $w^R_{p,tunn} = 0.058$ cm^2/s, and $w_{n,p,capt} = 0.1$ cm^2/s.

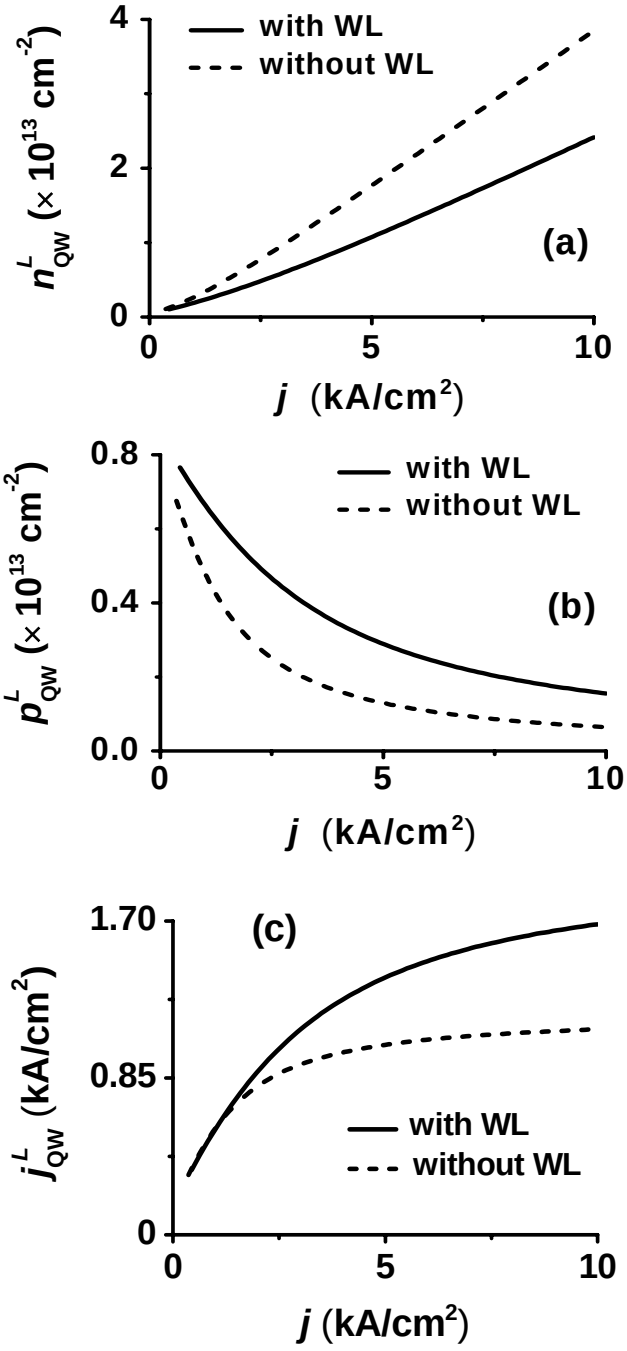

Fig. 4.5. 2-D densities of electrons (a) and holes (b) and recombination current density (c) in the electron-injecting QW against injection current density for the structures with (solid curve) and without (dashed curve) the WL.

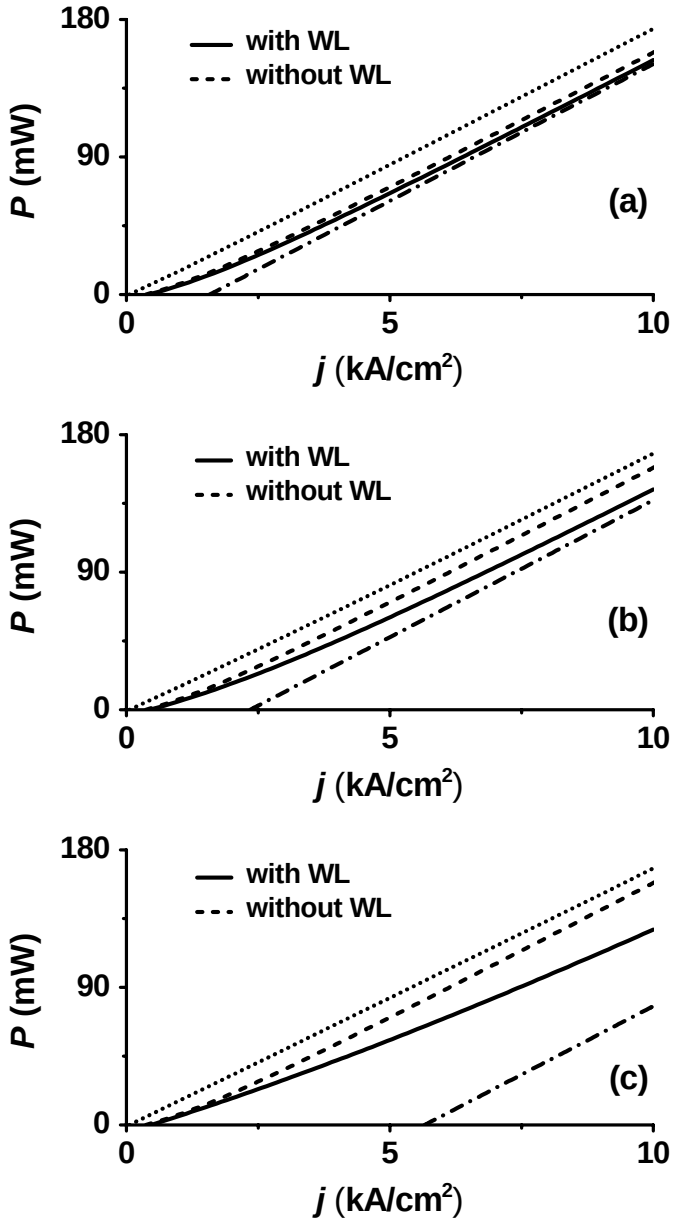

Fig. 4.6. Light-current characteristics of the tunneling-injection QD lasers with (solid curve) and without (dashed curve) the WL. The temporal cross-sections of electron and hole capture from the WL into a QD are $w_{\mathrm{n,p,\,capt}}$ = 0.03, 0.1, and 0.4 cm^2/s in (a), (b), and (c), respectively. The threshold current density is j_{th} = 417, 440, and 467 A/cm^2; for the structure without the WL, j_{th} = 366.3 A/cm^2. The dotted line given by (4.32) is the upper limit for the LCC. The dash-dotted line given by (4.30) is the asymptote and the lower limit for the LCC.

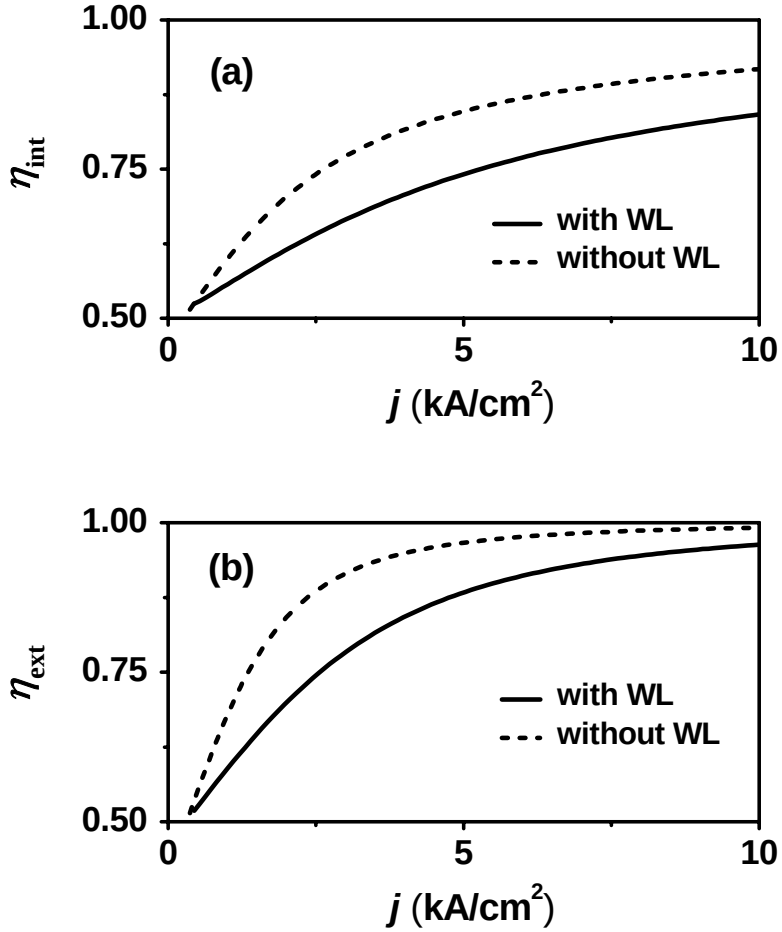

Fig. 4.7. Internal quantum efficiency (a) and slope efficiency (b) against injection current density for the tunneling-injection QD lasers with (solid curve) and without (dashed curve) the WL. Since η_{int} increases with j, η_{ext} also increases and is higher than η_{int} as is clear from (4.34).

Whatever the dependences of p_{QW}^{L}, n_{QW}^{R} and p_{WL} on j, it is clear from (4.29) that by dropping the last three terms in the brackets (the current densities of backward tunneling of minority carriers from the foreign QWs to QDs and of hole capture from the WL into QDs) we will obtain the lower limit for the output power,

$$P^{\text{lowest}} = \frac{\hbar\omega}{e} S\left(j - j_{\text{th}}^{\text{highest}}\right), \tag{4.30}$$

where

$$j_{\rm th}^{\rm highest} = eN_S \frac{f_{\rm n} f_{\rm p}}{\tau_{\rm QD}} + ew_{\rm p,tunn}^{L} p_1^{L,{\rm QW}} N_S f_{\rm p} + ew_{\rm n,tunn}^{R} n_1^{R,{\rm QW}} N_S f_{\rm n} + ew_{\rm p,capt} p_1^{\rm WL} N_S f_{\rm p} \tag{4.31}$$

is the upper limit for the threshold current density.

As seen from (4.30), the lower limit for the LCC is linear (dash-dotted line in Fig. 4.6) and its slope efficiency is unity.

The upper limit for the LCC is obtained in an ideal structure wherein out-tunneling from QDs to the foreign QWs and hence recombination in the QWs and OCL are completely blocked. Since recombination in the WL will still occur in such a structure, we have from (4.20)

$$P^{\rm highest} = \frac{\hbar\omega}{e} S \left(j - eN_S \frac{f_{\rm n} f_{\rm p}}{\tau_{\rm QD}} - eB_{\rm WL} n_{\rm WL} p_{\rm WL} \right). \tag{4.32}$$

In this case, we obtain from (4.25) that the recombination current density $eB_{\rm WL} n_{\rm WL} p_{\rm WL}$ in the WL is limited by the current density $ew_{\rm p,capt} p_1^{\rm WL} N_S f_{\rm p}$ of hole thermal escape from QDs to the WL,

$$B_{\rm 2D} n_{\rm WL} p_{\rm WL} \; < \; w_{\rm p,capt} p_1^{\rm WL} N_S f_{\rm p} \; < \; w_{\rm p,capt} p_1^{\rm WL} N_S \,. \tag{4.33}$$

With increasing j, $eB_{\rm WL} n_{\rm WL} p_{\rm WL}$ asymptotically approaches $ew_{\rm p,capt} p_1^{\rm WL} N_S f_{\rm p}$ and the upper limit (4.32) for the LCC becomes linear (dotted line in Fig. 4.6).

Hence, the actual LCC (obtained from the solution of the rate equations and shown by the solid curve in Fig. 4.6) in a structure with the WL is confined between the two parallel lines given by (4.30) and (4.32) (dash-dotted and dotted lines). Since the parasitic recombination current density remains restricted [see (4.25), (4.26) and Fig. 4.8], the fraction of the excess injection current density $j - j_{\rm th}$ that goes into the stimulated emission [the internal differential quantum efficiency, $\eta_{\rm int} = e\left(c/\sqrt{\epsilon_{\rm g}}\right)\beta(N/S)/(j - j_{\rm th})$] should rise with j [Fig. 4.7(a)]. As a result, the LCC should become increasingly linear (Fig. 4.6).

From (4.29), we have for the slope efficiency (external differential quantum efficiency)

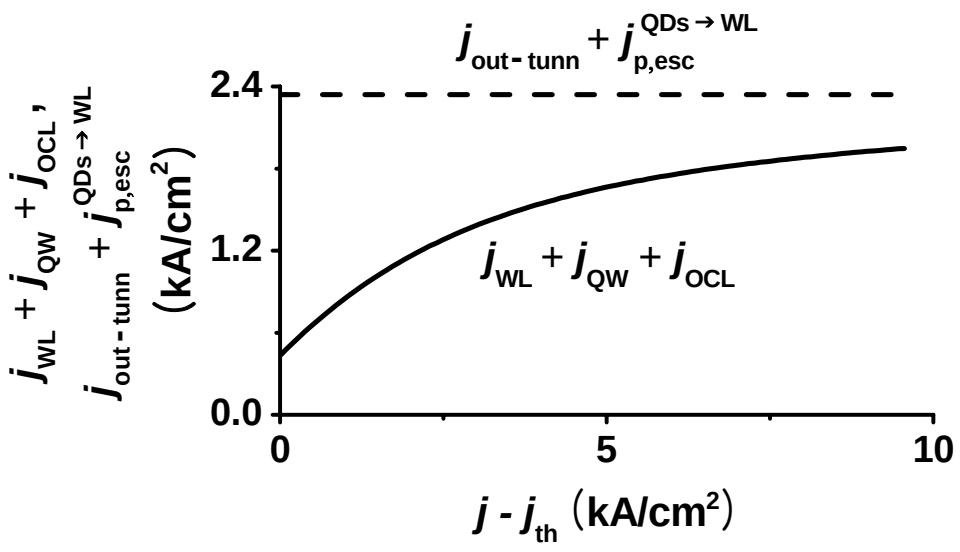

Fig. 4.8. Parasitic recombination current density outside QDs (solid curve). The horizontal dashed line is the sum of the current densities of electron and hole out-tunneling from QDs to the foreign QWs and hole thermal escape from QDs to the WL.

$$\eta_{\text{ext}} = \frac{1}{\frac{\hbar\omega}{e}S}\frac{\partial P}{\partial j} = \eta_{\text{int}} + (j - j_{\text{th}})\frac{\partial \eta_{\text{int}}}{\partial j}$$
$$= 1 + ew_{\text{p,tunn}}^{L} N_S (1 - f_{\text{p}})\frac{\partial p_{\text{QW}}^{L}}{\partial j} + ew_{\text{n,tunn}}^{R} N_S (1 - f_{\text{n}})\frac{\partial n_{\text{QW}}^{R}}{\partial j} + ew_{\text{p,capt}} N_S (1 - f_{\text{p}})\frac{\partial p_{\text{WL}}}{\partial j}. \tag{4.34}$$

Since η_{ext} should not be higher than unity, the derivatives of p_{QW}^{L}, n_{QW}^{R}, and p_{WL} with respect to j should be negative — the minority carrier density in each of the two QWs and the hole density in the WL decrease with j [Figs. 4.4(a) and 4.5(b)]. Hence, the last three terms in the brackets in (4.29) decrease with increasing j and the LCC asymptotically approaches the straight line given by (4.30) (Fig. 4.6).

4.3.1. Laser characteristics versus temporal cross-sections of electron and hole capture from the WL into a QD

Fig. 4.9 shows the dependences of the carrier densities and recombination current densities in the WL and QW, total parasitic recombination current density outside QDs, and

output power on the temporal cross-section $w_{\mathrm{n,\,capt}}$ of majority carrier (electron) capture from the WL into a QD at a fixed temporal cross-section $w_{\mathrm{p,\,capt}}$ of minority carrier (hole) capture. As $w_{\mathrm{n,\,capt}}$ increases, electrons are more efficiently captured into QDs and the electron densities in the WL and QW decrease [Fig. 4.9(a) and (b)]. Hence, the recombination current densities decrease [Fig. 4.9(e) and (f)], and the hole densities increase in the WL and QW [Fig. 4.9(c) and (d)]. Following the decrease of the recombination current densities in the WL and QW, the total parasitic recombination current density outside QDs decreases [Fig. 4.9(g)] and, consequently, the output power increases [Fig 4.9(h)]. As $w_{\mathrm{n,\,capt}} \to \infty$, the electron density in the WL saturates [dashed line in Fig. 4.9(a)],

$$n_{\mathrm{WL}}\Big|_{w_{\mathrm{n,capt}}\to\infty} = n_{1,\mathrm{WL}}\frac{f_{\mathrm{n}}}{1-f_{\mathrm{n}}}. \tag{4.35}$$

Eq. (4.35) is the equilibrium relation between n_{WL} and f_{n} and is easily obtained from eq. (4.11).

Fig. 4.10 shows the dependences of the carrier densities and recombination current densities in the WL and QW, total parasitic recombination current density outside QDs, and output power on the temporal cross-section $w_{\mathrm{p,\,capt}}$ of minority carrier (hole) capture from the WL into a QD at a fixed temporal cross-section $w_{\mathrm{n,\,capt}}$ of majority carrier (electron) capture. As $w_{\mathrm{p,\,capt}}$ increases, holes are efficiently provided to the WL and left-hand side QW and hence the hole densities there increase [Fig. 4.10(c) and (d)]. The increase of the hole densities leads to the increase of the recombination current densities in the WL and QW [Fig. 4.10(e) and (f)] and, consequently, the electron densities in the WL and QW decrease [Fig. 4.10(a) and (b)]. As a result, the parasitic recombination current density outside QDs increases [Fig. 4.10 (g)], and the output power decreases [Fig .4.10(h)]. As $w_{\mathrm{p,\,capt}} \to \infty$, the hole density in the WL saturates [dashed line in Fig. 4.10(c)],

$$p_{\mathrm{WL}}\Big|_{w_{\mathrm{p,capt}}\to\infty} = p_{1,\mathrm{WL}}\frac{f_{\mathrm{p}}}{1-f_{\mathrm{p}}}. \tag{4.36}$$

Eq. (4.36) is the equilibrium relation between p_{WL} and f_{p} and is easily obtained from eq. (4.12).

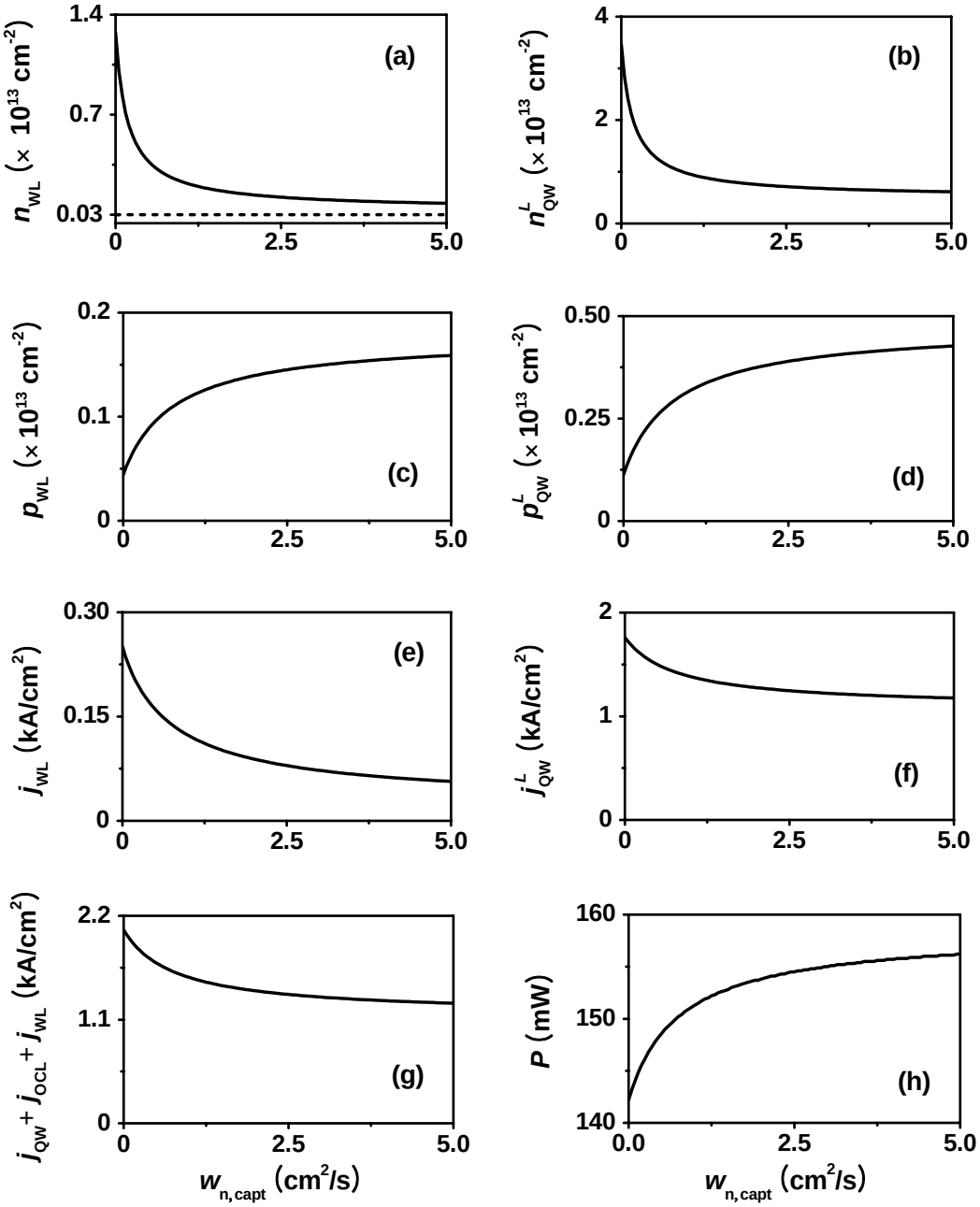

Fig. 4.9. 2-D densities of electrons and holes, recombination current densities in the WL [(a), (c), and (e), respectively] and QW [(b), (d), and (f), respectively], total parasitic recombination current density outside QDs (g), and output power (h) against temporal cross-section $w_{n,\,capt}$ of majority carrier (electron) capture from the WL into a QD at a fixed temporal cross-section $w_{p,\,capt}$ = 0.1 cm^2/s of minority carrier (hole) capture. The injection current density is j = 10 kA/cm^2.

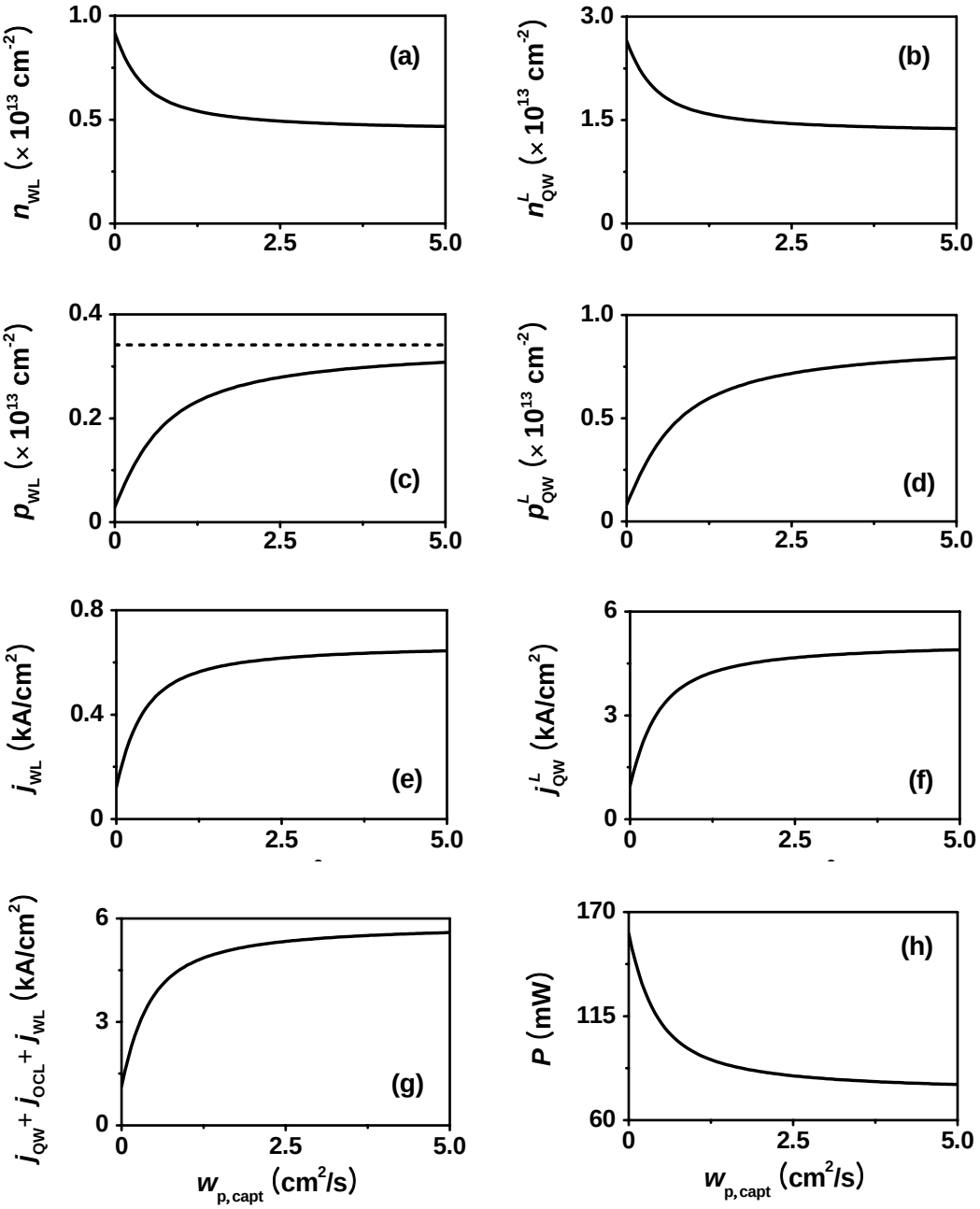

Fig. 4.10. 2-D densities of electrons and holes, recombination current densities in the WL [(a), (c), and (e), respectively] and QW [(b), (d), and (f), respectively], total parasitic recombination current density outside QDs (g), and output power (h) against temporal cross-section $w_{p,\,capt}$ of minority carrier (hole) capture from the WL into a QD at a fixed temporal cross-section $w_{n,\,capt}$ = 0.1 cm^2/s of majority carrier (electron) capture. The injection current density is j = 10 kA/cm^2.

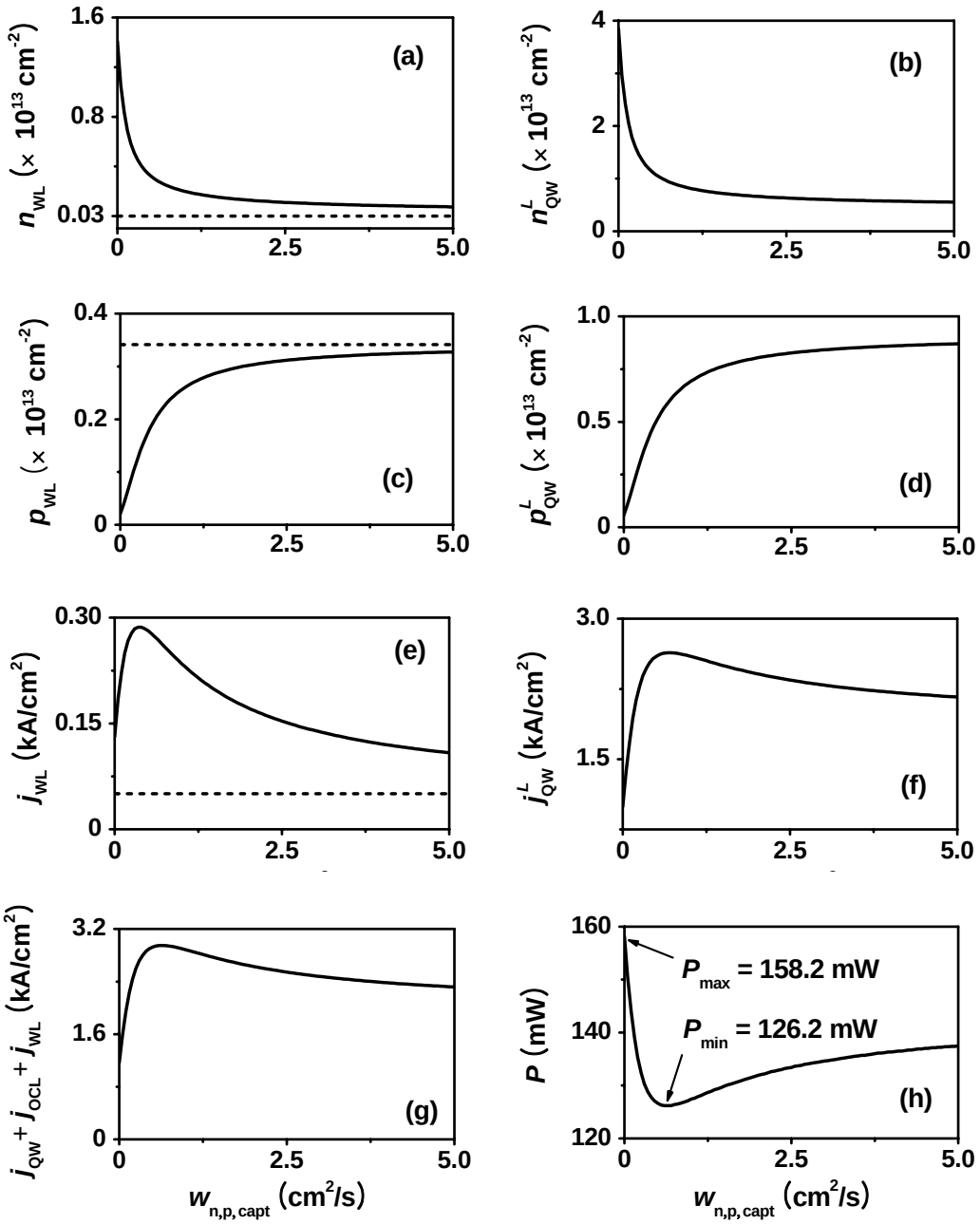

Fig. 4.11. 2-D densities of electrons and holes, recombination current densities in the WL [(a), (c), and (e), respectively] and QW [(b), (d), and (f), respectively], total parasitic recombination current density outside QDs (g), and output power (h) against temporal cross-sections of majority and minority carrier capture, which vary simultaneously and are equal to each other, $w_{n,\,capt} = w_{p,\,capt}$. The injection current density is j = 10 kA/cm^2.

Hence, as it could be expected and is natural, and is seen from Figs. 4.9 and 4.10, the parasitic recombination outside QDs becomes less (more) intensive and hence the output power increases (decreases) as the majority (minority) carrier capture from the WL into a QD becomes more intensive.

Both in Figs. 4.9 and 4.10, the electron densities decrease [(a) and (b)] and the hole densities increase [(c) and (d)] with increasing capture temporal cross-sections. The recombination current densities are controlled by the product of the electron and hole densities. The decrease of the recombination current densities in Fig. 4.9(e) and (f) reflects the fact that the electron densities decrease faster than the hole densities increase. In contrast, the increase of the recombination current densities in Fig. 4.10(e) and (f) reflects the fact that the electron densities decrease slower than the hole densities increase.

Fig. 4.11 shows the carrier densities and recombination current densities in the WL and QW, total parasitic recombination current density, and output power versus the temporal cross-sections of majority and minority carrier capture, which vary simultaneously and are equal to each other, $w_{\mathrm{n,\,capt}} = w_{\mathrm{p,\,capt}}$. Such a simultaneous increase of $w_{\mathrm{n,p,\,capt}}$ means that both the desirable electron capture from the WL into a QD and undesirable hole supply (by thermal escape) from a QD to the WL [and then the hole supply (by tunneling from the WL) to the electron-injecting QW] become more efficient. The electron (hole) densities decrease (increase) with increasing each of $w_{\mathrm{n,\,capt}}$ and $w_{\mathrm{p,\,capt}}$ [Figs. 4.9 and 4.10]. Hence, these tendencies remain the same as $w_{\mathrm{n,p,\,capt}}$ change simultaneously [Fig. 4.11(a, b, c, d)]. In contrast, the effects of varying $w_{\mathrm{n,\,capt}}$ and $w_{\mathrm{p,\,capt}}$ on the recombination current densities in the WL and QW, and hence on the total parasitic recombination current density outside QDs, are opposite to each other. As a result of the competition between these effects, the recombination current densities are nonmonotonic – they first increase and then decrease [Fig. 4.11(e, f, g)]. Consequently, the output power is also nonmonotonic – it first decreases and then increases [Fig. 4.11(h)]. Hence, as a function of $w_{\mathrm{n,\,capt}} = w_{\mathrm{p,\,capt}}$, the parasitic recombination current density has a maximum and the output power has a minimum. The total parasitic recombination current density is minimum [Fig. 4.11(g)] and the output power is maximum [Fig. 4.11(h)] at $w_{\mathrm{n,\,capt}} = w_{\mathrm{p,\,capt}} = 0$. This is because the hole densities in the WL and QW are minimum at $w_{\mathrm{n,\,capt}} = w_{\mathrm{p,\,capt}} = 0$.

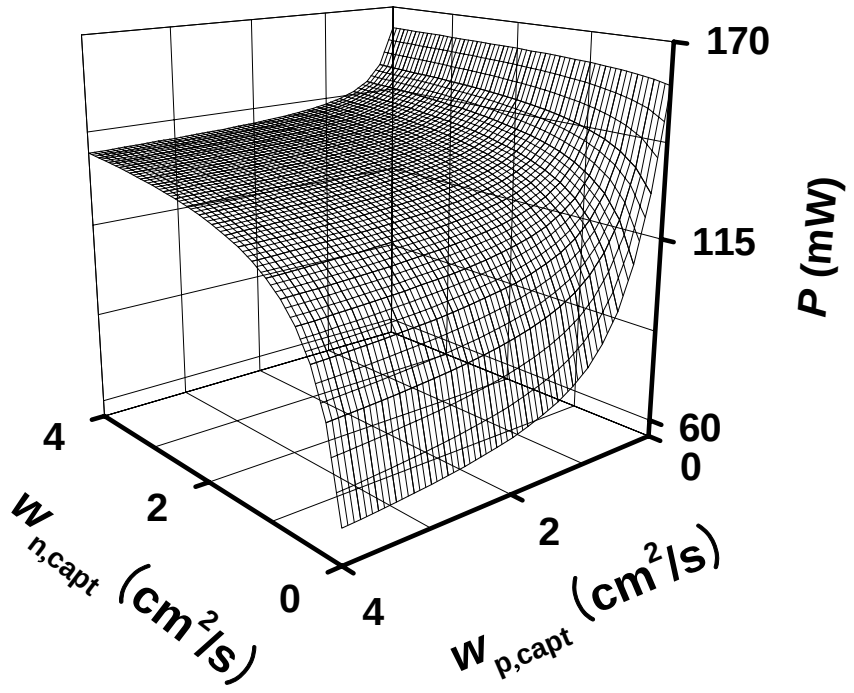

Fig. 4.12. Optical power against temporal cross-sections $w_{\mathrm{n,\,capt}}$ and $w_{\mathrm{p,\,capt}}$ of electron and hole capture from the WL into a QD. The injection current density is j = 10 kA/cm^2.

Note that the recombination current density in the WL is nonzero at a zero value of $w_{\mathrm{n,\,capt}}$ or (and) $w_{\mathrm{p,\,capt}}$ [Fig. 4.9(e), Fig. 4.10(e), and Fig. 4.11(e)]. This is because, even in such a case of absence of direct coupling between the WL and a QD, there is an alternative path for the electron and hole supply to the WL – the path from the electron-injecting QW (processes ④ and ⑨ in Fig. 4.3). As $w_{\mathrm{n,\,capt}} = w_{\mathrm{p,\,capt}} \to \infty$, the electron and hole densities in the WL saturate at (4.35) and (4.36) [dashed lines in Fig. 4.11(a) and (c)], respectively, and hence the recombination current density in the WL saturates [dashed line in Fig. 4.11(e)].

As seen from Figs. 4.9-4.11, the output power is strongly affected by the temporal cross-sections of carrier capture into a QD. Fig. 4.12 shows the dependence of the output power on both $w_{\mathrm{n,\,capt}}$ and $w_{\mathrm{p,\,capt}}$ in the most general form. The specific cases described by Figs. 4.9(h),

4.10(h), and 4.11(h) (changing only one of the two cross-sections at a fixed value of another, and changing them simultaneously) are easily seen from this general dependence.

As clear from Figs. 4.9-4.12, to properly optimize the tunneling-injection structure with the WL, the temporal cross-sections of electron and hole capture into a QD should be controlled in addition to the tunneling coefficients (chapter 3) – $w_{\mathrm{n,\,capt}}$ should be kept high and $w_{\mathrm{p,\,capt}}$ low.

4.4. Conclusion

The effect of the WL, which is inherently present in self-assembled Stranski-Krastanow grown structures, on the optical power of a tunneling-injection QD laser has been studied. Due to thermal escape of carriers from QDs, bipolar population establishes and hence electron-hole recombination occurs in the WL. Since the opposite sides of a tunneling-injection structure are only connected by the current paths through QDs, and the WL is located in the n-side of the structure, the only source of holes for the WL is provided by QDs. It has been shown that, due to the zero-dimensional nature of QDs, the rate of the hole supply to the WL remains limited with increasing injection current. For this reason, as in the other parts of the structure outside QDs (QWs and OCL), the parasitic electron-hole recombination remains restricted in the WL. As a result, even in the presence of the WL, the LCC of a tunneling-injection QD laser becomes increasingly linear at high injection currents, which is a further demonstration of robustness of such a laser and its potential for high-power operation.

Appendix I

Quantities $\widetilde{n}_1^{\mathrm{WL}}$ and $\widetilde{p}_1^{\mathrm{WL}}$ in the tunneling fluxes of electrons and holes from the electron-injecting QW to the WL

For definiteness, we consider in Appendixes I and II electrons. The derivation and expressions for holes are similar. Under thermal equilibrium, the flux $w_{\mathrm{n,\,tunn}}^{\mathrm{QW}\leftrightarrow\mathrm{WL}}\widetilde{n}_1^{\mathrm{WL}}n_{\mathrm{QW}}^{\mathrm{eq}}$ of electron tunneling from the electron-injecting QW to the WL is equal to the flux $w_{\mathrm{n,\,tunn}}^{\mathrm{QW}\leftrightarrow\mathrm{WL}}N_{\mathrm{c,2D}}^{\mathrm{QW}}n_{\mathrm{WL}}^{\mathrm{eq}}$ of backward tunneling of electrons from the WL to the QW, to give:

$$\widetilde{n}_1^{\mathrm{WL}} = N_{\mathrm{c,2D}}^{\mathrm{QW}}\frac{n_{\mathrm{WL}}^{\mathrm{eq}}}{n_{\mathrm{QW}}^{\mathrm{eq}}}. \tag{A1}$$

Using the closed-form expression for the 2-D equilibrium carrier density (see, e.g., [22]), we have for $n_{\mathrm{WL}}^{\mathrm{eq}}$ and $n_{\mathrm{QW}}^{\mathrm{eq}}$

$$n_{\mathrm{WL,\,QW}}^{\mathrm{eq}} = N_{\mathrm{c,2D}}^{\mathrm{WL,\,QW}}\ln\left[1+\exp\left(\frac{\mu^{\mathrm{eq}}-\varepsilon_{\mathrm{n}}^{\mathrm{WL,\,QW}}}{T}\right)\right], \tag{A2}$$

where $N_{\mathrm{c,2D}}^{\mathrm{WL,\,QW}} = m_{\mathrm{c}}^{\mathrm{WL,\,QW}}T/\left(\pi\hbar^2\right)$ are the 2-D effective densities of states in the conduction band in the WL and QW, respectively, $m_{\mathrm{c}}^{\mathrm{WL,\,QW}}$ are the electron effective masses there, T is the temperature (measured in units of energy), $\varepsilon_{\mathrm{n}}^{\mathrm{WL,\,QW}}$ are the energies of the lowest electron-subband edge in the WL and QW, respectively, and μ^{eq} is the equilibrium Fermi level.

With (A2), (A1) becomes

$$\widetilde{n}_1^{\mathrm{WL}} = N_{\mathrm{c,2D}}^{\mathrm{WL}}\frac{\ln\left[1+\exp\left(\dfrac{\mu^{\mathrm{eq}}-\varepsilon_{\mathrm{n}}^{\mathrm{WL}}}{T}\right)\right]}{\ln\left[1+\exp\left(\dfrac{\mu^{\mathrm{eq}}-\varepsilon_{\mathrm{n}}^{\mathrm{QW}}}{T}\right)\right]}. \tag{A3}$$

If both QW and WL materials are nondegenerate (the Fermi level μ^{eq} is below $\varepsilon_{\mathrm{n}}^{\mathrm{QW}}$ by several T), which is the case of undoped QW and WL considered here, then

$$\ln\left[1+\exp\left(\frac{\mu^{\mathrm{eq}}-\varepsilon_{\mathrm{n}}^{\mathrm{WL,\,QW}}}{T}\right)\right]\approx\exp\left(-\frac{\varepsilon_{\mathrm{n}}^{\mathrm{WL,\,QW}}-\mu^{\mathrm{eq}}}{T}\right). \qquad \text{(A4)}$$

With (A4), eq. (15) is obtained from (A3).

Appendix II

Quantities n_1^{WL} and p_1^{WL} in the thermal escape fluxes of electrons and holes from QDs to the WL

We now use the detailed balance condition under thermal equilibrium for the flux $w_{\mathrm{n,capt}} n_1^{\mathrm{WL}} N_S f_{\mathrm{n}}^{\mathrm{eq}}$ of carrier thermal escape from QDs to the WL and the flux $w_{\mathrm{n,capt}} N_S \left(1 - f_{\mathrm{n}}^{\mathrm{eq}}\right) n_{\mathrm{WL}}^{\mathrm{eq}}$ of capture from the WL to QDs to obtain

$$n_1^{\mathrm{WL}} = \frac{1 - f_{\mathrm{n}}^{\mathrm{eq}}}{f_{\mathrm{n}}^{\mathrm{eq}}} n_{\mathrm{WL}}^{\mathrm{eq}}, \tag{A5}$$

where

$$f_{\mathrm{n}}^{\mathrm{eq}} = \frac{1}{\exp\left(\dfrac{\varepsilon_{\mathrm{n}}^{\mathrm{QD}} - \mu^{\mathrm{eq}}}{T}\right) + 1}, \tag{A6}$$

is the equilibrium occupancy of the energy level $\varepsilon_{\mathrm{n}}^{\mathrm{QD}}$ in a QD.

With (A2) for $n_{\mathrm{WL}}^{\mathrm{eq}}$, (A5) becomes

$$n_1^{\mathrm{WL}} = N_{\mathrm{c,2D}}^{\mathrm{WL}} \exp\left(\frac{\varepsilon_{\mathrm{n}}^{\mathrm{QD}} - \mu^{\mathrm{eq}}}{T}\right) \ln\left[1 + \exp\left(\frac{\mu^{\mathrm{eq}} - \varepsilon_{\mathrm{n}}^{\mathrm{WL}}}{T}\right)\right]. \tag{A7}$$

If a WL material is nondegenerate (μ^{eq} is below $\varepsilon_{\mathrm{n}}^{\mathrm{WL}}$ by several T), which is the case of an undoped WL considered here, the use of (A4) in (A7) yields eq. (16). In (16), the separation $\varepsilon_{\mathrm{n}}^{\mathrm{WL}} - \varepsilon_{\mathrm{n}}^{\mathrm{QD}}$ between the energies of the lowest subband edge in the WL and the level in a QD can be controlled by post-growth annealing [11] or changing the growth temperature [12].

REFERENCES[*)]

[A1] D.-S. Han and L. V. Asryan, "Light-current curve of a tunneling-injection quantum dot laser," *Proc. SPIE*, vol. 6902, pp. B9020-1–B9020-12, Jan. 2008.

[A2] D.-S. Han and L. V. Asryan, "Tunneling-injection of electrons and holes into quantum dots: A tool for high-power lasing," *Appl. Phys. Lett.*, vol. 92, no. 25, pp. 251113-1–251113-3, June 2008.

[A3] D.-S. Han and L. V. Asryan, "Output power of a tunneling-injection quantum dot laser," under review.

[A4] D.-S. Han and L. V. Asryan, "Effect of the wetting layer on the output power of a tunneling-injection quantum dot laser," accepted for publication in *IEEE/OSA J. Lightwave Technol.*

[A5] D.-S. Han and L. V. Asryan, "Tunneling-injection quantum dot laser: Effect of the wetting layer," *Proc. SPIE,* vol. 7610, Jan. 2010.

[1] Y. Arakawa and H. Sakaki, "Multidimensional quantum well laser and temperature dependence of its threshold current," *Appl. Phys. Lett.*, vol. 40, no. 3, pp. 217–219, June 1982.

[2] N. Kirstädter, N. N. Ledentsov, M. Grundmann, D. Bimberg, V. M. Ustinov, S. S. Ruvimov, M. V. Maximov, P. S. Kop'ev, Zh. I. Alferov, U. Richter, P. Werner, U. Gösele, and J. Heydenreich, "Low threshold, large T_0 injection laser emission from (InGa)As quantum dots," *Electron. Lett.*, vol. 30, no. 17, pp. 1416–1417, Aug. 1994.

[3] R. Mirin, A. Gossard, and J. Bowers, "Room temperature lasing from InGaAs quantum dots," *Electron. Lett.*, vol. 32, no. 18, pp. 1732–1734, Aug. 1996.

[4] G. Park, O. B. Shchekin, D. L. Huffaker, and D. G. Deppe, "Low-threshold oxide-confined 1.3-μm quantum-dot laser," *IEEE Phot. Technol. Lett.*, vol. 13, no. 3, pp. 230–232, Mar. 2000.

[*)] "A" in the reference number indicates the publications of the author of this dissertation.

[5] Y. Qiu, P. Gogna, S. Forouhar, A. Stintz, and L. F. Lester, "High-performance InAs quantum-dot lasers near 1.3 μm," *Appl. Phys. Lett.*, vol. 79, no. 22, pp. 3570–3572, Nov. 2001.

[6] P. Bhattacharya and S. Ghosh, "Tunnel injection $In_{0.4}Ga_{0.6}As$/GaAs quantum dot lasers with 15 GHz modulation bandwidth at room temperature," *Appl. Phys. Lett.*, vol. 80, no. 19, pp. 3482–3484, May 2002.

[7] D. Zhou, R. Piron, F. Grillot, O. Dehaese, E. Homeyer, M. Dontabactouny, T. Batte, K. Tavernier, J. Even, and S. Loualiche, "Study of the characteristics of 1.55 μm quantum dash/dot semiconductor lasers on InP substrate," *Appl. Phys. Lett.*, vol. 93, no. 16, pp. 161104-1–161104-3, Oct. 2008.

[8] V. A. Shchukin, N. N. Ledentsov, and D. Bimberg, "Epitaxy of Nanostructures," Berlin, Springer, 2003, 400 p.

[9] K. Nishi, R. Mirin, D. Leonard, G. Medeiros-Ribeiro, P. M. Petroff, and A. C. Gossard, "Structural and optical characterization of InAs/InGaAs self-assembled quantum dots grown on (311)*B* GaAs," *J. Appl. Phys.,* vol. 80, no. 6, pp. 3466–3470, Sept. 1996.

[10] R. Leon, Y. Kim, C. Jagadish, M. Gal, J. Zou, and D. J. H. Cockayne, "Effects of interdiffusion on the luminescence of InGaAs/GaAs quantum dots," *Appl. Phys. Lett.*, vol. 69, no. 13, pp. 1888–1890, Sept. 1996.

[11] A. Patanè, A. Polimeni, P. C. Main, M. Henini, and L. Eaves, "High-temperature light emission from InAs quantum dots," *Appl. Phys. Lett.*, vol. 75, no. 6, pp. 814–816, Aug. 1999.

[12] J. S. Kim and I.-H. Bae, "Optical properties of wetting layer in InAs quantum dots at different growth temperatures," *J. Korean Phys. Soc.*, vol. 42, no. 92, pp. S483–S486, Feb. 2003.

[13] H. S. Kim, J. H. Suh, C. G. Park, S. J. Lee, S. K. Noh, J. D. Song, Y. J. Park, W. J. Choi, and J. I. Lee, "Effects of the thickness of GaAs spacer layers on the structure of multilayer stacked InAs quantum dots," *J. Cryst. Growth*, vol. 311, no. 2, pp. 258-262, Jan. 2009.

[14] L. V. Asryan and R. A. Suris, "Inhomogeneous line broadening and the threshold current density of a semiconductor quantum dot laser," *Semicond. Sci. Technol.*, vol. 11, no. 4, pp. 554–567, Apr. 1996.

[15] L. V. Asryan and R. A. Suris, "Temperature dependence of the threshold current density of a quantum dot laser," *IEEE J. Quantum Electron*., vol. 34, no. 5, pp. 841–850, May 1998.

[16] M. V. Maximov, L. V. Asryan, Y. M. Shernyakov, A. F. Tsatsul'nikov, I. N. Kaiander, W. Nikolaev, A. R. Kovsh, S. S. Mikhrin, V. M. Ustinov, A. E. Zhukov, Z. I. Alferov, N. N. Ledentsov, and D. Bimberg, "Gain and threshold characteristics of long wavelength lasers based on InAs/GaAs quantum dots formed by activated alloy phase separation," *IEEE J. Quantum Electron*., vol. 37, no. 5, pp. 676–683, May 2001.

[17] L. V. Asryan and S. Luryi, "Tunneling-injection quantum-dot laser: Ultrahigh temperature stability," *IEEE J. Quantum Electron*., vol. 37, no. 7, pp. 905–910, Jul. 2001.

[18] L. V. Asryan and S. Luryi, "Temperature-insensitive semiconductor quantum dot laser," *Solid-State Electron*., vol. 47, no. 2, pp. 205–212, Feb. 2003.

[19] L. V. Asryan and S. Luryi, "Semiconductor laser with reduced temperature sensitivity," *U.S. Patent 6 870 178 B2*, Mar. 22, 2005.

[20] S. Raymond, S. Fafard, K. Hinzer, S. Charbonneau, and J. L. Merz, "Temporal cross-section for carrier capture by self-assembled quantum dots," *Microelectron. Eng.*, vol. 53, no. 1, pp. 241–244, Jun. 2000.

[21] S. Raymond, K. Hinzer, S. Fafard, and J. L. Merz, " Experimental determination of Auger capture coefficients in self-assembled quantum dots," *Phys*. *Rev*. *B,* vol. 61, no. 24, pp. R16 331–334, Jun. 2000.

[22] K. J. Vahala and C. E. Zah, "Effect of doping on the optical gain and the spontaneous noise enhancement factor in quantum well amplifiers and lasers studied by simple analytical expressions," *Appl*. *Phys*. *Lett*., vol. 52, no. 23, pp. 1945–1947, Jun. 1988.